ENGINEERING EXPERIMENT STATION

OF THE GEORGIA INSTITUTE OF TECHNOLOGY

ATLANTA, GEORGIA

FINAL REPORT AND REVISED FINAL REPORT, PART A-B

PROJECT NO. 218

A NOTE ON THE FLOW INDUCED BY AN "IDEALIZED" LIFTING ROTOR IN VERTICAL FLIGHT

BY

WALTER CASTLES, JR.

CONTRACT NO. Naw-6230

NATIONAL ADVISORY COMMITTEE FOR AERONAUTICS

1953-1957

CONTENTS

ENGINEERING EXPERIMENT STATION
of the Georgia Institute of Technology
Atlanta, Georgia

FINAL REPORT

PROJECT NO. 218

A NOTE ON THE FLOW INDUCED BY AN "IDEALIZED" LIFTING ROTOR IN VERTICAL FLIGHT

By

WALTER CASTLES, JR.
Daniel Guggenheim School of Aeronautics

o - o - o - o - o - o - o - o - o - o - o

CONTRACT NO. Naw-6230

NATIONAL ADVISORY COMMITTEE FOR AERONAUTICS

o - o - o - o - o - o - o - o - o - o - o

FEBRUARY, 1953

ENGINEERING EXPERIMENT STATION
of the Georgia Institute of Technology
Atlanta, Georgia

FINAL REPORT

PROJECT NO. 218

A NOTE ON THE FLOW INDUCED BY AN "IDEALIZED" LIFTING ROTOR IN VERTICAL FLIGHT

By

WALTER CASTLES, JR.
Daniel Guggenheim School of Aeronautics

o - o - o - o - o - o - o - o - o - o - o

CONTRACT NO. Naw-6230

NATIONAL ADVISORY COMMITTEE FOR AERONAUTICS

o - o - o - o - o - o - o - o - o - o - o

FEBRUARY, 1953

Final Report, Project No. 218

A NOTE ON THE FLOW INDUCED BY AN "IDEALIZED" LIFTING ROTOR IN VERTICAL FLIGHT

Prepared by [redacted]
Walter Castles, Jr., Assoc. Prof.
Daniel Guggenheim School of
Aeronautics

Approved by [redacted]
Donnell W. Dutton, Director
Daniel Guggenheim School of
Aeronautics

Released by [redacted]
Herschel H. Cudd, Acting Director
Engineering Experiment Station

February, 1953

TABLE OF CONTENTS

Final Report, Project No. 218

A NOTE ON THE FLOW INDUCED BY AN "IDEALIZED" LIFTING ROTOR IN VERTICAL FLIGHT

By

Walter Castles, Jr.

SUMMARY

Equations are derived for the relation between the nondimensional mean-induced velocity and the nondimensional flight-path velocity of an "idealized" lifting rotor in vertical flight. The equations are based upon the assumption that the vortex sheet enclosing the wake unrolls from around the periphery of the rotor disk in the form of a spiral which may be considered, as far as the flow outside the spiral is concerned, to be approximately equivalent to the "core" of a "bound" vortex ring.

The present analysis indicates that previous theory considerably underestimated the magnitude of the mean-axial component of the induced velocity and consequently the induced power required for the helicopter vertical-flight range.

INTRODUCTION

The usual propeller theory is based upon the assumption that the induced velocities are small compared to the freestream velocity. This assumption is not valid for the large relative induced velocities of lifting rotors operating at the smaller rates of vertical ascent, hovering, or vertical descent. Also, the flow studies of references 1 and 2 and numerous other observations have shown that, for at least a part of the above flight range, the wake originates from a vortex-ring-type flow enclosing the

periphery of the rotor.

A simplifying assumption which appears to be sufficiently accurate for the small torque loadings encountered in helicopter-rotor analysis is the assumption that the induced and freestream velocities are small compared with the tip rotor-blade-section tangential velocity. This assumption, which has been used in the present report, places no limit upon the relative magnitude of the induced and freestream velocities and is equivalent to assuming the vortex wake elements to be vortex rings of small strength.

In order to satisfy continuity and boundary conditions for the flow patterns under consideration, the periphery of the rotor must apparently be enclosed in a vortex ring type of flow. The present paper attempts to explain this phenomena by making the assumption that the vortex sheet enclosing the wake of a rotor having blades with constant circulation along the radii unrolls from around the periphery of the rotor disk in the form of a spiral (shown schematically in figure 1) which, for some mathematical purposes, may be considered to be the core of a bound vortex ring.

In the case of an actual rotor blade the circulation must decrease over the outer blade-elements to a zero value at the blade tips. Consequently there will be a vortex sheet shed from the trailing edges of these outer blade elements and the free outer edge of this sheet will immediately start to roll up in a spiral. For propeller flight conditions where the freestream velocity is large, this roll up occurs far behind the propeller and can be neglected in the theory. However, for the helicopter flight conditions considered in this report, it appears that a significant amount of the rolled up sheet can be accumulated at or near the periphery of the rotor and thus furnish the vorticity for the previously mentioned bound vortex ring.

SYMBOLS

$\frac{d\Gamma}{dt}$	rate at which vorticity is transported along wake (also rate at which it is generated)
$\frac{d\Gamma}{dz}$	strength of unit length of wake vortex sheet
$\left(\frac{d\Gamma}{dz}\right)_\infty$	strength of unit length of ultimate wake vortex sheet
$\frac{dz}{dt}$	axial component of wake vortex sheet velocity
$E(\ )$	complete elliptic integral of the first kind
$K(\ )$	complete elliptic integral of the second kind
P_i	induced power required
Q_x	flux of bound vortex ring at radius x
Q_y	flux of bound vortex ring at radius y
R	rotor radius
R_∞	ultimate wake radius
T	rotor thrust
V	flight-path velocity
V_x	induced velocity at nondimensional radius $x > 1$ in the rotor plane

V_y induced velocity at nondimensional radius $y < 1$ in the rotor plane

v mean induced velocity over rotor disk

x nondimensional radius at which wake vortex sheet leaves plane of rotor ($x > 1$, wake up)

y nondimensional radius at which wake vortex sheet leaves plane of rotor ($y < 1$, wake down)

z axial distance of wake element from plane of rotor

Γ circulation of bound vortex ring

λ_i nondimensional mean induced velocity $\left(\frac{v}{\sqrt{\frac{T}{2 \rho \pi R^2}}} \right)$

λ_z nondimensional flight-path velocity $\left(\frac{V}{\sqrt{\frac{T}{2 \rho \pi R^2}}} \right)$

ρ air density

ANALYSIS

A. Some Properties of a Vortex Ring

The velocity V_y induced by a vortex ring of unit radius and circulation Γ at a point lying in the plane of the ring and located at a radius $y < 1$ from the ring axis, as shown in figure 1, is

$$V_y = \frac{\Gamma \left[E(y) \right]}{\pi (1 - y^2)} \tag{1}$$

where $E(y)$ is the complete elliptic integral of the first kind.

The velocity V_x induced at a point in the ring plane having a radius $x > 1$, as shown in figure 2, is

$$V_x = \frac{\Gamma}{\pi x} \left[\frac{E\left(\frac{1}{x}\right)}{1 - \frac{1}{x^2}} - K\left(\frac{1}{x}\right) \right] \tag{2}$$

where $K\left(\frac{1}{x}\right)$ is the complete elliptic integral of the second kind.

The flux Q_y induced across the ring plane inside radius $y < 1$ by the ring circulation is

$$Q_y = 2\Gamma \left[K(y) - E(y) \right] \tag{3}$$

The flux Q_x induced across the ring plane outside radius $x > 1$ is

$$Q_x = 2x\Gamma \left[K\left(\frac{1}{x}\right) - E\left(\frac{1}{x}\right) \right] \tag{4}$$

B. Some Considerations as to the Nature of the Rotor Wake for Steady State, Axially Symmetric Flight.

The strength of the spiral vortex-filament shed from the tip of a rotor blade having uniform circulation along the radius is constant along the length of the filament and is equal to the circulation about the blade. Consequently, if each turn of the spiral be replaced by an equivalent vortex ring, it follows that the vortex strength of each vortex ring enclosing the wake is a constant value and equal to the strength of the corresponding turn of the equivalent spiral vortex-filament.

If the induced rotation be neglected, there are no additional turns of the vortex spiral created in the wake. This follows since the number of turns per second of the spiral wake-vortex-filament passing all planes cutting the wake at fixed distances from the rotor is constant and equal to the number of blades in the rotor times the revolutions per second of the rotor. It follows that, for the equivalent wake composed of a succession of vortex rings, the number of rings per second passing all cutting planes at fixed distances from the rotor is constant. If the vortex ring strength and spacing is small, the wake may be considered to be enclosed by a vortex sheet. Since both the strength of each vortex-ring-element composing the sheet and the number of rings per second passing any point in the wake has been shown to be constant along the wake, it follows for the wake vortex sheet of strength $\frac{d\Gamma}{dz}$ moving at an axial velocity $\frac{dz}{dt}$ that

$$\frac{d\Gamma}{dz} \cdot \frac{dz}{dt} = \frac{d\Gamma}{dt} = \text{a constant} \qquad (5)$$

where z is the distance measured from the rotor along the axis of the wake.

The wake-vortex-sheet strength must everywhere be equal to the difference in velocity between the inside and outside surfaces of the sheet.

C. Approximate Solutions for the Boundary Conditions that Determine the Strength of the Bound Vortex Ring.

In order to eliminate physically impossible, infinite velocities and pressure gradients it appears to be necessary to isolate the end of the wake-vortex-sheet at the periphery of the rotor from the flow field. The free edges of the vortex sheets in known steady-state flows all terminate in spirals. The assumption will therefore be made that the vortex sheet enclosing the wake unrolls from the periphery of the rotor in the form of a spiral as shown schematically in figure 1.

The flow induced at points outside the spiral by the vortex elements composing the spiral can be considered for mathematical purposes to be approximately equivalent to the flow induced by a bound-vortex-ring with circular axis located at the periphery of the rotor.

The strength Γ of the bound vortex ring and the radius, denoted by y in figure 1 and x in figure 2, at which the wake vortex sheet finally leaves the plane of the rotor may be approximately determined from the following two boundary considerations:

1. The wake vortex sheet strength at y is the difference in the velocities induced at points $y - \varepsilon$ just inside and $y + \varepsilon$ just outside of y by the wake vortex elements extending from y downstream to infinity since the velocity components arising from the freestream velocity and the bound vortex ring are continuous across the distance $y - \varepsilon$ to $y + \varepsilon$. If the wake vortex-ring-elements were uniformly distributed on the surface of a cylinder, the jump in velocity across the sheet at y

would be half the ultimate-wake sheet strength, as shown in reference 3. Under the present concept of the wake-vortex-sheet being continuous at y the required sheet strength at y would be half the ultimate-wake sheet strength. In an exact solution the value of the vortex sheet strength at y probably differs somewhat from the approximate value of half the ultimate-wake sheet strength. However, the approximate value appears to be sufficiently accurate for the present purposes of evaluating the bound-vortex-ring strength and will be so used.

It has been shown that the value of $\frac{d\Gamma}{dt}$ of the wake-vortex-sheet is constant along the wake. For a given thrust, T, and rotor radius, R, the value of $\frac{d\Gamma}{dt}$ is

$$\frac{d\Gamma}{dt} = \frac{T}{\rho \pi R^2} \tag{6}$$

from impulse considerations as shown in reference 4. If the freestream velocity be denoted by V, it follows from the equilibrium velocity of the ultimate-wake-vortex-sheet that for vertical ascent

$$\frac{d\Gamma}{dt} = \left(\frac{d\Gamma}{dz}\right)_\infty \left[V + \frac{1}{2}\left(\frac{d\Gamma}{dz}\right)_\infty\right] \tag{7}$$

where $\left(\frac{d\Gamma}{dz}\right)_\infty$ is the ultimate-wake sheet strength.

Thus

$$\left(\frac{d\Gamma}{dz}\right)_\infty = -V + \sqrt{V^2 + \frac{2T}{\rho \pi R^2}} \tag{8}$$

The wake-vortex-sheet velocity $\left(\frac{dz}{dt}\right)_y$ at y is then

$$\left(\frac{dz}{dt}\right)_y = \frac{\frac{d\Gamma}{dt}}{\left(\frac{d\Gamma}{dz}\right)_y} \approx \frac{\frac{d\Gamma}{dt}}{\frac{1}{2}\left(\frac{d\Gamma}{dz}\right)_\infty} \approx V + \sqrt{V^2 + \frac{2T}{\rho \pi R^2}} \quad (9)$$

and the induced velocity V_y at y is $\left(\frac{dz}{dt}\right)_y - V$ or

$$V_y \approx \sqrt{V^2 + \frac{2T}{\rho \pi R^2}} \approx V + \left(\frac{d\Gamma}{dz}\right)_\infty \quad (10)$$

Since the velocity induced at y by that portion of the wake extending from y to infinity is necessarily included in the line integral for the value of the circulation of the bound vortex ring, it follows that V_y as given by equation 10 is the approximate value of the velocity induced at y by the bound vortex-ring.

It is the author's opinion that air viscosity has only a minor effect on rotor thrust except for the flight conditions very close to the endpoint of the "windmill brake" state where the bound-vortex-ring strength approaches infinity. If the effects of viscosity be neglected the wake will extend down to infinity in the "vortex ring" or power-on vertical descent state and equation 10 may be used upon the substitution of $-V$ for V.

In the "windmill brake" state a similar derivation gives, for the ring velocity at the radius x, as shown in figure 2, the value

$$V_x = V - \left(\frac{d\Gamma}{dz}\right)_\infty \quad (11)$$

2. In order to determine an approximate value for the flux of the bound vortex-ring at radius y, consider again the properties of a uniform cylindrical wake. For such a wake all of the induced flow passing through the rotor originates in the upper quadrants and the flow in lower quadrants is of a ficticious nature as sketched in figure 3.

In the desired potential flow this ficticious flow in the lower quadrants must be eliminated. Consequently the induced flow outside the wake, when viewed from a very great distance from the wake, must correspond to the flow for a sink located at the position of the rotor and having a strength equal to the induced flow through the rotor. In such a potential flow approximately half of the induced flow originates below the plane of the sink. Since the cylindrical wake induces no flow across the plane of the rotor outside the rotor and all of the flow of the bound vortex ring crosses this plane, it follows that the ring flux Q_y at y, as in figure 1, or Q_x at x, as in figure 2, must be such as to induce approximately half the value of the induced flow at the plane of the rotor. Although taking the ring flux as half the induced flow across the rotor is only an approximation, it appears to be sufficiently accurate for present purposes and will be used. Since the values of the bound-vortex-ring-velocity, V_y, and flux, Q_y, at y, or V_x and Q_x at x may be determined, the value of the ring circulation Γ and the radius, y, or x at which the wake leaves the rotor, may be found from equations 1 and 3, or 2 and 4.

There remains the question of the nature of the flow within the vortex sheets of the assumed spiral enclosing the periphery of the rotor or the core of the equivalent bound-vortex-ring. As the spiral or core

radius is small compared to the rotor radius, the assumption will be made that the induced ring-core-flow is that of a two-dimensional vortex core where the velocity is proportional to the radius from the core axis which, in this paper, is assumed to be the periphery of the rotor. Although this assumption is probably sufficiently accurate for the present purpose of determining the mean induced velocity over the whole of the rotor, it could not be used to determine blade-tip loadings.

It may be noted that there will be a flow of fluid out of the spiral core which is not taken into account by the bound-vortex-ring analogy.

D. Equations for Induced Flow in Vertical Ascent and Power-On Vertical Descent.

Let the rotor radius and ultimate wake vortex sheet strength be unity in order to simplify the equations and let the geometry and notation be as shown in figure 1. Then, from impulse considerations as shown in reference 4, the rotor thrust, T , is

$$T = \rho \pi \frac{d\Gamma}{dt} \tag{12}$$

The ultimate wake sheet velocity $\left(\frac{dz}{dt}\right)_\infty$ is

$$\left(\frac{dz}{dt}\right)_\infty = V + \frac{1}{2}\left(\frac{d\Gamma}{dz}\right)_\infty = V + \frac{1}{2} \tag{13}$$

and the value of $\frac{d\Gamma}{dt}$, which has been shown to be constant along the wake, is

$$\frac{d\Gamma}{dt} = \left(\frac{d\Gamma}{dz}\right)_\infty \left(\frac{dz}{dt}\right)_\infty = V + \frac{1}{2} \tag{14}$$

or, from equation 12,

$$T = \rho \pi (V + \tfrac{1}{2}) \tag{15}$$

The thrust is also equal to the rate of change of momentum of the fluid in the ultimate wake. Thus

$$T = \rho \pi R_\infty^2 \left(\frac{d\Gamma}{dz}\right)_\infty \left[V + \left(\frac{d\Gamma}{dz}\right)_\infty\right] = \rho \pi R_\infty^2 (1 + V) \tag{16}$$

where R_∞ is the ultimate wake radius.

It follows from equations 15 and 16 that

$$R_\infty^2 = \frac{\frac{1}{2} + V}{1 + V} \tag{17}$$

Equating the values of the bound-vortex-ring-velocity at y given by equations 1 and 10

$$V_y = V + 1 = \frac{\Gamma \left[E(y)\right]}{\pi (1 - y^2)} \tag{18}$$

The sink flow at the rotor is equal to the flow in the ultimate wake minus πV. The ring flux, Q_y, at y from the second boundary condition is then half the sink flow at the rotor, or

$$Q_y = \frac{1}{2}\left[\pi R_\infty^2 (1 + V) - \pi V\right] \tag{19}$$

It follows from equations 3 and 17 that

$$Q_y = \frac{\pi}{4} = 2\Gamma\left[K(y) - E(y)\right] \tag{20}$$

For given values of V, equations 18 and 20 may be solved for the values of the bound-vortex-ring-circulation Γ and the radius y at which the wake vortex sheet leaves the plane of the rotor.

Define a nondimensional flight path velocity λ_z, taken positive for descent, as

$$\lambda_z = \pm \frac{V}{\sqrt{\frac{T}{2\rho\pi R^2}}} \tag{21}$$

Then, from equation 15,

$$\lambda_z = \frac{-2V}{\sqrt{1+2V}} \tag{22}$$

Define a nondimensional induced velocity λ_i as

$$\lambda_i = \frac{v}{\sqrt{\frac{T}{2\rho\pi R^2}}} \tag{23}$$

where v is the average induced velocity over the rotor.

Then following the previous approximation that the circular axis of the bound vortex ring coincides with the periphery of the rotor

$$v = \frac{\text{flow in ultimate wake} - \pi V + \text{induced flow within ring core}}{\pi} \tag{24}$$

It follows from the previously stated assumption for the induced "core" flow that for the ring of unit radius the

$$\text{induced ring-core-flow} \approx \frac{\pi}{2}(1 - y^2)\, v_y \tag{25}$$

Or by using equation 18 equation 23 becomes

$$\lambda_i = \frac{1 + (1 - y^2)(V + 1)}{\sqrt{1 + 2V}} \tag{26}$$

For comparison purposes the value of λ_i given by the simple momentum theory or that derived on the assumption of an uniform cylindrical wake vortex system is

$$\lambda_i = \frac{1}{\sqrt{1 + 2V}} \tag{27}$$

It is seen that the only difference arises from the bound-vortex-ring core flow.

The assumed "idealized" rotor has constant circulation along the blade radii and thus constant thrust loading over the rotor disk. Consequently the value of λ_i is a measure of the induced power required P_i since

$$P_i = T v = T\lambda_i \sqrt{\frac{T}{2\rho\pi R^2}} \tag{28}$$

at

$$V = -\lambda_z \sqrt{\frac{T}{2\rho\pi R^2}}$$

Table 1 gives the values of λ_i , y , and $\frac{\Gamma_{ring}}{\left(\frac{d\Gamma}{dz}\right)_\infty R}$ versus λ_z for the vertical ascent and power-on vertical-descent range. Values of $(\lambda_i)_{cylindrical\ wake}$ are included for comparison.

Figure 4 shows a comparison of the values of λ_i versus λ_z obtained from the present analysis with the experimental values given in reference 4 for the model rotor with 12 degrees negative twist in the blades and, consequently, nearly the constant circulation along the blade radii assumed in the present derivation. It is seen that the agreement is good although the theoretical values of λ_i do not cover the whole power-on vertical-descent range $0 < \lambda_z < 2$. One reason for this limitation is the approximations introduced in equations 9 and 19 by the present boundary conditions, namely, that the bound vortex ring flux is half the induced flow and that the wake sheet strength at the rotor is half the ultimate wake sheet strength.

E. Equations for Induced Flow in The Autorotative and Windmill-Brake Ranges of Vertical Descent.

Using the notation and geometry outlined in figure 2 and following the same order as in the previous section,

$$T = \rho \pi \frac{d\Gamma}{dt} = \rho \pi \left(V - \frac{1}{2}\right) \tag{29}$$

$$T = \rho \pi R_\infty^2 (V - 1) \tag{30}$$

$$R_\infty^2 = \frac{V - \frac{1}{2}}{V - 1} \tag{31}$$

The bound-vortex-ring velocity at x, from equations 2 and 11, is

$$V_x = V - 1 = \frac{\Gamma}{\pi x}\left[\frac{E\left(\frac{1}{x}\right)}{1-\frac{1}{x^2}} - K\left(\frac{1}{x}\right)\right] \qquad (32)$$

Noting that the ring flux at radius x is the same as that passing through the rotor and down the wake, it follows from the second boundary condition and equation 4 that

$$Q_x = \frac{1}{2}\left[\pi V - \pi R_\infty^2 (V-1)\right] = \frac{\pi}{4} = 2\Gamma x\left[K\left(\frac{1}{x}\right) - E\left(\frac{1}{x}\right)\right] \qquad (33)$$

The values of x and Γ at given values of V may thus be determined from equations 32 and 33.

The value of λ_z for the windmill-brake state is

$$\lambda_z = \frac{2V}{\sqrt{2V-1}} \qquad (34)$$

In setting up the expression for λ_i for this case, the approximation will be made that all of the bound-vortex-ring core-flow passing through the annulus $\pi(x^2-1)$ is returned through the rotor although, in the actual case, a part of this fluid would pass downstream. It follows that

$$v = \frac{\pi V - \text{flow in ultimate wake} + \pi V(x^2-1) + \text{induced core flow}}{\pi} \qquad (35)$$

or, from equation 32,

$$\lambda_i = \frac{1 + (3V - 1)(x^2 - 1)}{\sqrt{2V - 1}} \qquad (36)$$

The value of λ_i for this flight condition given by the simple momentum theory or the assumption of a cylindrical wake is

$$(\lambda_i)_{CYL.} = \frac{1}{\sqrt{2V - 1}} \qquad (37)$$

Table 2 gives the values of λ_i , $1/x$ and $\Gamma_{ring} \Big/ \left(\frac{d\Gamma}{dz}\right)_{\infty} R$ versus λ_z for the autorotative and windmill brake states. Values of $(\lambda_i)_{\text{cylindrical wake}}$ are again included for comparison.

Plots of the calculated values are shown in figure 4 along with the experimental points from reference 2 for the model rotor with twelve degrees negative thrust.

It is seen from figure 4 that the present relations furnish the values of λ_i and thus the induced power over the autorotation flight-range.

The progressively larger disagreement at the higher rates of descent in the windmill brake state between the experimental points from reference 2 and the theoretical value of λ_i is probably a result of the neglect of the inboard blade-element stall in the computations for the experimentally determined values of λ_i .

As a check on the equations, the approximate wake-vortex-distribution and consequent velocity distribution across the rotor were computed for the point $\lambda_z = 2.02$, $\lambda_i = 1.99$, or approximately the point for "ideal" autorotation or zero net flow through the rotor. The results obtained from a first numerical iteration starting with the theoretical values of R_∞, Γ_{ring} and a cylindrical wake are shown in figure 5. As can be seen

from the figure, the first iteration gives good results since the error of closure at x is 1.5 per cent of x. Further iterations diverge possibly on account of the necessary neglect of the flow from the spiral core and the approximate nature of the boundary conditions.

F. Effects of Bound Vortex Ring on the Efficiency of Rotors with Blades Whose Circulation Increases Towards the Tips.

The previous derivations for the values of λ_i and thus the induced power required are based upon the assumption that the rotor has constant circulation along the blade radii. Although it is impossible to obtain a constant circulation along the radii in practice, rotor blades having negative twists of the order of eight to twelve degrees have circulation distributions in hovering and vertical descent which approach the assumed constant value. Consequently, for the flight range from hovering to autorotation, the theoretical results of the present investigation should be applicable to such rotors. Rotors which have untwisted blades and thus values of the blade circulation which are increasing towards the blade tip are less efficient in hovering and vertical ascent than rotors having blades with negative twist and thus more nearly constant blade circulation. The reason for this is well known and easily explained on the basis of the increased kinetic energy in the wake. However, the experimental results of reference 2 show that the rotor with constant-chord, untwisted blades is more efficient at autorotation and the larger rates of power-on descent than the rotor having blades with twelve degrees of negative twist. This seeming paradox may be qualitatively accounted for as follows:

Consider two otherwise identical rotors operating at the same angular and freestream velocities, one having a constant circulation Γ along the blade radii and the other having the same circulation Γ from $r = 0$ to $r = y$ but increasing from Γ at $r = y$ to $\Gamma + \Delta\Gamma$ at $r = R$. The former rotor will shed a vortex filament of strength Γ at the blade tip and the latter rotor will shed a vortex sheet of total strength $-\Delta\Gamma$ from the portion of the trailing edge extending from $r = y$ to $r = R$ and a vortex filament of strength $\Gamma + \Delta\Gamma$ from the blade tip. The vortex sheet shed from the tip-trailing-edge sections of the blades of the latter rotor lies within the closed streamlines of the bound vortex ring. As a consequence the sheet of strength $-\Delta\Gamma$ is rolled up with the tip-vortex filament of strength $\Gamma + \Delta\Gamma$ and the resultant-emitted-wake-vortex sheet has the same strength as that of the former rotor. The ultimate-wake sheet strengths of the two rotors are therefore identical although the rotor with the non-uniform radial blade-circulation distribution has the higher thrust and thus efficiency. This favorable effect of the bound vortex ring on the efficiency of a rotor having blades whose circulation increases towards the tips is small in hovering and negligible at the larger rates of vertical ascent where the bound-vortex-ring strength is low and $y \approx R$ but becomes important at the larger rates of power-on descent or at autorotative vertical descent where the bound-vortex-ring strength is high and y is considerably less than R.

It does not appear that quantitative results can be obtained for rotors with non-uniform blade circulation by the present approach.

CONCLUSIONS

1. The vortex-ring type of flow which has been observed to enclose the periphery of a propeller operating in the static-thrust condition or a lifting rotor in hovering or power-on vertical descent is shown to be a necessary part of the wake vortex system. Approximate relations are presented for the required equilibrium strength of the bound-vortex-ring for rotors having constant circulation along the blade radii.

2. The results of the present investigation indicate that the simple momentum theory, or vortex theory based upon the assumption of a cylindrical wake, underestimates the mean-axial-induced-velocity and induced power required over the whole vertical-flight range. The increase in induced power required, as furnished by the present analysis, is a function of the relative loading or value of $\frac{\Delta p}{q}$ at the rotor. It is negligible for the lightly-loaded propeller or windmill, but amounts to about ten per cent at static thrust or hovering and increases to a maximum at the endpoint of the windmill brake state. The increase in induced power near the latter point over that given by previous theory has the effect of placing the vertical-autorotation-flight-range within what is normally considered the windmill brake state and thus furnishes the previously missing theoretical solution for the induced flow at autorotation for the rotor with constant circulation along the blade radii.

3. Although the present investigation was limited to a consideration of rotors with blades having a constant circulation along the radii, a comparison of the calculated values of the nondimensional-mean-induced-velocity with the experimental values given in reference 2 indicates that

the results are applicable to conventional rotors having blades with negative twist of the order of twelve degrees.

REFERENCES

1. Glauert, E: The Analysis of Experimental Results in the Windmill Brake and Vortex Ring States of an Airscrew. R and M No. 1026, British A.R.C., 1926.

2. Castles, Walter, Jr., and Gray, Robin B.: Empirical Relation Between Induced Velocity, Thrust, and Rate of Descent of a Helicopter Rotor as Determined by Wind-tunnel Tests On Four Model Rotors. NACA TN 2474, 1951.

3. Knight, Montgomery, and Hefner, Ralph A.: Static Thrust Analysis of the Lifting Airscrew. NACA TN 626, 1937.

4. Karman, Th. von, and Burgers, J. M.: General Aerodynamic Theory - Perfect Fluids. Mathematical Foundation of the Theory of Wings with Finite Span. Vol. II of Aerodynamic Theory, div. E, ch. III, sec. 3, W. F. Durand, ed., Julius Springer (Berlin), 1935, pp 103-106.

TABLE I

CALCULATED VALUES OF THE NONDIMENSIONAL INDUCED VELOCITY, WAKE RADIUS AT ROTOR, AND BOUND VORTEX RING STRENGTH FOR VERTICAL ASCENT, POWER-ON VERTICAL DESCENT, AND WINDMILL BRAKE STATE (AUTOROTATION POINTS)

A. VERTICAL ASCENT (PROPELLER STATE)

λ_z	λ_i	$(\lambda_i)_{cylindrical}$	γ	$\frac{\Gamma_{ring}}{\left(\frac{d\Gamma}{dz}\right)_\infty R}$
0.000	1.09	1.00	0.954	0.257
-0.146	1.01	0.93	0.960	0.244
-0.287	0.94	0.87	0.965	0.233
-0.456	0.86	0.80	0.970	0.222
-0.646	0.78	0.73	0.975	0.210
-0.886	0.69	0.65	0.980	0.198
-1.205	0.60	0.57	0.985	0.185
-1.663	0.49	0.47	0.990	0.168
-2.573	0.36	0.34	0.995	0.144
-3.40	0.28	0.27	0.997	0.130
-4.22	0.24	0.23	0.998	0.118

TABLE I. - Continued

CALCULATED VALUES OF THE NONDIMENSIONAL INDUCED VELOCITY, WAKE RADIUS AT ROTOR, AND BOUND VORTEX RING STRENGTH FOR VERTICAL ASCENT, POWER-ON VERTICAL DESCENT, AND WINDMILL BRAKE STATE (AUTOROTATION POINTS)

B. POWER-ON VERTICAL DESCENT (VORTEX RING STATE)

λ_z	λ_i	$(\lambda_i)_{cylindrical}$	η	$\frac{\Gamma_{ring}}{\left(\frac{d\Gamma}{dz}\right)_{\infty} R}$
0.000	1.09	1.00	0.954	0.257
0.317	1.29	1.17	0.940	0.283
0.501	1.42	1.28	0.930	0.302
0.677	1.56	1.39	0.920	0.318
0.822	1.68	1.49	0.910	0.337
0.976	1.81	1.60	0.900	0.354
1.221	2.05	1.78	0.880	0.390
1.475	2.32	1.98	0.850	0.446
1.578	2.48	2.06	0.820	0.505
1.597	2.52	2.08	0.810	0.525
- - -	- - -	- - -	- - -	- - -
1.590	2.53		0.800	
1.531	2.52		0.780	

Note: Last two values are included to show limit imposed by present equations.

TABLE I. - Concluded

CALCULATED VALUES OF THE NONDIMENSIONAL INDUCED VELOCITY, WAKE RADIUS AT ROTOR, AND BOUND VORTEX RING STRENGTH FOR VERTICAL ASCENT, POWER-ON VERTICAL DESCENT, AND WINDMILL BRAKE STATE (AUTOROTATION POINTS)

C. AUTOROTATIVE AND WINDMILL BRAKE STATE

λ_z	λ_i	$(\lambda_i)_{cylindrical}$	$\frac{1}{\chi}$	$\frac{\Gamma_{ring}}{\left(\frac{d\Gamma}{dz}\right)_\infty R}$
2.000	∞	1.00	0.00	∞
2.000	49.10	0.99	0.20	2.47
2.000	11.60	0.98	0.40	1.17
2.004	4.61	0.94	0.60	0.71
2.009	3.10	0.91	0.70	0.56
2.013	2.55	0.89	0.75	0.50
2.022	2.08	0.86	0.80	0.44
2.037	1.68	0.82	0.85	0.38
2.080	1.31	0.76	0.90	0.32
2.178	0.94	0.65	0.95	0.25
2.480	0.63	0.51	0.98	0.19
2.880	0.48	0.40	0.99	0.17
∞	0.00	0.00	1.00	0.00

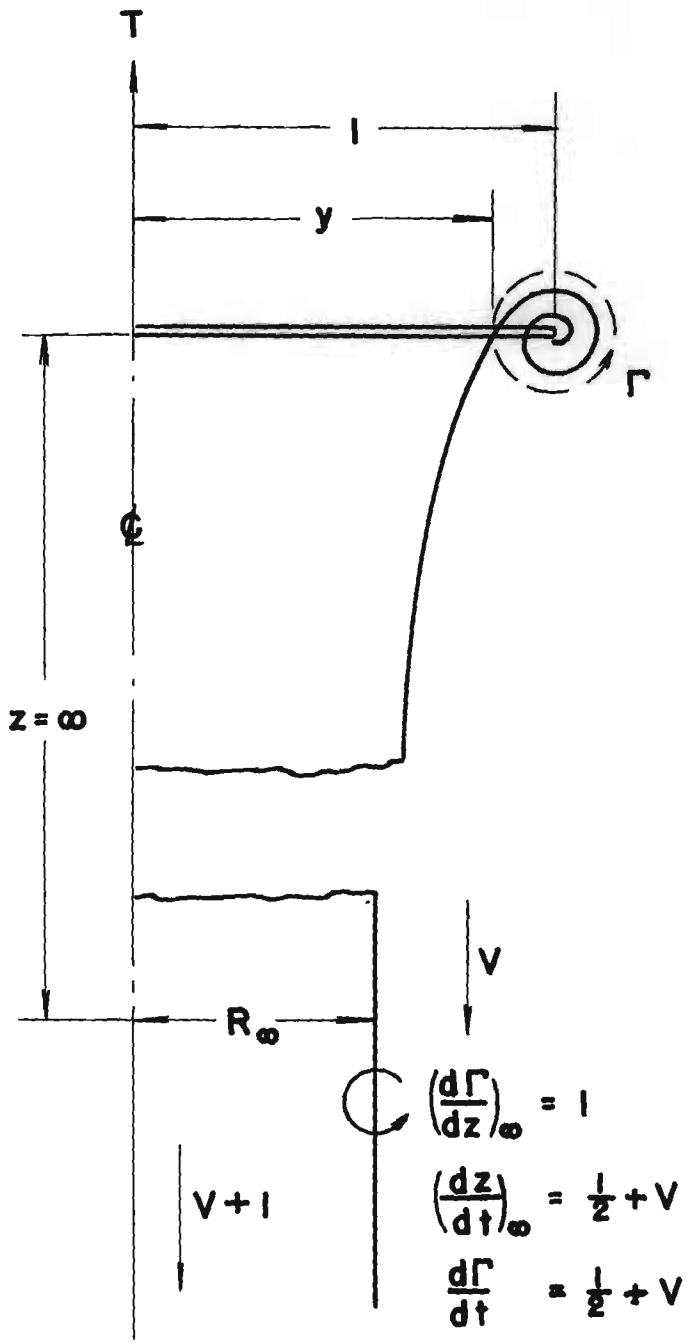

Figure 1. Geometry and Notation for Vertical Ascent, and Power-on Vertical Descent.

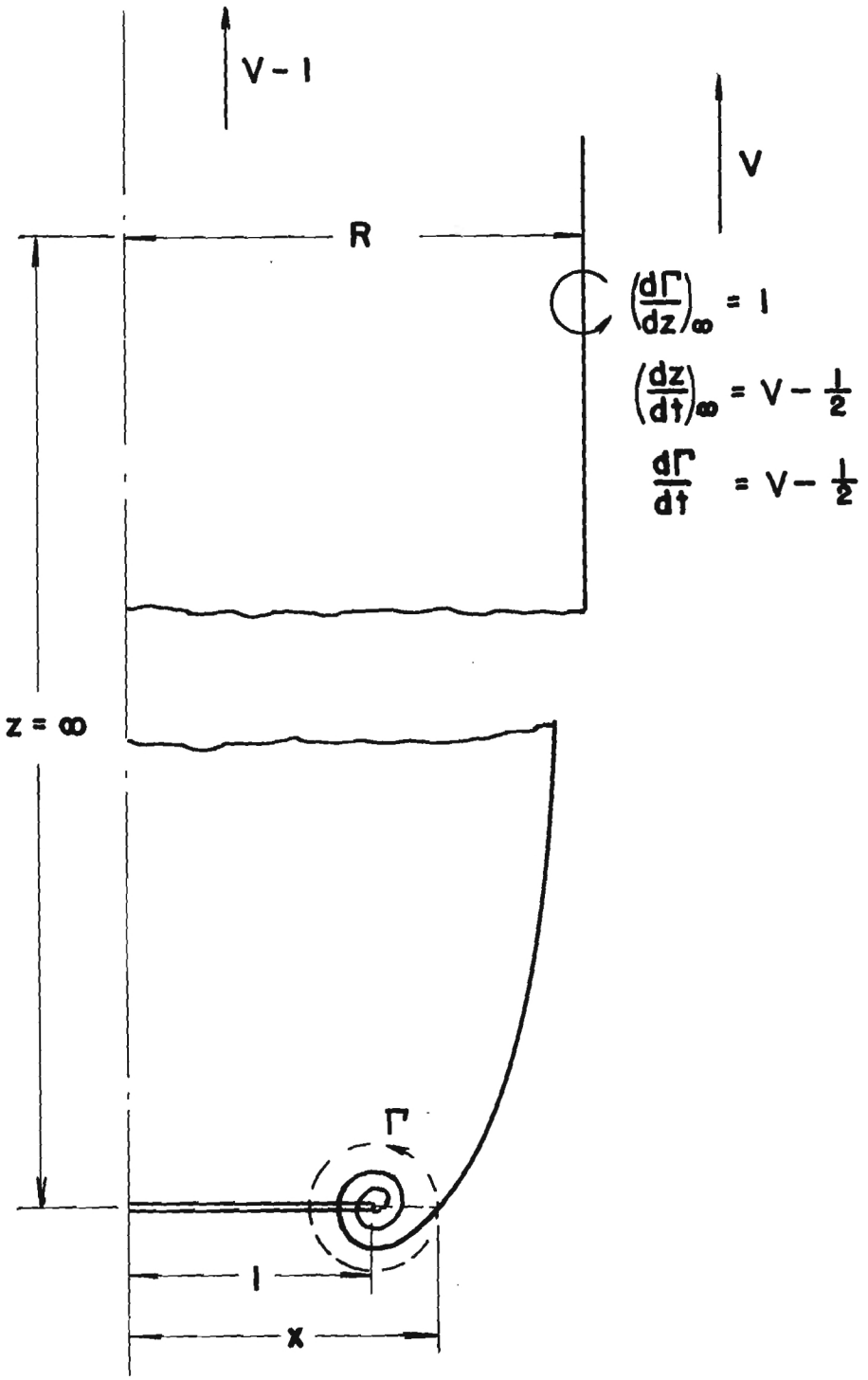

Figure 2. Geometry and Notation for Windmill Brake State.

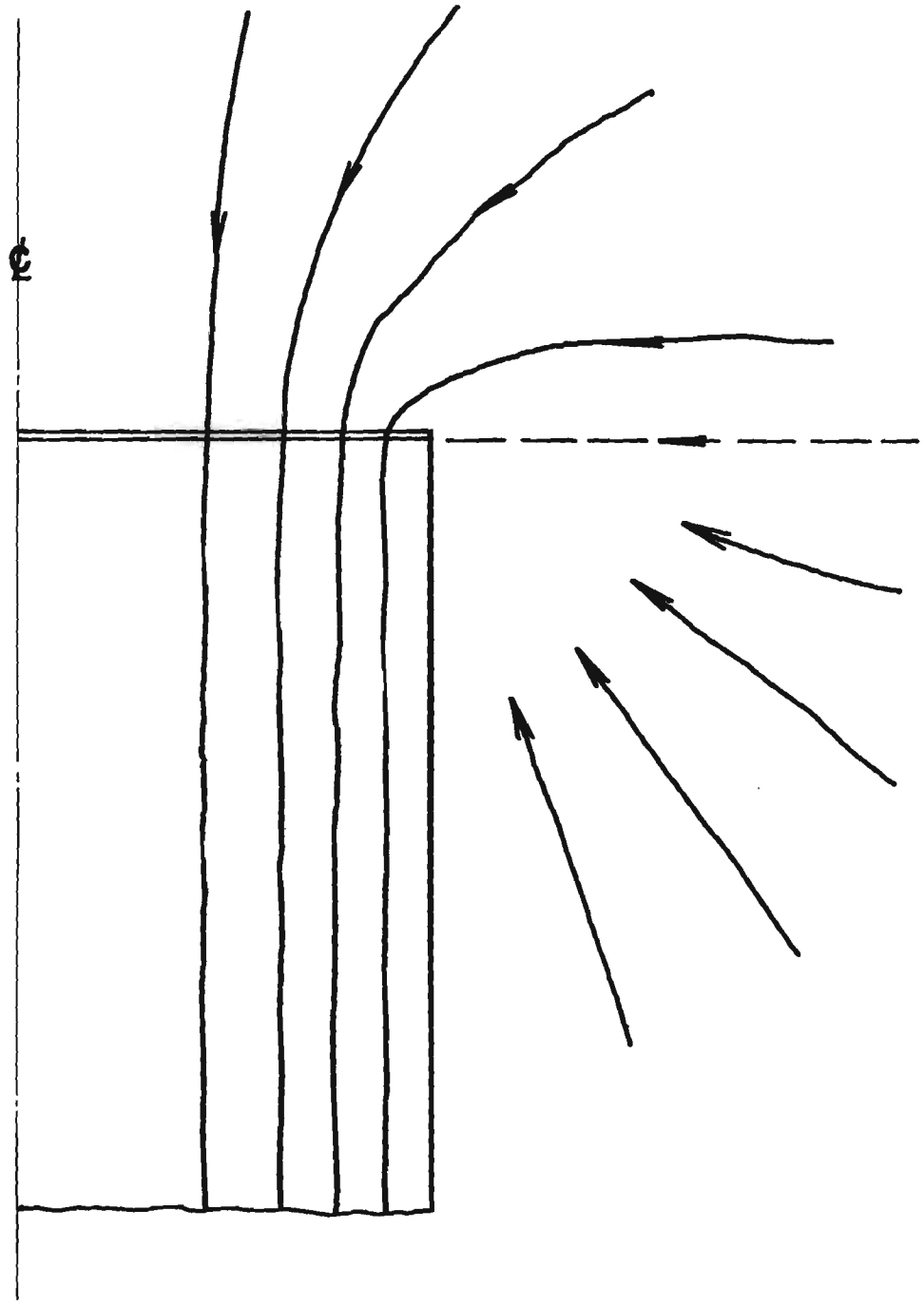

Figure 3. Schematic Induced Flow for Cylindrical Wake.

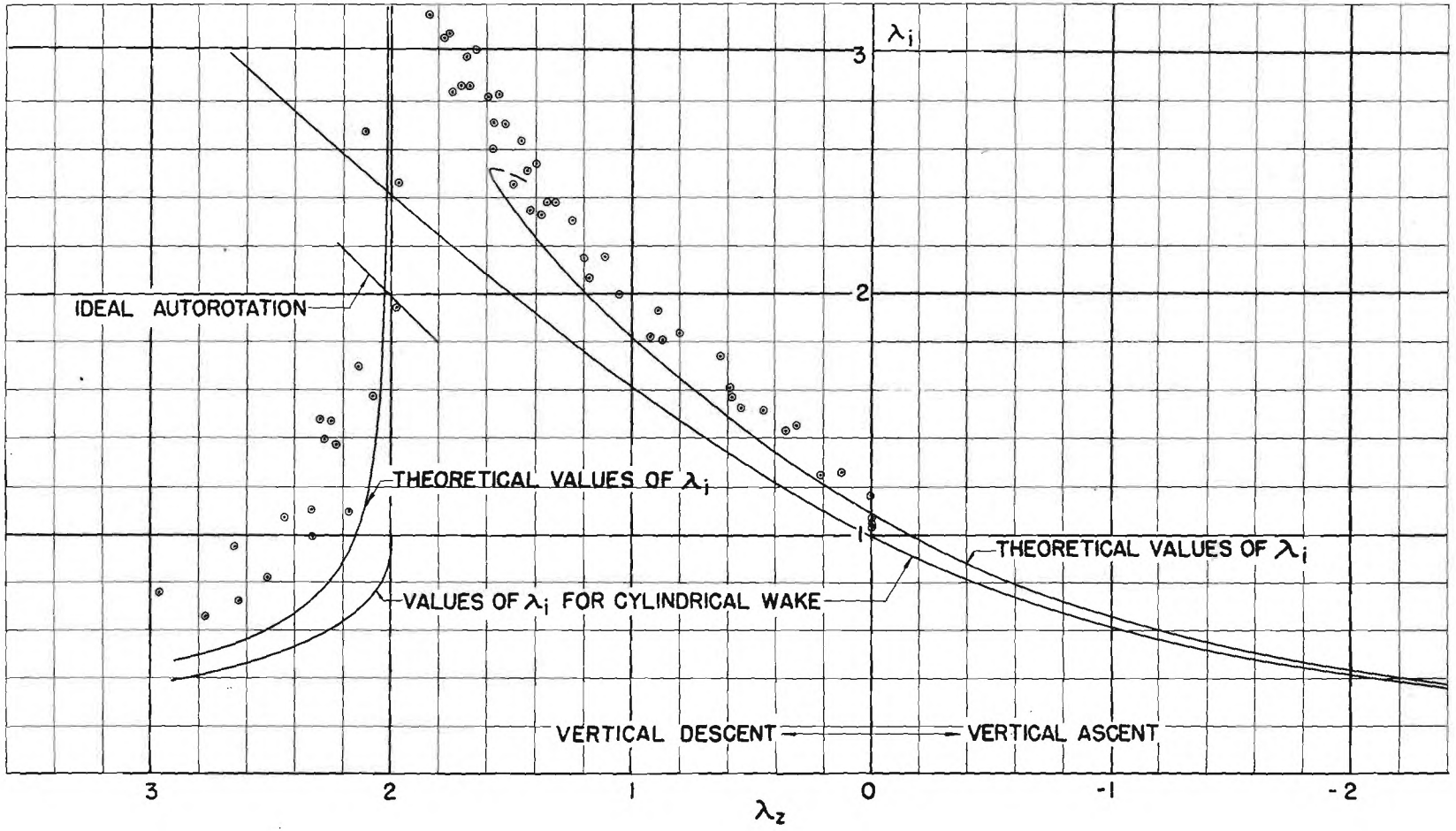

Figure 4. Comparison of Theoretical Values of λ_i with Experimental Points from Reference 2.

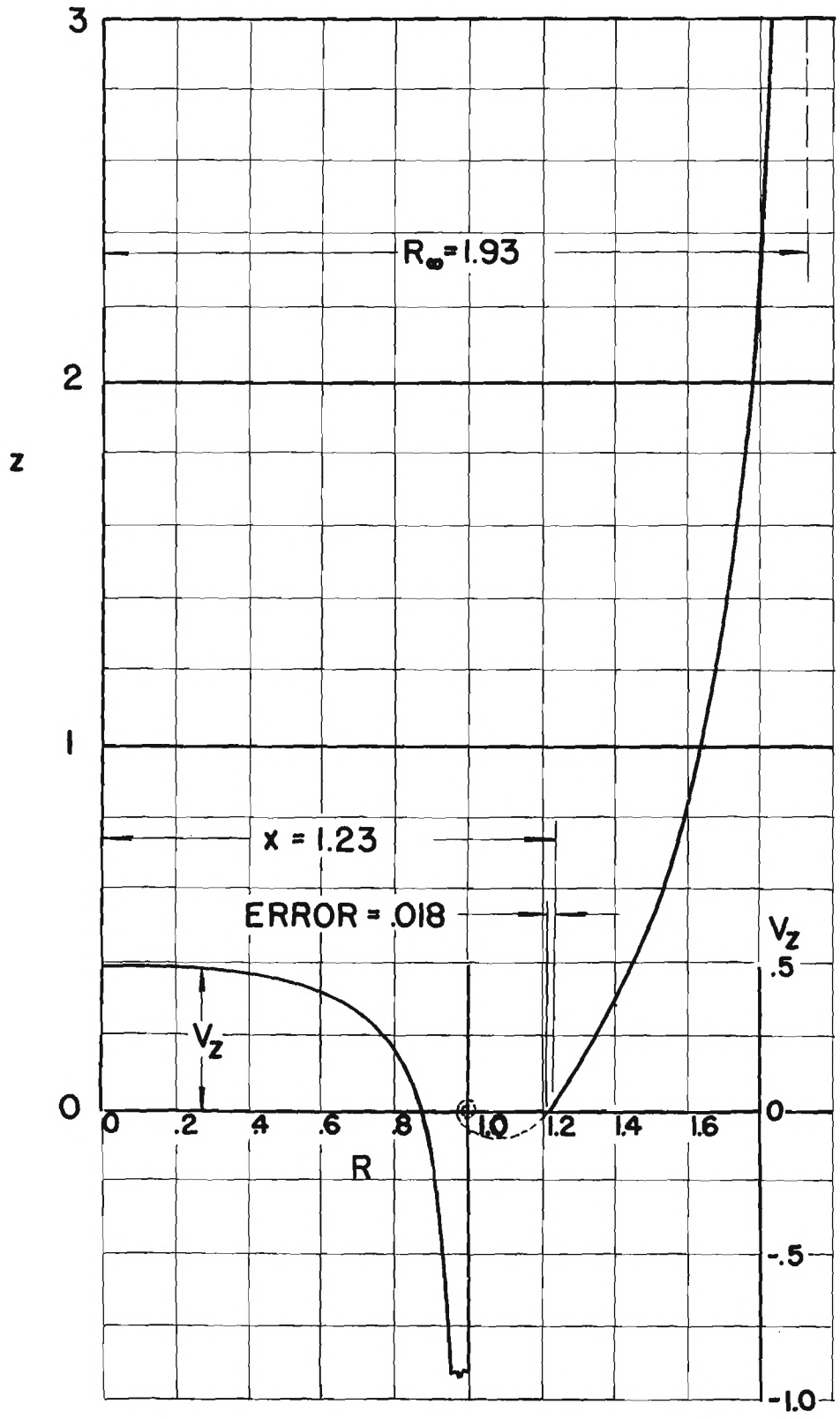

Figure 5. Approximate Wake Shape and Velocity Distribution for Autorotation ($\lambda_i = \lambda_z = 2.02$).

ENGINEERING EXPERIMENT STATION
of the Georgia Institute of Technology
Atlanta, Georgia

REVISED FINAL REPORT - PART A

PROJECT NO. 218

A NOTE ON THE FLOW BY A LIFTING ROTOR IN VERTICAL DESCENT

By

WALTER CASTLES, JR.
Daniel Guggenheim School of Aeronautics

o - o - o - o - o - o - o - o - o - o

CONTRACT NO. Naw-6230

NATIONAL ADVISORY COMMITTEE FOR AERONAUTICS

o - o - o - o - o - o - o - o - o - o

MAY, 1955

ENGINEERING EXPERIMENT STATION
of the Georgia Institute of Technology
Atlanta, Georgia

REVISED FINAL REPORT - PART A

PROJECT NO. 218

A NOTE ON THE FLOW BY A LIFTING ROTOR IN VERTICAL DESCENT

By

WALTER CASTLES, JR.
Daniel Guggenheim School of Aeronautics

o - o - o - o - o - o - o - o - o - o

CONTRACT NO. Naw-6230

NATIONAL ADVISORY COMMITTEE FOR AERONAUTICS

o - o - o - o - o - o - o - o - o - o

MAY, 1955

A NOTE ON THE FLOW INDUCED BY A LIFTING ROTOR IN VERTICAL DESCENT

Prepared by [redacted]
Walter Castles, Jr., Assoc. Prof.
Daniel Guggenheim School of
Aeronautics

Approved by [redacted]
Thomas W. Jackson, Head
Mechanical Sciences Division

Released by [redacted]
Paul K. Calaway, Director
Engineering Experiment Station

May, 1955

TABLE OF CONTENTS

A NOTE ON THE FLOW INDUCED BY A LIFTING ROTOR IN VERTICAL DESCENT

By Walter Castles, Jr.

SUMMARY

Approximate equations are derived for the mean induced velocity of a lifting rotor with uniform loading operating in the vertical descent flight range. The equations, which are based upon certain assumptions as to the type and progression of the flow patterns, yield results which are in general agreement with the available experimental data.

INTRODUCTION

The theoretical determination of the relation between the mean induced velocity, the freestream velocity, and the disk loading for a lifting rotor operating in the vertical descent flight range presents certain difficulties because of the lack of sufficient experimental evidence as to the nature of the flow patterns. Furthermore, the flow patterns have certain turbulent mixing regions where the familiar perfect fluid relations cannot be applied.

The present report is an attempt to devise a logical progression of flow patterns for the vertical descent flight range which are in accord with the available experimental flow studies and to derive the approximate theoretical relation between the thrust, freestream velocity, and average induced velocity for each flow pattern.

The derivation of useful equations for the case of the rotor with uniform loading is a necessary preliminary step before the working hypothesis of the "independence of blade elements" can be correctly applied to obtain the blade loadings for rotors with arbitrary geometry.

NOTATION

k_1 k_2	parameters
p_o	freestream static pressure
p_1	static pressure on upper surface of rotor
p_2	static pressure on lower surface of rotor
v	mean induced velocity at rotor
R	rotor radius
T	rotor thrust
V	freestream velocity (descent velocity)
V_w	wake velocity
ρ	air density
λ_i	nondimensional induced velocity
λ_z	nondimensional descent velocity

ANALYSIS

A. The power-unstable range of power-on vertical descent

For this flight range the smoke flow studies of reference 1 indicate that a developed wake extends an appreciable distance below the rotor and the smoke flow studies of reference 2 indicate that the segment of wake ends in a stagnation region. The fluid that constituted the wake undergoes turbulent mixing with the adjacent freestream fluid in the stagnation region with the result that the wake boundaries are spread, the strength of the original vortex sheet enclosing the wake is degraded, and the wake fluid and vorticity are folded back in the form of a secondary wake boundary around the region occupied by the rotor and carried downstream (i.e. above the rotor) by the freestream flow. The flow pattern is as shown schematically in figure 1.

The static pressure in the stagnation region at the end of the wake and in the cross section of wake just above the stagnation region is necessarily of the order of the freestream total head for the present flow pattern where the freestream velocity V is less than the counter directed wake velocity V_w.

If the secondary wake boundaries be assumed to extend downstream to infinity, and to approach parallelism, the velocity in the ultimate sections of the secondary wake above the rotor must be of the order of zero. This follows since an upward velocity would not satisfy the necessary continuity with the flow through the rotor and, conversely, a downward velocity would result in a rate of change of momentum of the wake fluid in a direction such that the rotor thrust would be negative.

The static pressure a large distance above the rotor and inside the secondary wake boundaries will be of the order of the freestream static pressure

p_o .

It appears to be a reasonable assumption that the effects of viscosity can be neglected for the central region inside the secondary wake boundary and for the limited region inside the primary wake and above the stagnation region or turbulent mixing region at the end of the primary wake. Thus, writing Bernoulli's equation along an entering streamline from point 1 a large distance above the rotor to point 2 on the upper surface of the rotor (see fig. 1)

$$p_o = p_1 + \frac{1}{2} \rho (v - V)^2 \qquad (1)$$

where v = mean induced velocity at rotor

V = freestream (descent) velocity

Similarly, for point 3 on the lower surface of the rotor and point 4 at the end of the primary wake where the static pressure is approximately $p_o + \frac{1}{2} \rho V^2$

$$p_2 + \frac{1}{2} \rho (v - V)^2 = p_o + \frac{1}{2} \rho V^2 + \frac{1}{2} \rho V_w^2 \qquad (2)$$

where V_w = velocity at end of primary wake

The average pressure difference $p_2 - p_1$ across the plane of the rotor is then of the order of

$$p_2 - p_1 = \frac{T}{\pi R^2} = \frac{1}{2} \rho (V^2 + V_w^2) \qquad (3)$$

or

$$V_w = \sqrt{\frac{2T}{\rho \pi R^2} - V^2} \qquad (4)$$

The type of flow pattern under consideration (fig. 1) can only exist when $V_w > V$ since, if the freestream velocity predominates, the stagnation region moves up to the lower surface of the rotor and the primary wake extending from the plane of the rotor to the stagnation region no longer exists. The range for the power-unstable flow pattern is thus

$$0 \leqq V \leqq \sqrt{\frac{T}{\rho \pi R^2}} \tag{5}$$

or, in nondimensional form obtained by dividing through by $\sqrt{\frac{T}{2\rho\pi R^2}}$

$$0 \leqq \lambda_z \leqq \sqrt{2} \tag{6}$$

where

$$\lambda_z = \sqrt{\frac{V}{\frac{T}{2\rho\pi R^2}}}$$

Although the usual momentum relations cannot be applied to the present type of flow pattern since the ultimate secondary wake diameter is, in a sense, indeterminate, (i.e., using difference in momentum transfer across control surfaces) it appears from the principle of the conservation of momentum that the rotor thrust can be no less than the rate of transfer of momentum across final sections of the primary wake (although it could be slightly greater if there exists some conversion of the excess energy of the flow at the end of the primary wake into additional momentum). Thus

$$T = \rho\pi R^2 \left(v - V \right) V_w \tag{7}$$

or from equation 4, the rotor thrust T is

$$T = \rho\pi R^2 \left(v - V \right) \left[v - V + \sqrt{v^2 - 2Vv} \right] \tag{8}$$

Solving for the mean induced velocity v

$$v = V + \frac{\frac{T}{2\rho\pi R^2}}{\sqrt{\frac{T}{2\rho\pi R^2} - \left(\frac{V}{2}\right)^2}} \tag{9}$$

Reducing equation 9 to nondimensional form

$$\lambda_i = \lambda_z + \sqrt{\frac{1}{1 - \left(\frac{\lambda_z}{2}\right)^2}} \qquad \text{for} \quad 0 \leq \lambda_z \leq \sqrt{2} \tag{10}$$

where

$$\lambda_i = \frac{v}{\sqrt{\frac{T}{2\rho\pi R^2}}}$$

It will be noted that λ_i increases faster than λ_z over the whole range and thus the rotor will be power unstable (i.e. engine power required will increase with rate of steady descent) since, for the assumed rotor with uniform loading, the induced power is proportional to λ_i and the rate of decrease of potential energy is proportional to λ_z .

B. The power-stable range of power-on vertical descent

When the freestream velocity V (descent velocity) is increased to the value it equals the wake velocity V_w (fig. 1) the stagnation region moves up

to the lower surface of the rotor and the flow pattern is as shown in figure 2. At this descent velocity ($V = \sqrt{\frac{T}{\rho \pi R^2}}$) the static pressure within the wake a large distance above the rotor is of the order of p_o . As the rate of descent increases it appears that the ultimate wake static pressure must decrease below p_o (i.e. the wake must have a finite expansion angle) in order to approach the condition at the autorotation point where $\lambda_i = \lambda_z$. Writing the static pressure within the wake a large distance above the rotor as

$$p = p_o - \frac{1}{2} \rho k_1 V^2 \tag{11}$$

and using Bernoulli's equation to find the static pressure p_1 at the upper surface of the rotor disk

$$p_1 = p_o - \frac{1}{2} \rho k_1 V^2 - \frac{1}{2} \rho (v - V)^2 \tag{12}$$

It will be noted that the flow pattern is completely determined by specifying a value for λ_z . Thus k_1 is some function of λ_z .

The static pressure p_2 at the lower surface of the rotor is approximately equal to freestream stagnation pressure $p_o + \frac{1}{2} \rho V^2$. Thus

$$T = \pi R^2 (p_2 - p_1) = \frac{1}{2} \rho \pi R^2 \left[(1 + k_1) V^2 + (v - V)^2 \right]$$

or

$$T = \frac{1}{2} \rho \pi R^2 \left[v^2 - 2 Vv + (2 + k_1) V^2 \right] \tag{13}$$

Solving for the mean induced velocity v

$$v = V + \sqrt{\frac{2T}{\rho\pi R^2} - (1 + k_1) V^2} \tag{14}$$

or in nondimensional form

$$\lambda_i = \lambda_z + \sqrt{4 - (1 + k_1) \lambda_z^2} \tag{15}$$

The form of the relation for $k_1 = f(\lambda_z)$ remains to be determined, but $k_1 = 0$ at $\lambda_z = \sqrt{2}$ since at this value of λ_z the wake static pressure is p_o from section A.

The range of the power-stable vertical descent flow pattern is from $V = \sqrt{\frac{T}{\rho\pi R^2}}$ to $V = v$ since the stagnation region just below the plane of the rotor will disappear as soon as there is any upflow through the rotor disk.

C. The power-off range of vertical descent

The static pressure on the upper surface of the rotor for this flight range must be identical with that for the familiar windmill brake state at $v = \frac{1}{2} V$ or $\lambda_z = 2$, the endpoint of the windmill brake state. Also the wake must be identical with that of the power-stable range of power-on descent at the ideal autorotation point or value of V at which $v = V$. It follows that the static pressure on the upper surface of the rotor must vary from $p_o - \frac{1}{2} \rho k_1 V^2$ at the ideal autorotation point to $p_o - \frac{1}{2} \rho (V - v)^2$ at the endpoint of the windmill brake state.

The equality of k_1 and k_2 at the ideal autorotation point follows from the theory of the drag of bluff bodies (i.e. free streamline flow) which indicates that, for points near ideal autorotation where the upflow through the rotor is very small, the static pressure within the wake should be very

nearly constant and considerably below p_o (see reference 3). The flow pattern is therefore taken to be of the type shown in figure 3. The static pressure on the upper surface of the rotor can then be taken as

$$p_1 = p_o - \frac{1}{2} \rho k_2 V^2 \tag{16}$$

Using Bernoulli's equation to determine the static pressure on the lower surface of the rotor gives

$$p_2 = p_o + \frac{1}{2} \rho V^2 - \frac{1}{2} \rho (V - v)^2 \tag{17}$$

or finally

$$T = \pi R^2 (p_2 - p_1) = \frac{1}{2} \rho \pi R^2 \left[(1 + k_2) V^2 - (V - v)^2 \right] \tag{18}$$

or

$$V - v = \sqrt{(1 + k_2) V^2 - \frac{2T}{\rho \pi R^2}} \tag{19}$$

Solving for the mean induced velocity v gives

$$v = V - \sqrt{(1 + k_2) V^2 - \frac{2T}{\rho \pi R^2}} \tag{20}$$

for

$$v \leq V \leq \sqrt{\frac{2T}{\rho \pi R^2}}$$

or in nondimensional form

$$\lambda_i = \lambda_z - \sqrt{(1 + k_2) \lambda_z^2 - 4} \tag{21}$$

$$k_1 = f(\lambda_z) = \frac{c_1}{\lambda_z^2} \tag{26}$$

At the endpoint of the power-unstable range ($\lambda_z = \sqrt{2}$), the value of the wake static pressure is p_o . Thus at this point $k_1 = 0$ from section B. Thus c_1 can be written as $c_1 = \lambda_z^2 - 2$ and

$$k_1 = f(\lambda_z) = \frac{\lambda_z^2 - 2}{\lambda_z^2} \tag{27}$$

or from equation 24

$$k_1 = \frac{\lambda_z^2 - 2}{\lambda_z^2} = 1 - \frac{T}{\rho\pi R^2 V^2} \tag{28}$$

E. Resumé of equations for a rotor with uniform loading in vertical flight

(Note: Let V and λ_z be negative for vertical ascent by definition).

1. For vertical ascent ($0 \geq \lambda_z \geq -\infty$)

$$T = 2\rho\pi R^2 v (v - V) \tag{29}$$

$$v = \frac{V}{2} + \sqrt{\left(\frac{V}{2}\right)^2 + \frac{T}{2\rho\pi R^2}} \tag{30}$$

$$\lambda_i = \frac{\lambda_z}{2} + \sqrt{\left(\frac{\lambda_z}{2}\right)^2 + 1} \tag{31}$$

2. For the power-unstable range of power-on vertical descent ($0 \leq \lambda_z < \sqrt{2}$

$$T = \rho\pi R^2 \left(v - V \right) \left[v - V + \sqrt{v^2 - 2 V v} \right] \tag{32}$$

$$v = V + \sqrt{\frac{\frac{T}{2\rho\pi R^2}}{\frac{T}{2\rho\pi R^2} - \left(\frac{V}{2}\right)^2}} \tag{33}$$

$$\lambda_i = \lambda_z + \sqrt{\frac{1}{1 - \left(\frac{\lambda_z}{2}\right)^2}} \tag{34}$$

3. For the power-stable range of power-on vertical descent ($\sqrt{2} \leq \lambda_z \leq \sqrt{3}$)

$$T = \frac{1}{3} \rho\pi R^2 \left(v^2 - 2 v V + 3 V^2 \right) \tag{35}$$

$$v = V + \sqrt{\frac{3T}{\rho\pi R^2} - 2 V^2} \tag{36}$$

$$\lambda_i = \lambda_z + \sqrt{6 - 2 \lambda_z^2} \tag{37}$$

4. For the power-off range of vertical descent ($\sqrt{3} \leq \lambda_z \leq 2$)

$$T = \frac{2}{3} \rho\pi R^2 v \left(2 V - v \right) \tag{38}$$

$$v' = V - \sqrt{V^2 - \frac{3T}{2\rho\pi R^2}} \tag{39}$$

$$\lambda_i = \lambda_z - \sqrt{\lambda_z^2 - 3} \tag{40}$$

5. For the windmill range ($2 \leq \lambda_z \leq \infty$)

$$T = 2\rho\pi R^2 \, v \, (V - v) \tag{41}$$

$$v = \frac{V}{2} - \sqrt{\left(\frac{V}{2}\right)^2 - \frac{T}{2\rho\pi R^2}} \tag{42}$$

$$\lambda_i = \frac{\lambda_z}{2} - \sqrt{\left(\frac{\lambda_z}{2}\right)^2 - 1} \tag{43}$$

Calculated values of λ_i versus λ_z for the vertical flight range are given in table 1.

DISCUSSION

Figure 4 shows a comparison of the theoretical values of the nondimensional, mean induced velocity λ_i with the experimental values from runs 51 and 61 of reference 1. These two runs were the high rpm, low C_T runs on a model rotor with three to one taper and untwisted blades and were chosen for the comparison because it is believed that they are the least affected by inboard blade stall.

If the effects of the non-uniform loading of the model rotor were to be taken into account in the theory by making the assumption of the "independence of blade elements" for the theoretical comparison, the agreement between the theoretical and experimental values would be improved. This follows since, at any appreciable rate of descent, there will always be inboard blade elements operating in the windmill and power-off ranges.

The only empiricism in the present report which appears likely to effect the engineering accuracy of the final equations lies in the choice of $\lambda_i = \lambda_z = \sqrt{3}$ for the ideal autorotation point, since any reasonable form for the relations $k_1 = f(\lambda_z)$ and $k_2 = f(\lambda_z)$ which fit the endpoints of the power-stable, and power-off ranges will yield essentially the same results.

REFERENCES

1. Castles, Walter, Jr. and Gray, Robin B. : Empirical Relation Between Induced Velocity, Thrust, and Rate of Descent of a Helicopter Rotor As Determined by Wind-tunnel Tests on Four Model Rotors. NACA TN 2474, Oct. 1951.

2. Drees, J. Meijer and Hendal, W. P. : The Field of Flow Through a Helicopter Rotor Obtained from Wind Tunnel Smoke Tests. Netherlands, NLL Rep. A. 1205, Feb. 1950, pp 7.

3. Roshko, Anatol: On the Wake and Drag of Bluff Bodies. J.A.S. Vol. 22, No. 2 , Feb. 1955, pp 124.

TABLE I

THEORETICAL VALUES OF THE NONDIMENSIONAL INDUCED VELOCITY λ_i FOR A LIFTING ROTOR WITH UNIFORM LOADING OPERATING IN VERTICAL FLIGHT

A. - VALUES FOR VERTICAL ASCENT

λ_z	λ_i
0.0	1.000
-0.4	0.820
-1.0	0.618
-2.0	0.414
-4.0	0.236

B. - VALUES FOR THE POWER-UNSTABLE RANGE OF POWER-ON VERTICAL DESCENT

λ_z	λ_i
0.0	1.000
.2	1.205
.4	1.420
.6	1.658
.8	1.892
1.0	2.155
1.2	2.450
1.4	2.801
1.414	2.828

TABLE I continued -

C. - VALUES FOR THE POWER-STABLE RANGE OF POWER-ON VERTICAL DESCENT

λ_z	λ_i
1.414	2.828
1.50	2.725
1.55	2.643
1.60	2.538
1.65	2.395
1.70	2.169
1.732	1.732

D. - VALUES FOR THE POWER-OFF RANGE OF VERTICAL DESCENT

λ_z	λ_i
1.732	1.732
1.75	1.501
1.80	1.310
1.85	1.200
1.90	1.119
1.95	1.055
2.00	1.000

E. - VALUES FOR THE WIND-MILL RANGE

λ_z	λ_i
2.00	1.000
2.05	0.800
2.10	.730
2.20	.642
2.40	.537
3.00	.382
4.00	.268

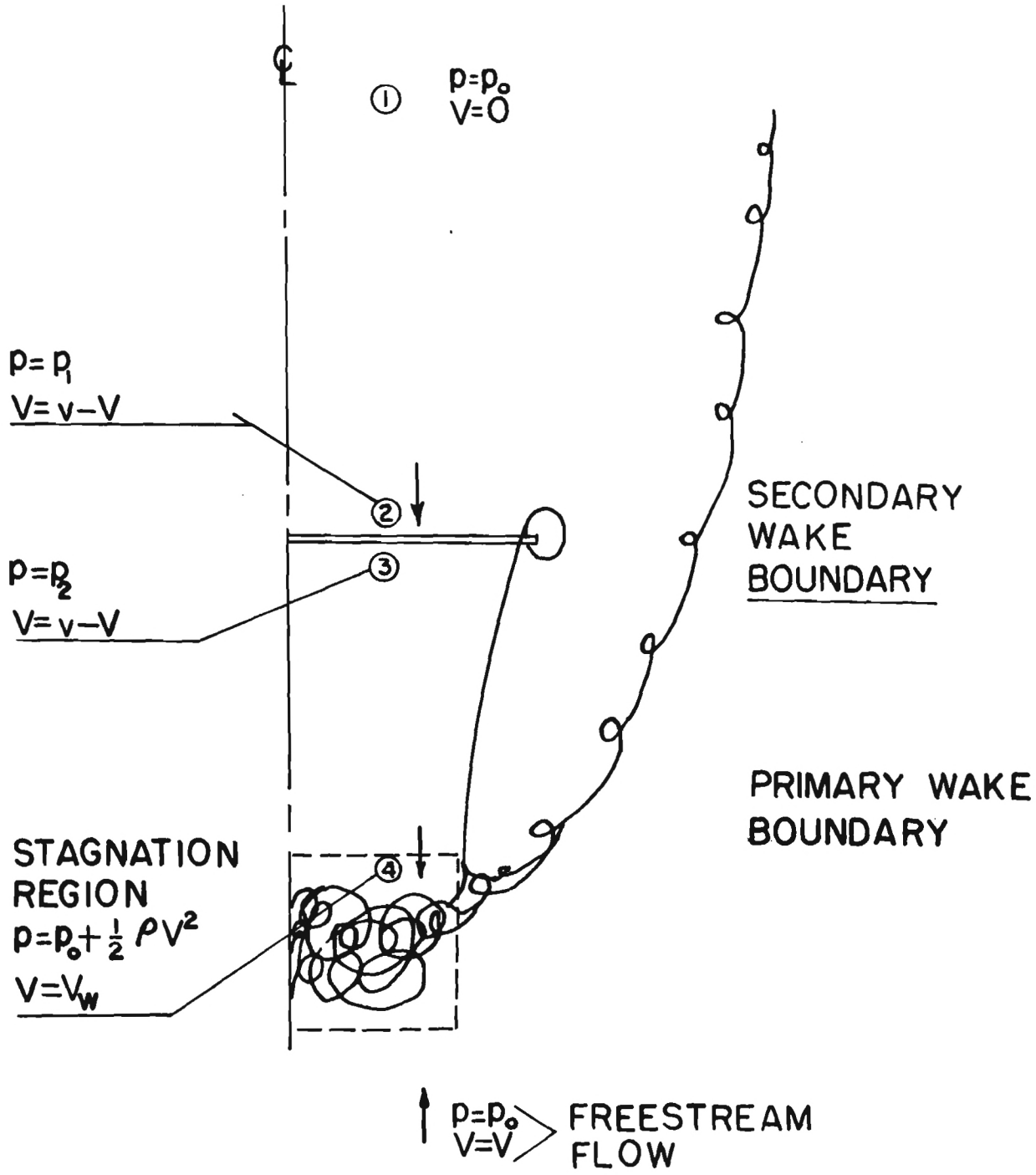

Figure 1. Schematic Flow Pattern for Power-Unstable Range of Power-On Vertical Descent ($0 \leq \lambda_z \leq -\sqrt{2}$).

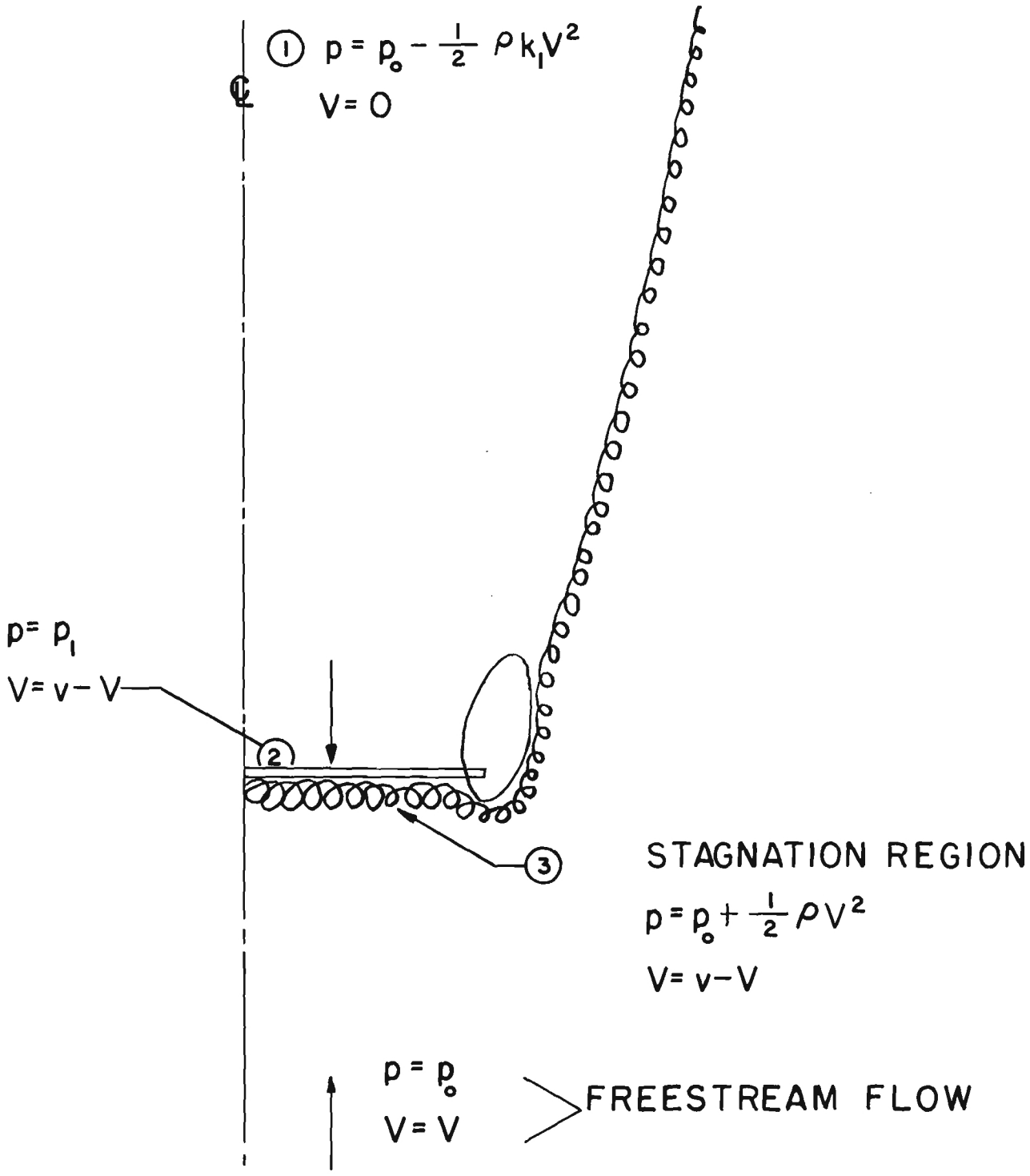

Figure 2. Schematic Flow Pattern for Power-Stable Range of Power-On Descent ($-\sqrt{2} \leq \lambda_z \leq -\sqrt{3}$).

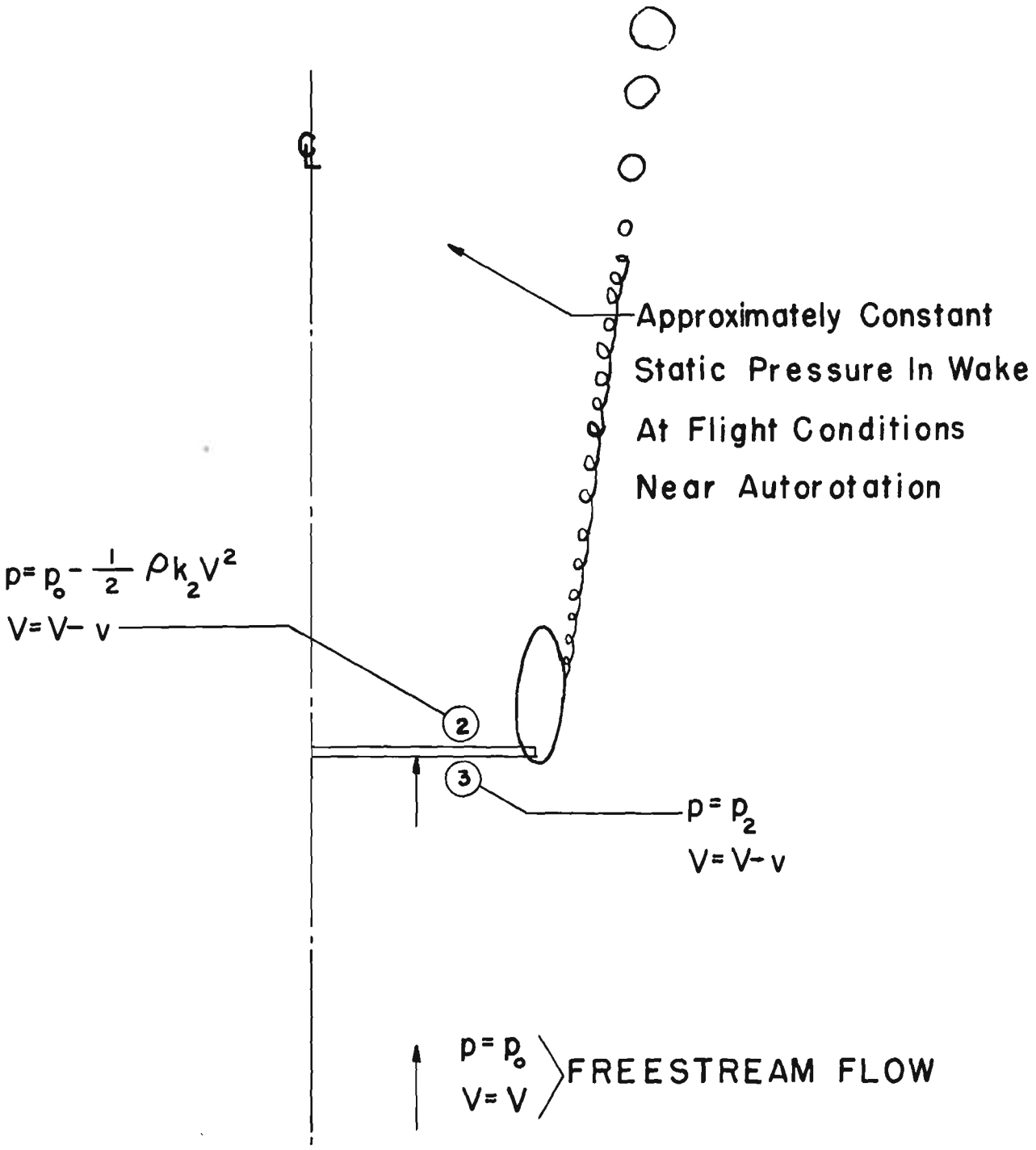

Figure 3. Schematic Flow Pattern for Power-Off Range of Vertical Descent ($\sqrt{3} \leq \lambda_z \leq 2$).

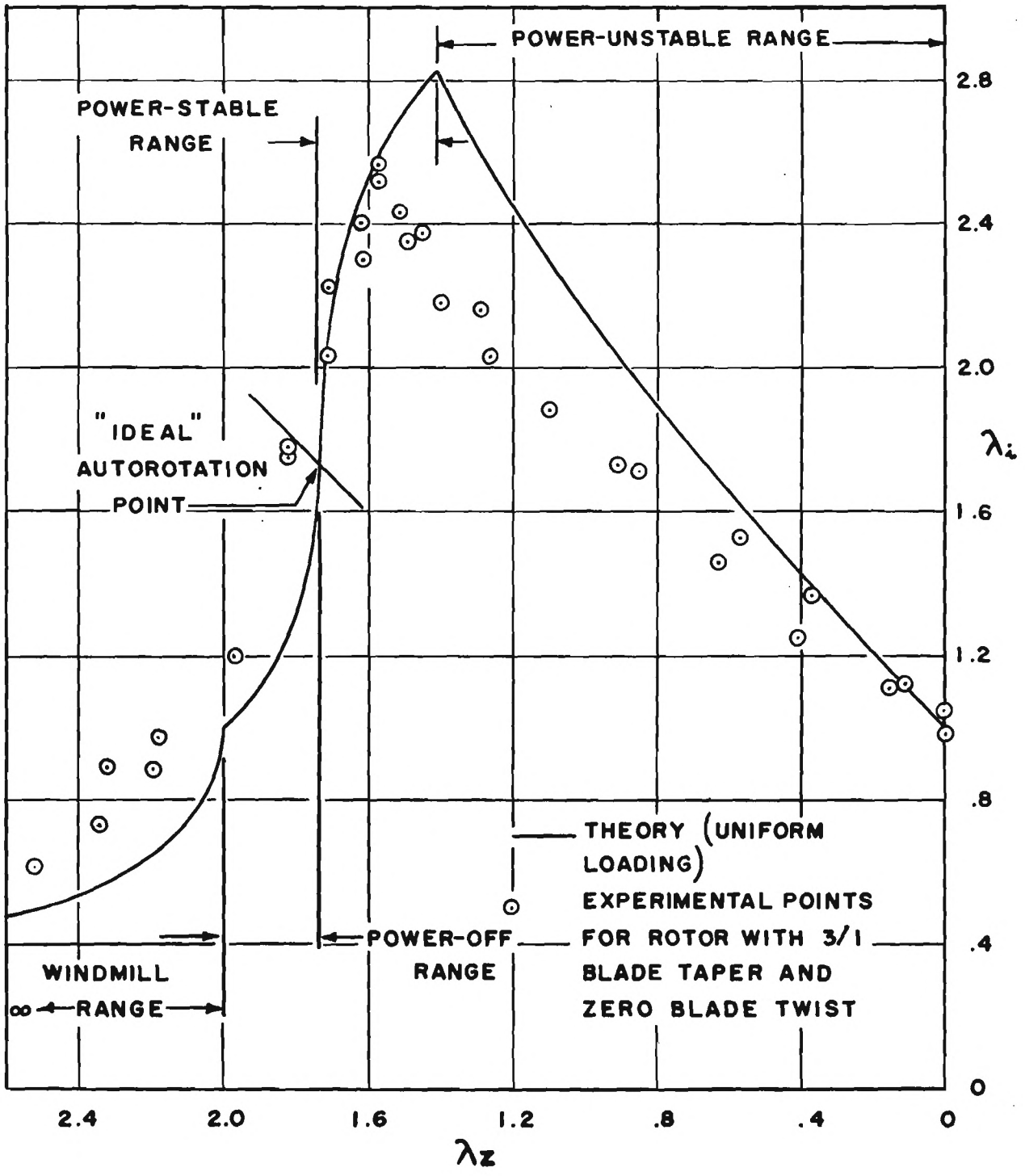

Figure 4. Comparison of Theoretical and Experimental Values of the Nondimensional Induced Velocity λ_i.

ENGINEERING EXPERIMENT STATION
of the Georgia Institute of Technology
Atlanta, Georgia

REVISED FINAL REPORT - PART B

PROJECT NO. 218

AN APPROXIMATE SOLUTION FOR THE STREAMLINES ABOUT A LIFTING ROTOR HAVING UNIFORM LOADING AND OPERATING IN THE HOVERING OR LOW-SPEED VERTICAL-ASCENT FLIGHT CONDITIONS

By

WALTER CASTLES, JR.
Daniel Guggenheim School of Aeronautics

o - o - o - o - o - o - o - o - o - o

CONTRACT NO. Naw-6230

NATIONAL ADVISORY COMMITTEE FOR AERONAUTICS

o - o - o - o - o - o - o - o - o - o - o

JULY, 1955

ENGINEERING EXPERIMENT STATION
of the Georgia Institute of Technology
Atlanta, Georgia

REVISED FINAL REPORT - PART B

PROJECT NO. 218

AN APPROXIMATE SOLUTION FOR THE STREAMLINES ABOUT A LIFTING ROTOR HAVING UNIFORM LOADING AND OPERATING IN THE HOVERING OR LOW-SPEED VERTICAL-ASCENT FLIGHT CONDITIONS

By

WALTER CASTLES, JR.
Daniel Guggenheim School of Aeronautics

o - o - o - o - o - o - o - o - o

CONTRACT NO. Naw-6230

NATIONAL ADVISORY COMMITTEE FOR AERONAUTICS

o - o - o - o - o - o - o - o - o - o

JULY, 1955

AN APPROXIMATE SOLUTION FOR THE STREAMLINES ABOUT A LIFTING ROTOR HAVING UNIFORM LOADING AND OPERATING IN THE HOVERING OR LOW-SPEED VERTICAL-ASCENT FLIGHT CONDITIONS

Prepared by [redacted]

Walter Castles, Jr., Assoc. Prof.
Daniel Guggenheim School of
Aeronautics

Approved by [redacted]

Thomas W. Jackson, Head
Mechanical Sciences Division

Released by [redacted]

Paul K. Calaway, Director
Engineering Experiment Station

July, 1955

TABLE OF CONTENTS

TABLE OF CONTENTS (CONTINUED)

TABLE OF CONTENTS (CONTINUED)

AN APPROXIMATE SOLUTION FOR THE STREAMLINES ABOUT A LIFTING ROTOR HAVING UNIFORM LOADING AND OPERATING IN THE HOVERING OR LOW-SPEED VERTICAL-ASCENT FLIGHT CONDITIONS

By Walter Castles, Jr.

SUMMARY

It is shown that the usual assumption of a uniform vortex-cylinder for the wake-vortex-structure of a uniformly loaded, lifting rotor operating in the hovering or low speed vertical ascent flight conditions does not yield useful results for the induced velocities in the region about the periphery of the rotor.

It is then shown that a useful approximation for the flow patterns can be constructed by adding the stream function for the displacement velocity of the actuator-disk assumed to be generating the wake-vortex-cylinder and the stream function for a ring source coincident with the rim of the rotor to the stream functions for a uniform vortex-cylinder and the freestream velocity. Equations are derived for the relative values of the component stream functions.

The present analysis indicates that there is an appreciable induced upflow in the region around the periphery of a rotor operating in the hovering or low speed vertical ascent flight conditions. For a point located at 120% radius and in the plane of rotation of a hovering rotor the magnitude of the induced upflow-velocity is of the order of 22% of the mean induced velocity over the rotor disk. The induced upward velocity component decreases rapidly with increasing distance from the edge of the rotor and, at a point in the vicinity of the center of the second rotor of a twin rotor helicopter in hovering flight, the upwash has decreased to a value of about 2-1/2% of the

mean induced velocity over the rotor disk.

INTRODUCTION

The assumption of a uniform wake-vortex-cylinder for purposes of computing the mean normal component of induced velocity over the rotor disk of a lifting rotor with uniform loading has been successfully used for many years (see ref. 1 for example) and yields results which are in good agreement with experimental data. In fact, for vertical ascent, the equations that are obtained from this assumption are identical with those obtained from the simple momentum theory provided that the displacement velocity of the vortex-cylinder relative to the rotor is taken to be equal to the resultant normal component of velocity at the rotor. (i.e. The proper motion of the vortex-cylinder relative to the adjacent fluid is taken to be the equilibrium value at a large distance downstream from the end of the cylinder). Furthermore, the assumption of the "independence of blade elements" which is, in effect, the assumption of a wake-vortex-structure consisting of an infinite set of coaxial vortex-cylinders having a radial distribution of vortex strength proportional in magnitude and opposite in sign to the change in blade-bound-vortex-strength (ref. 1) has furnished the basis for calculating the induced velocities along the radii of rotors with nonuniform loading. With the exception of the values near the rim of the rotor, the induced velocity distributions along the rotor radii that are computed by this method appear to be in reasonable agreement with the available experimental data.

The use of a uniform skewed-vortex-cylinder to compute the induced velocity fields of rotors operating in the higher speed helicopter-flight conditions has also yielded useful results of engineering accuracy (ref. 2). However, in the course of computing the induced flow fields for reference 2,

it was noticed that, for the smaller advance ratios there exist large discrepancies between the positions of the boundary streamlines for the flow inside and outside the wake. Further investigations of the flow induced by a uniform right-circular-vortex-cylinder showed that, although the streamlines for the internal wake boundaries converged to the correct ultimate wake-diameter (i.e. the value given by momentum theory), the streamlines bounding the outer surface of the wake not only in general converged to a different ultimate wake-diameter but did not even exist for vertical ascent velocities less than the normal component of induced velocity at the rotor.

It was therefore thought that, for low speed vertical flight and probably for all low speed flight conditions where the magnitude of the induced velocity is of the order of the freestream velocity, or greater, it would be necessary to obtain a more accurate approximation for the induced flow in the region around the rotor.

The present report presents one approximate solution of the low speed flow problem for a rotor with uniform loading operating in hovering or vertical ascent.

NOTATION

r	radius of point P (r, z) from rotor axis (figure 5)
r_o	radius of wake-vortex-sheet at rotor disk
r_w	wake-radius
r_∞	radius of wake-vortex-sheet a large distance downstream of the rotor (or at point of minimum wake-radius)
s	distance along wake-vortex-sheet streamline
v	mean normal component of induced velocity over rotor disk ($v = \frac{1}{2}\gamma$)
v_o	normal component of velocity at rotor disk arising from stream function ψ_o for the actuator-disk displacement velocity
v_{ri}	radial component of induced velocity at a point of radius r_o on upper surface of rotor inside wake-vortex-sheet
v_{ro}	radial component of induced velocity at a point of radius r_o on lower surface of rotor and outside wake-vortex-sheet
v_s	normal component of velocity at rotor disk arising from the stream function ψ_s for the uniform distribution of sinks over the disk (i.e. induced by a uniform wake-vortex-cylinder)
z	normal distance of a point P from the rotor disk
R	rotor radius
T	rotor thrust
V	freestream velocity

V_z resultant Z component of velocity at a point P (r, z)

V_r the radial component of velocity at point P (r, z)

γ wake-vortex-sheet-strength a large distance downstream of the rotor (or at point of minimum wake-radius)

ρ mass density of fluid

ψ stream function for rotor flow pattern as computed from the results of the present report

ψ' stream function for rotor flow pattern as computed using a uniform vortex-cylinder for the wake-vortex-system

ψ_o stream function for the displacement velocity of the actuator-disk assumed to be generating the wake-vortex-rings

ψ_r stream function for a ring source

ψ_s stream function for a uniform distribution of sinks over the rotor disk (i.e. a uniform vortex-cylinder)

$\frac{d\gamma}{dt}$ rate of transport of vorticity along wake boundary

$\frac{d\gamma}{dz}$ value of line integral taken about a unit length (measured in the Z direction) of the wake-vortex-sheet

ANALYSIS

A. Demonstration of the Approximation Involved in the Assumption that the Wake-Vortex-Distribution Consists of a Uniform Vortex-Cylinder

It is shown in reference 3 that the flow induced by a uniform vortex-cylinder is identical with the flow induced by a uniform distribution of sinks of proper strength over the end of the cylinder apart from the addition, for the region inside the cylinder, of an axial velocity component equal to the strength of the bounding vortex-sheet. A table of the values of the stream function ψ_s for a uniform distribution of sinks over a disk (i.e. - a uniform right-circular vortex-cylinder) is given in appendix table 17 in reference 3. Consequently, it is easier to compute the streamlines for the axially symmetric case where the values of the stream function for the free-stream flow and the flow induced by the vortex-cylinder are additive by using the tabulated values of ψ_s than by the method used in reference 2.

The value of the stream function ψ' for the freestream flow plus vortex-cylinder is thus

$$\psi' = \pi r^2 (V + \gamma) - \psi_s \qquad (1)$$

for the region inside the wake and

$$\psi' = \pi r^2 V + \psi_s \qquad (2)$$

for the region outside the wake

where ψ_s = value of stream function at r, z for uniform distribution of sinks over rotor disk (i.e. vortex-cylinder)

r = radius of point from axis of symmetry

z = axial distance of point from rotor plane

V = freestream velocity

γ = wake-vortex-sheet-strength (i.e. $\gamma = 2v$)

v = normal component of induced velocity at rotor disk

and for the full sphere

$$(\psi_s)_{total} = 2\pi R^2 v = \pi R^2 \gamma \qquad (3)$$

Figure 1, plotted from the computed values of ψ' given in table 1, shows the streamlines for the vortex-cylinder in a freestream flow for the case where the freestream velocity V is four times the normal component of the induced velocity v at the rotor disk. It is seen that for this large a ratio of freestream velocity to induced velocity the assumption of a uniform vortex-cylinder for the wake-vortex-structure gives a reasonable flow pattern except for the slight overlapping of streamlines along the wake boundary. However, for the case where the freestream velocity V is of the order of magnitude of the induced velocity v there is a complete overlap in the streamlines below the rotor as shown in figure 2 for the computed values of ψ' given in table 2. For the case of $V = \frac{1}{4} v$ and the case of hovering flight where $V = 0$, the streamlines induced by the uniform vortex-cylinder give the inaccurate representation shown plotted in figures 3 and 4 for the computed values of ψ' given in tables 3 and 4.

It is obvious from figures 1, 2, 3 and 4 that the assumption of a uniform vortex-cylinder for the wake-vortex-structure will not furnish a useful basis for computing the velocity field in the vicinity of the

periphery of a lifting rotor unless the freestream velocity V is several times as large as the mean normal component of the induced velocity v at the rotor disk.

B. Determination of a Useful Approximation for the Stream Function for Vertical Ascent.

It appears that in the physical case the wake-vortex-sheet must unroll from around the periphery of a uniformly loaded rotor in the form of a spiral somewhat as shown schematically in figure 5 and that the lumped vorticity around the periphery of the rotor should be taken into account in computing the induced flow for hovering and the smaller rates of vertical ascent.

The effects of the spiral vortex-sheet at the periphery of the rotor might be approximated by a finite strength vortex-ring coincident with the edge of the rotor. However, this approximation for the wake-vortex-structure does not furnish the necessary "feeder-sheet" connecting the rotor rim with the initial radius r_o of the wake-vortex-cylinder (see figure 5) and consequently, does not afford a very good approximation for the rotor streamlines.

It appears that a better approximation, and one based upon a certain logic, can be obtained by adding the stream function for the displacement-velocity of the actuator-disk assumed to be generating the wake-vortex-rings to the stream function ψ_s for the uniform distribution of sinks over the rotor disk (i.e. the uniform wake-vortex-cylinder). This approximation inherently contains the necessary "feeder-sheet" and affords a particularly simple solution since both ψ_o and ψ_s furnish a uniform value for the normal component of induced velocity at the rotor disk.

Values of the stream function ψ_o for the displacement velocity of the

actuator-disk are given in table 5. These values were computed from the limiting case of the solution for the flow about an oblate spheroid given in reference 4. In addition, it is necessary to add the stream function ψ_r for a ring source located at the periphery of the rotor, or a similar singularity distribution, in order to cancel the distributed sink strength located within the closed streamlines of the spiral. A table of the values of ψ_r are given in appendix table 6 in reference 3.

Let the rotor thrust be T and uniformly distributed over the rotor disk of radius R. Let the radius of the wake-boundary-streamline at the rotor disk be r_o and the ultimate wake-radius be r_∞. Let the ultimate wake-vortex-sheet-strength be γ and the freestream velocity be V as shown in figure 5.

Vortex theory demonstrates that, for a lifting surface with uniform loading, the force is equal to the product of the fluid mass density, the area over which the force acts, and the rate of generation of vorticity. In the steady state system under consideration the rate of generation of vorticity is constant and equal to the rate of transport of vorticity along the wake which is, in turn, equal to the product of the wake-vortex-sheet-strength times the wake-vortex-sheet-velocity. Thus, using values at a section across the ultimate-wake where the sheet-strength is the known value γ and the sheet velocity is $V + \frac{1}{2}\gamma$,

$$T = \rho \pi R^2 \gamma \left(V + \frac{1}{2}\gamma \right) \tag{4}$$

or

$$\gamma = -V + \sqrt{V^2 + \frac{2T}{\rho \pi R^2}} \tag{5}$$

The thrust is also equal to the rate of transport of excess momentum across a section of the ultimate wake of radius r_∞ or

$$T = \rho \pi r_\infty^2 \gamma (V + \gamma) \tag{6}$$

It follows from equations 4 and 6, that

$$\left(\frac{r_\infty}{R}\right)^2 = \frac{V + \frac{1}{2}\gamma}{V + \gamma} \tag{7}$$

Let v_o be the uniform normal-component of velocity over the rotor disk that is attributable to the stream function ψ_o for the displacement velocity of the actuator-disk. Let v_s denote the similar velocity component for the stream function ψ_s of the uniform sink distribution (i.e. vortex-cylinder). Then equating the values of ψ on opposite faces of the wake-vortex-sheet a large distance downstream of the rotor where the sheet strength is the known value γ, the wake radius is the known value r_∞, the velocity outside the wake is the freestream value V, and the value of ψ_o is zero, gives

$$\pi r_\infty^2 \quad (V + \gamma) = \pi r_\infty^2 \quad V + 2 \pi R^2 v_s - (\psi_r)_{total} \tag{8}$$

However, for continuity of flow within the closed streamline enclosing the rotor rim the strength $(\psi_r)_{total}$ of the ring source located at the rotor rim is

$$(\psi_r)_{total} = 2 \pi \ (R^2 - r_o^2) v_s \tag{9}$$

Solving equations 8 and 9 for v_s

$$v_s = \frac{1}{2}\gamma \left(\frac{r_\infty}{r_o}\right)^2 \tag{10}$$

Equating the value of ψ on the wake boundary at radius r_o at the rotor disk to the value of ψ at radius r_∞ in the ultimate wake

$$\pi r_o^2 \ (V + v_o + v_s) = \pi r_\infty^2 \ (V + \gamma) \tag{11}$$

Substituting the value of v_s from equation 10 and solving for v_o gives

$$v_o = \left(\frac{r_\infty}{r_o}\right)^2 \ (V + \frac{1}{2}\gamma) - V \tag{12}$$

For the larger rates of vertical ascent, say $V \geq \frac{\gamma}{2}$, where the stagnation point on the entering ψ_{total} streamline is above the plane of the rotor disk, the value of the initial wake-radius r_o is fixed by the requirement that the ψ_{total} streamline be single-valued over the portion of the rotor-disk-plane outside the rotor-disk-radius. The following proceedure may thus be used to compute the values of the stream function outside the wake:

1. For the given values of the disk loading $\frac{T}{\pi R^2}$, freestream velocity V, and air density ρ, compute the ultimate wake-vortex-sheet-strength γ from equation 5
2. Compute the value of the square of the ultimate-wake radius-ratio $\left(\frac{r_\infty}{R}\right)^2$ from equation 7

3. Choose three or more initial-wake radius-ratios $\left(\frac{r_o}{R}\right)$ covering the range from $\frac{r_o}{R} \approx \sqrt{\frac{r_\infty}{R}}$ to $\frac{r_o}{R} = 1$ and calculate the values of v_o and v_s for each ratio from equations 10 and 12

4. For each initial-wake radius-ratio $\left(\frac{r_o}{R}\right)$ compute the values of ψ/ψ_{total} along a radial line in the plane of the rotor disk for the interval $1 \leq \frac{r}{R} \leq 1.10$. It is to be noted that $\psi_s + \psi_r = \pi r_o^2 v_s$ = constant for points in the rotor plane outside the rim of the rotor so that for these plots

$$\psi = \pi r^2 V + \psi_o + \pi r_o^2 v_s \tag{13}$$

where

$$\psi_o = 2 R^2 v_o \psi_o^* \tag{14}$$

(ψ_o^* from table 5 b)

and

$$\psi_{total} = \pi r_o^2 (V + v_o + v_s) \tag{15}$$

(It will be noted that if the trial value of $\left(\frac{r_o}{R}\right)$ is too small there will be no intercept of the ψ/ψ_{total} versus $\frac{r}{R}$ curve with the $\psi/\psi_{total} = 1$ line as in curve (a) of figure 6, whereas if the trial value of $\left(\frac{r_o}{R}\right)$ is too large there will be a double intercept as in curve (b). The correct value of $\left(\frac{r_o}{R}\right)$ may thus be determined by plotting the ordinates of the minimum points of the ψ/ψ_{total} curves versus $\left(\frac{r_o}{R}\right)$ and reading the values of $\left(\frac{r_o}{R}\right)$ for the point at which $\psi/\psi_{total} = 1$).

5. Compute the values of v_o, v_s and $(\psi_r)_{total}$ for the given values of V, γ, $\frac{r_\infty}{R}$, and $\frac{r_o}{R}$

6. Then for the region outside the wake

$$\psi = \pi r^2 V + \psi_o + \psi_s - \psi_r \tag{16}$$

where

$$\psi_o = 2 R^2 v_o \psi_o^*$$

$$\psi_s = 2 R^2 v_s \psi_s^* \quad \text{for upper quadrants}$$

$$\psi_s = 2 R^2 v_s (\pi - \psi_s^*) \quad \text{for lower quadrants}$$

$$\psi_r = \frac{(\psi_r)_{total}}{2 \pi} \psi_r^*$$

and the nondimensional starred values of psi are those given in the aformentioned tables.

For hovering and the smaller rates of vertical ascent where the stagnation point on the entering ψ_{total} streamline is below the rotor-disk-plane, the value of the initial wake-radius r_o can be found by equating the rate of transport of vorticity (i.e. product of wake-vortex-sheet-strength and wake-vortex-sheet-velocity) across the rotor plane at radius r_o to the value across a section of the ultimate wake. It is shown in appendix I that this procedure gives the solution

$$\left(\frac{r_\infty}{r_o}\right)^4 (1 + \tan^2 \theta) = 1 \tag{17}$$

where

θ = angle between streamline at $z = 0$ and $r = r_o$ and the normal to the rotor disk (see figure 5)

and

$$\tan \theta = \frac{2 v_o}{\pi v_s} \sqrt{\frac{r_o}{1 - r_o^2}} \qquad (18)$$

It is found from numerical computations that it is necessary, for all cases except hovering, to reduce the value of r_∞ slightly (i.e. a few per cent) below that given by equation 7 in order to obtain a real solution for r_o from equations 17 and 18. This discrepancy in the present analysis may arise from considering the rotor loading as constant to the rotor edge rather than decreasing to zero over some small final radius-increment as it would necessarily have to do.

For hovering and very small rates of vertical ascent (i.e. $V = \frac{1}{4} v$) there would in an exact solution apparently be an appreciable outflow of fluid from the vortex-spiral enclosing the rotor rim. Consequently, in order to simulate the effect of this outflow in the present approximate solution it is necessary to reduce the value of v_o given by equation 12 by about 5% in order to make the minimum wake radius equal to r_∞ for hovering and in order to eliminate a bulge in the wake boundary streamlines just below the rotor for the case where $V = \frac{1}{4} v$.

The streamlines computed by the above procedure for the cases of $V = 4\ v = 2\gamma$, $V = v = \frac{1}{2}\gamma$, $V = \frac{1}{4} v = \frac{1}{8}\gamma$, and $V = 0$ are shown in figures 7, 8, 9, and 10 respectively. The corresponding tabular values of ψ/ψ_{total} are given in tables 6, 7, 8, and 9.

For the present solution, where the wake-vortex-sheet-strength varies

from a value of $\frac{d\gamma}{dz} = 2\, v_s$ at radius r_o at the rotor disk to a value of $\frac{d\gamma}{dz} = \gamma$ at r_∞ in the ultimate wake, there does not appear to be any simple way to obtain an exact solution for the values of the stream function within the wake. However, it appears to be a good approximation to assume that the axial velocity component is uniform over each wake cross-section since this component is uniform over the sections in the plane of the rotor disk and in the ultimate wake. The tabulated values of ψ for the region inside the wake have therefore been computed using the aforementioned approximation for which

$$\psi = \left(\frac{r}{r_w}\right)^2 \psi_{total} \tag{19}$$

where r_w = radius of wake boundary streamline as determined from the solution for the external flow.

The axial and radial velocity components V_z and V_r at any point P (r, z) in the flow field may be readily computed from the values of the stream function by means of the relations

$$V_z = \frac{1}{2\pi r}\left(\frac{\partial \psi}{\partial r}\right) \tag{20}$$

and

$$V_r = -\frac{1}{2\pi r}\left(\frac{\partial \psi}{\partial z}\right) \tag{21}$$

C. Application of Results.

Although the whole flow field out to the limits of the tables at $r = \pm\, z = 2\,R$ might be mapped for any given flight condition by following

For points in the plane of a hovering rotor and outside the closed streamline the axial component of velocity arises solely from the stream function ψ_o and can thus be expressed in explicit form as

$$V_z = \frac{1}{2\pi r}\left(\frac{\partial \psi_o}{\partial r}\right)_{z=0}$$

or

$$\frac{V_z}{v} = \frac{4 v_o}{\pi \gamma}\left\{\frac{1}{\sqrt{r^2-1}} - \cot^{-1}\sqrt{r^2-1}\right\} \qquad (22)$$

Values of $\frac{V_z}{v}$ calculated from equation 22 for points in the plane of a hovering rotor are given in figure 11 and table 10.

DISCUSSION

As in most attempts to obtain an approximate solution of engineering accuracy for a complicated three-dimensional flow pattern, the choice and distribution of the singularities used in the present report are in a sense arbitrary. However, the identity of the flow about a uniform vortex-cylinder with that of a uniform sink distribution over the end of the cylinder suggests that the sink distribution represented in the present report by ψ_s will be a part of the total singularity distribution. Similarly, since the wake-vortex-rings may be assumed to be generated by the application of uniform impulse-pressures over an actuator-disk and, for a finite thrust, the generating actuator-disk must have a certain displacement velocity relative to the surrounding fluid, the addition of the singularity distribution ψ_o for the actuator-disk displacement velocity appears to be in order. The inclusion of the singularity distribution ψ_r for the ring source, or one of similar type, is necessary in order to

satisfy continuity at the closed streamline about the rotor rim and thus furnish the required stagnation points on the wake-boundary-streamlines.

The flow patterns computed on the basis of the present report inherently satisfy all conditions for continuity at all points in the flow that do not lie on the flow boundaries (i.e. the rotor disk or the wake boundary streamlines). Consequently, since the wake boundaries exist and have a reasonable geometry, the velocity components computed on the basis of the present report should be sufficiently accurate for most engineering purposes provided that the points in the flow lie a reasonable distance (say 0.1 R) from the flow boundaries at the rotor disk and the periphery of the wake.

The computed initial wake-radius r_o for hovering is in good agreement with experimental values, of the order of 0.85 R, obtained from smoke flow studies (see reference 5 for example). There does not appear to be any experimental data on the values of r_o at small rates of vertical ascent for comparison with the theoretical values.

It is unlikely that the axial velocity distribution along the radius of an actual rotor with a finite angular velocity will show the discontinuous change from a value of $V + v_o + v_s$ inside the initial wake radius r_o to the value $V + v_o - v_s$ just outside r_o that occurs in the present approximate solution for an actuator-disk. However, it appears that the present analysis should qualitatively describe the actual flow and that there should thus be an appreciable decrease in axial velocity component across the inner boundary of the closed streamline enclosing the rim of a rotor operating in hovering or very low-speed vertical ascent. The equilibrium blade coning and pitch angles for these flight conditions should thus be somewhat larger than the values computed by contemporary theory.

APPENDIX I

SOLUTION FOR INITIAL WAKE-RADIUS r_o FOR HOVERING AND THE VERY LOW RATES OF VERTICAL ASCENT

Let the angle between the normal to the rotor and the tangent to the wake boundary streamline at $z = 0$ and $r = r_o$ be denoted by θ as shown in figure 12. Let the radial velocity component at a point on the upper surface of the rotor and just inside the wake boundary be v_{ri} and the radial velocity component on the lower surface just outside the wake boundary be $v_{r\,o}$. Then the difference in radial velocity component Δv_r across the wake-vortex-sheet at r_o is

$$\Delta v_r = v_{r\,i} - v_{r\,o} \tag{A1}$$

The discontinuity in radial velocity Δv_r at r_o arises solely from the stream function ψ_o since the radial velocity components arising from ψ_s and ψ_r are continuous at this point. Thus the value of Δv_r is equal to twice the radial velocity component at r_o that arises from ψ_o.

Thus

$$\frac{1}{2}\,\Delta v_r = \frac{1}{2\pi r}\,\frac{\partial \psi_o}{\partial z} \tag{A2}$$

However, from reference 4 the value of ψ_o in elliptic coordinates is

$$\psi_o = 2 v_o (1 - \mu^2)\,(\varepsilon^2 + 1)\left\{\frac{\varepsilon}{\varepsilon^2 + 1} - \cot^{-1}\varepsilon\right\} \tag{A3}$$

where

$$z = \mu\varepsilon \tag{A4}$$

$$r = \sqrt{1 - \mu^2}\ \sqrt{\varepsilon^2 + 1} \tag{A5}$$

It follows from equations A1, A2, A3, A4, and A5 that

$$\Delta v_r = \frac{4 v_o r_o}{\pi \sqrt{1 - r_o^2}} \tag{A6}$$

For the singularity distributions used in the present report the difference in normal-velocity-component across the wake-vortex-sheet at r_o is merely $2 v_s$. Thus from the geometry and equation A6

$$\tan \theta = \frac{\Delta v_r}{2 v_s} = \frac{2 v_o}{\pi v_s} \left(\frac{r_o}{\sqrt{1 - r_o^2}} \right) \tag{A7}$$

The wake-vortex-sheet-strength γ at $z = 0$ and $r = r_o$ is the difference in velocities on opposite sides of the sheet or

$$(\gamma)_{\substack{z = 0 \\ r = r_o}} = \left[(V + v_o + v_s) - (V + v_o - v_s) \right] \sec \theta \tag{A8}$$

$$= 2 v_s \sec \theta$$

and the vortex-sheet-velocity $\frac{ds}{dt}$ is half the sum of the velocities on opposite sides of the sheet or

$$\left(\frac{ds}{dt} \right)_{\substack{z = 0 \\ r = r_o}} = \frac{1}{2} \left[(V + v_o + v_s) + (V + v_o - v_s) \right] \sec \theta \tag{A9}$$

$$= (V + v_o) \sec \theta$$

The rate of transport of vorticity $\left(\frac{d\gamma}{dt}\right)$ across the plane of the rotor at r_o is equal to the product of the sheet-strength and sheet-velocity or from equations A8 and A9

$$\left(\frac{d\gamma}{dt}\right)_{r_o} = 2\, v_s\, (V + v_o)\ \ (1 + \tan^2 \theta) \qquad \text{(A10)}$$

Equating the rate of transport of vorticity across the rotor plane to the known value $\gamma\,(V + \frac{1}{2}\gamma)$ across a section of the ultimate wake and using equations 10 and 12 to eliminate v_s and v_o gives

$$\left(\frac{r_\infty}{r_o}\right)^4 \ (1 + \tan^2 \theta) = 1 \qquad \text{(A11)}$$

Equations A7 and A11 can be solved for the value of r_o for any given flight condition by use of equations 5, 7, 10, and 12.

Figure 13 gives the resulting computed values of r_o for the smaller rates of vertical ascent.

REFERENCES

1. Knight, Montgomery: Static Thrust Analysis of the Lifting Airscrew. NACA TN 626, Dec. 1937.

2. Castles, Walter, Jr. and De Leeuw, Jacob Henri: The Normal Component of the Induced Velocity in the Vicinity of a Lifting Rotor and Some Examples of its Application. NACA Rep. (previously NACA TN 2912, March 1953)

3. Kuchemann, Dietrich, and Weber, Johanna: Aerodynamics of Propulsion. Section 3-6. McGraw-Hill Book Co., Inc. (New York). 1953. First Edition, pp. 55-57. (Table 17 - Appendix)

4. Lamb, Horace: Hydrodynamics. Ch. V, Sections 107 and 108. Dover Publications, 1945. Sixth ed. pp 142-145.

5. Castles, Walter, Jr. and Gray, Robin B.: Empirical Relation Between Induced Velocity, Thrust, and Rate of Descent of a Helicopter Rotor as Determined by Wind-Tunnel Tests on Four Model Rotors. NACA TN 2474, Oct. 1951.

TABLE I a

VALUES OF THE STREAM FUNCTION ABOVE THE PLANE OF THE ROTOR FOR

$V = 4v = 2\gamma$ FOR WAKE CONSISTING OF A UNIFORM VORTEX-CYLINDER

$\frac{r}{R}$ =	0	.2	.4	.6	.8	1.0	1.2	1.4	1.6	1.8	2.0
$\frac{z}{R}$	ψ/ψ_{total}										
0	0	.040	.160	.360	.640	1.000	1.352	1.768	2.248	2.792	3.400
.2	0	.038	.153	.343	.605	.932	1.307	1.734	2.219	2.767	3.378
.4	0	.037	.148	.330	.581	.897	1.272	1.703	2.193	2.743	3.357
.6	0	.036	.143	.320	.564	.874	1.245	1.677	2.169	2.722	3.337
.8	0	.035	.139	.313	.553	.858	1.226	1.656	2.149	2.703	3.320
1.0	0	.034	.137	.308	.545	.847	1.213	1.642	2.133	2.687	3.304
1.2	0	.034	.135	.304	.539	.839	1.203	1.631	2.122	2.675	3.290
1.4	0	.033	.134	.301	.534	.833	1.196	1.622	2.112	2.664	3.279
1.6	0	.033	.133	.299	.530	.827	1.189	1.614	2.103	2.655	3.270
1.8	0	.033	.132	.297	.527	.823	1.183	1.607	2.096	2.647	3.262
2.0	0	.032	.131	.296	.525	.819	1.178	1.601	2.089	2.639	3.255

TABLE I b

VALUES OF THE STREAM FUNCTION BELOW THE PLANE OF THE ROTOR FOR

$V = 4v = 2\gamma$ FOR WAKE CONSISTING OF A UNIFORM VORTEX-CYLINDER

$\frac{r}{R}$ =	0	.2	.4	.6	.8	1.0	1.2	1.4	1.6	1.8	2.0
$\frac{z}{R}$	ψ/ψ_{total}										
0	0	.040	.160	.360	.640	1.000	1.352	1.768	2.248	2.792	3.400
-.2	0	.042	.166	.377	.674	1.068	1.397	1.802	2.277	2.817	3.422
-.4	0	.043	.172	.390	.699	1.103	1.432	1.833	2.303	2.840	3.443
-.6	0	.044	.177	.400	.716	1.126	1.459	1.859	2.326	2.861	3.462
-.8	0	.045	.180	.407	.727	1.142	1.478	1.879	2.347	2.880	3.480
-1.0	0	.045	.183	.412	.735	1.153	1.491	1.894	2.363	2.896	3.496
-1.2	0	.046	.185	.416	.741	1.160	1.500	1.905	2.374	2.909	3.509
-1.4	0	.047	.186	.419	.746	1.167	1.508	1.914	2.384	2.919	3.520
-1.6	0	.047	.187	.421	.749	1.173	1.514	1.921	2.392	2.928	3.529
-1.8	0	.047	.187	.423	.753	1.177	1.521	1.928	2.400	2.936	3.537
-2.0	0	.047	.189	.424	.755	1.181	1.526	1.935	2.407	2.944	3.545

TABLE II a

VALUES OF THE STREAM FUNCTION ABOVE THE PLANE OF THE ROTOR FOR

$V = v = \frac{1}{2}\gamma$ FOR WAKE CONSISTING OF A UNIFORM VORTEX-CYLINDER

$\frac{r}{R}$ =	0	.2	.4	.6	.8	1.0	1.2	1.4	1.6	1.8	2.0
$\frac{z}{R}$	Ψ/Ψ_{total}										
0	0	.041	.159	.360	.640	1.000	1.220	1.480	1.780	2.120	2.500
.2	0	.036	.143	.318	.554	.829	1.108	1.395	1.708	2.057	2.445
.4	0	.033	.129	.285	.492	.742	1.019	1.317	1.643	1.999	2.393
.6	0	.030	.118	.259	.450	.685	.952	1.252	1.584	1.946	2.344
.8	0	.028	.108	.242	.422	.645	.905	1.201	1.533	1.898	2.299
1.0	0	.026	.102	.229	.403	.618	.873	1.165	1.493	1.859	2.259
1.2	0	.025	.097	.220	.388	.599	.849	1.138	1.464	1.827	2.226
1.4	0	.023	.094	.212	.376	.583	.830	1.115	1.439	1.801	2.199
1.6	0	.023	.093	.207	.366	.568	.814	1.096	1.418	1.779	2.177
1.8	0	.023	.091	.202	.358	.557	.798	1.079	1.399	1.758	2.156
2.0	0	.022	.088	.199	.352	.548	.785	1.063	1.382	1.739	2.137

TABLE II b

VALUES OF THE STREAM FUNCTION BELOW THE PLANE OF THE ROTOR FOR

$V = v = \frac{1}{2}\gamma$ FOR WAKE CONSISTING OF A UNIFORM VORTEX-CYLINDER

$\frac{r}{R}$ =	0	.2	.4	.6	.8	1.0	1.2	1.4	1.6	1.8	2.0
$\frac{z}{R}$	ψ/ψ_{total}										
0	0	.039	.160	.360	.640	1.000	1.220	1.480	1.780	2.120	2.500
- .2	0	.044	.176	.401	.726	1.170	1.332	1.565	1.852	2.182	2.554
- .4	0	.047	.191	.435	.788	1.258	1.421	1.643	1.917	2.241	2.607
- .6	0	.050	.202	.460	.829	1.315	1.488	1.708	1.976	2.294	2.656
- .8	0	.052	.211	.478	.858	1.355	1.535	1.759	2.027	2.341	2.700
-1.0	0	.053	.218	.490	.877	1.382	1.567	1.795	2.067	2.381	2.740
-1.2	0	.055	.222	.500	.891	1.401	1.591	1.822	2.095	2.413	2.774
-1.4	0	.057	.226	.508	.904	1.417	1.610	1.845	2.121	2.438	2.801
-1.6	0	.057	.227	.513	.914	1.431	1.626	1.864	2.142	2.461	2.823
-1.8	0	.057	.229	.517	.922	1.442	1.642	1.881	2.161	2.481	2.844
-2.0	0	.058	.232	.521	.928	1.452	1.655	1.897	2.178	2.501	2.863

TABLE III a

VALUES OF THE STREAM FUNCTION ABOVE THE PLANE OF THE ROTOR FOR $V = \frac{1}{4}$ $v = \frac{1}{8}\gamma$ FOR WAKE CONSISTING OF A UNIFORM VORTEX-CYLINDER

$\frac{r}{R}$ =	0	.2	.4	.6	.8	1.0	1.2	1.4	1.6	1.8	2.0
$\frac{z}{R}$	Ψ/Ψ_{total}										
0	0	.041	.159	.359	.640	1.000	1.088	1.192	1.312	1.448	1.600
.2	0	.034	.134	.293	.502	.727	.909	1.056	1.197	1.348	1.513
.4	0	.029	.111	.240	.403	.587	.767	.931	1.092	1.254	1.429
.6	0	.023	.093	.199	.337	.495	.660	.827	.998	1.170	1.350
.8	0	.021	.078	.171	.291	.432	.583	.746	.917	1.093	1.279
1.0	0	.018	.068	.151	.261	.388	.532	.687	.853	1.030	1.215
1.2	0	.016	.060	.135	.238	.358	.494	.644	.807	.979	1.162
1.4	0	.013	.055	.123	.217	.332	.464	.608	.767	.938	1.118
1.6	0	.013	.052	.115	.202	.309	.438	.578	.733	.902	1.083
1.8	0	.013	.050	.107	.189	.292	.413	.550	.703	.869	1.050
2.0	0	.011	.045	.102	.179	.276	.392	.524	.675	.839	1.019

TABLE III b

VALUES OF THE STREAM FUNCTION BELOW THE PLANE OF THE ROTOR FOR $V = \frac{1}{4} v = \frac{1}{8}\gamma$ FOR WAKE CONSISTING OF A UNIFORM VORTEX-CYLINDER

$\frac{r}{R}$ =	0	.2	.4	.6	.8	1.0	1.2	1.4	1.6	1.8	2.0
$\frac{z}{R}$	ψ/ψ_{total}										
0	0	.039	.161	.360	.640	1.000	1.088	1.192	1.312	1.448	1.600
-.2	0	.046	.186	.427	.777	1.272	1.266	1.327	1.427	1.547	1.687
-.4	0	.051	.209	.480	.876	1.412	1.409	1.452	1.531	1.642	1.771
-.6	0	.056	.227	.521	.943	1.504	1.516	1.556	1.625	1.726	1.850
-.8	0	.059	.242	.549	.988	1.568	1.592	1.637	1.707	1.802	1.921
-1.0	0	.062	.252	.569	1.019	1.611	1.643	1.696	1.770	1.865	1.985
-1.2	0	.064	.260	.584	1.042	1.642	1.681	1.739	1.816	1.916	2.038
-1.4	0	.067	.265	.597	1.061	1.667	1.712	1.775	1.857	1.957	2.081
-1.6	0	.067	.268	.605	1.078	1.690	1.737	1.805	1.890	1.993	2.117
-1.8	0	.667	.270	.612	1.090	1.708	1.763	1.833	1.920	2.026	2.150
-2.0	0	.069	.275	.617	1.100	1.723	1.783	1.859	1.948	2.056	2.181

TABLE IV a

VALUES OF THE STREAM FUNCTION ABOVE THE PLANE OF THE ROTOR FOR

V = 0 FOR WAKE CONSISTING OF A UNIFORM VORTEX-CYLINDER

$\frac{r}{R}$ =	0	.2	.4	.6	.8	1.0	1.2	1.4	1.6	1.8	2.0
$\frac{z}{R}$	ψ/ψ_{total}										
0	0	.041	.159	.360	.640	1.000	1.000	1.000	1.000	1.000	1.000
.2	0	.032	.127	.277	.468	.659	.777	.831	.856	.875	.891
.4	0	.025	.099	.210	.344	.434	.598	.675	.726	.757	.786
.6	0	.019	.076	.159	.261	.369	.464	.544	.608	.652	.687
.8	0	.016	.057	.124	.204	.290	.369	.442	.506	.557	.598
1.0	0	.013	.044	.099	.165	.235	.305	.369	.426	.477	.519
1.2	0	.009	.035	.079	.137	.197	.258	.315	.369	.414	.452
1.4	0	.006	.029	.064	.111	.165	.220	.270	.318	.363	.398
1.6	0	.006	.025	.054	.092	.137	.188	.232	.277	.318	.353
1.8	0	.006	.022	.044	.076	.114	.156	.197	.239	.277	.312
2.0	0	.003	.016	.038	.064	.095	.130	.165	.204	.239	.274

TABLE IV b

VALUES OF THE STREAM FUNCTION BELOW THE PLANE OF THE ROTOR FOR

V = 0 FOR WAKE CONSISTING OF A UNIFORM VORTEX-CYLINDER

$\frac{r}{R}$ =	0	.2	.4	.6	.8	1.0	1.2	1.4	1.6	1.8	2.0
$\frac{z}{R}$	ψ/ψ_{total}										
0	0	.041	.161	.360	.640	1.000	1.000	1.000	1.000	1.000	1.000
- .2	0	.048	.193	.443	.812	1.341	1.223	1.169	1.144	1.125	1.109
- .4	0	.055	.221	.510	.936	1.156	1.402	1.325	1.274	1.242	1.214
- .6	0	.061	.244	.561	1.739	1.631	1.535	1.456	1.392	1.347	1.312
- .8	0	.064	.263	.596	1.796	1.710	1.631	1.558	1.494	1.443	1.402
-1.0	0	.067	.276	.621	1.834	1.764	1.694	1.631	1.573	1.523	1.481
-1.2	0	.071	.285	.640	1.863	1.803	1.742	1.685	1.631	1.586	1.548
-1.4	0	.074	.291	.656	1.889	1.834	1.780	1.729	1.682	1.637	1.602
-1.6	0	.074	.295	.666	1.908	1.863	1.812	1.768	1.723	1.682	1.647
-1.8	0	.074	.298	.675	1.924	1.885	1.844	1.803	1.761	1.723	1.688
-2.0	0	.077	.304	.682	1.936	1.904	1.869	1.834	1.796	1.761	1.726

TABLE V a

VALUES OF THE STREAM FUNCTION ψ_o^* FOR

THE DISPLACEMENT VELOCITY OF A DISK

$\frac{r}{R}$ =	0	.2	.4	.6	.8	1.0	1.2	1.4	1.6	1.8	2.0
$\frac{z}{R}$	ψ_o										
0	0	.063	0.251	0.565	1.005	1.571	0.755	0.579	0.478	0.410	0.362
.2	0	.047	.184	.395	0.632	0.740	.652	.540	.459	.397	.355
.4	0	.033	.128	.266	.407	.492	.495	.457	.410	.370	.332
.6	0	.023	.088	.182	.274	.342	.372	.369	.349	.327	.305
.8	0	.016	.061	.124	.191	.244	.279	.294	.294	.283	.271
1.0	0	.011	.042	.085	.137	.180	.213	.232	.240	.239	.237
1.2	0	.008	.030	.063	.100	.135	.164	.185	.198	.203	.204
1.4	0	.006	.022	.047	.075	.103	.128	.148	.164	.173	.175
1.6	0	.004	.017	.034	.057	.080	.101	.120	.131	.144	.152
1.8	0	.003	.013	.027	.044	.063	.081	.097	.111	.121	.130
2.0	0	.002	.010	.021	.035	.050	.065	.080	.092	.103	.111

TABLE V b

VALUES OF ψ_o^* FOR $\frac{z}{R} = 0$

$\frac{r}{R}$	ψ_o
1.01	1.3168
1.02	1.2269
1.03	1.1630
1.04	1.1125
1.05	1.0700
1.06	1.0334
1.07	1.0012
1.08	0.9724
1.09	0.9463
1.10	0.9226

TABLE VI a

VALUES OF THE STREAM FUNCTION ABOVE THE

PLANE OF THE ROTOR FOR $V = 4v = 2\gamma$

$\frac{r}{R}$ =	0	.2	.4	.6	.8	1.0	1.2	1.4	1.6	1.8	2.0
$\frac{z}{R}$	ψ/ψ_{total}										
0	0	.040	.160	.360	.640	1.000	1.335	1.747	2.225	2.767	3.374
.2	0	.038	.153	.342	.603	.925	1.295	1.718	2.200	2.746	3.356
.4	0	.037	.147	.329	.578	.891	1.262	1.690	2.177	2.726	3.338
.8	0	.035	.139	.311	.550	.853	1.219	1.648	2.138	2.690	3.305
1.2	0	.034	.134	.302	.537	.836	1.198	1.624	2.114	2.665	3.280
1.6	0	.033	.132	.298	.528	.824	1.185	1.609	2.097	2.648	3.262
2.0	0	.032	.131	.295	.523	.817	1.175	1.597	2.084	2.634	3.248

TABLE VI b

VALUES OF THE STREAM FUNCTION BELOW THE

PLANE OF THE ROTOR FOR $V = 4v = 2\gamma$

$\frac{r}{R}$ =	0	.2	.4	.6	.8	1.0	1.2	1.4	1.6	1.8	2.0
$\frac{z}{R}$	ψ/ψ_{total}										
0	0	.040	.160	.360	.640	1.000	1.335	1.747	2.225	2.767	3.374
-.2	0	.042	.169	.381	.677	1.039	1.370	1.774	2.248	2.788	3.392
-.4	0	.043	.174	.391	.694	1.063	1.396	1.798	2.269	2.807	3.409
-.8	0	.045	.181	.407	.724	1.089	1.430	1.834	2.303	2.838	3.439
-1.2	0	.046	.185	.416	.740	1.103	1.446	1.853	2.324	2.861	3.462
-1.6	0	.047	.187	.420	.747	1.112	1.456	1.865	2.338	2.875	3.478
-2.0	0	.047	.188	.423	.753	1.118	1.465	1.875	2.349	2.888	3.490

TABLE VII a

VALUES OF THE STREAM FUNCTION ABOVE THE PLANE OF THE ROTOR FOR $V = v = \frac{1}{2}\gamma$

$\frac{r}{R}$ =	0	.2	.4	.6	.8	1.0	1.2	1.4	1.6	1.8	2.0
$\frac{z}{R}$	ψ/ψ_{total}										
0	0	.042	.164	.370	.659	1.020 1.030	1.143	1.382	1.670	2.002	2.376
.2	0	.036	.145	.321	.554	.811	1.058	1.322	1.621	1.959	2.340
.4	0	.032	.129	.283	.485	.721	.980	1.260	1.571	1.917	2.302
.8	0	.027	.107	.236	.411	.626	.876	1.163	1.484	1.840	2.232
1.2	0	.024	.095	.214	.378	.582	.826	1.107	1.427	1.783	2.175
1.6	0	.022	.090	.202	.358	.556	.795	1.072	1.388	1.744	2.136
2.0	0	.021	.086	.195	.345	.538	.771	1.045	1.359	1.712	2.104

TABLE VII b

VALUES OF THE STREAM FUNCTION BELOW THE PLANE OF THE ROTOR FOR $V = v = \frac{1}{2}\Upsilon$

$\frac{r}{R}$ =	0	.2	.4	.6	.8	1.0	1.2	1.4	1.6	1.8	2.0
$\frac{z}{R}$	Ψ/Ψ_{total}										
0	0	.041	.165	.371	.659	1.020 1.010	1.143	1.382	1.670	2.002	2.376
-.2	0	.044	.176	.397	.705	1.032	1.204	1.433	1.716	2.042	2.412
-.4	0	.047	.189	.425	.756	1.062	1.245	1.475	1.753	2.078	2.444
-.8	0	.052	.206	.464	.826	1.098	1.296	1.533	1.812	2.134	2.499
-1.2	0	.054	.216	.487	.866	1.116	1.320	1.563	1.847	2.172	2.540
-1.6	0	.055	.221	.498	.885	1.130	1.336	1.583	1.870	2.197	2.566
-2.0	0	.057	.226	.510	.906	1.141	1.351	1.601	1.889	2.219	2.588

TABLE VIII a

VALUES OF THE STREAM FUNCTION ABOVE THE PLANE OF THE ROTOR FOR $V = \frac{1}{4} v = \frac{1}{8} \gamma$

$\frac{r}{R}$ =	0	.2	.4	.6	.8	1.0	1.2	1.4	1.6	1.8	2.0
$\frac{z}{R}$	ψ/ψ_{total}										
0	0	.052	.204	.460	.818	$\frac{1.153}{1.280}$	.986	1.038	1.129	1.246	1.387
.2	0	.041	.162	.352	.583	.772	.868	.957	1.061	1.187	1.336
.4	0	.032	.127	.269	.438	.601	.738	.862	.989	1.128	1.283
.6	0	.025	.100	.213	.348	.494	.634	.774	.917	1.067	1.230
.8	0	.022	.081	.175	.292	.422	.558	.702	.852	1.009	1.179
1.0	0	.018	.068	.149	.256	.376	.507	.648	.798	.959	1.132
1.2	0	.016	.059	.132	.229	.342	.469	.609	.758	.918	1.091
1.6	0	.012	.050	.110	.193	.295	.416	.548	.695	.856	1.029
2.0	0	.010	.044	.098	.172	.266	.376	.504	.647	.805	.979

TABLE VIII b

VALUES OF THE STREAM FUNCTION BELOW THE PLANE OF THE ROTOR FOR $V = \frac{1}{4}$ $v = \frac{1}{8}\gamma$

$\frac{r}{R}$ =	0	.2	.4	.6	.8	1.0	1.2	1.4	1.6	1.8	2.0
$\frac{z}{R}$ =	ψ/ψ_{total}										
0	0	.052	.204	.460	.818	1.153 1.026	.986	1.038	1.129	1.246	1.387
-.2	0	.052	.207	.465	.826	1.012	1.038	1.094	1.183	1.296	1.432
-.4	0	.054	.216	.487	.865	1.026	1.070	1.136	1.224	1.339	1.471
-.6	0	.058	.232	.523	.929	1.038	1.097	1.169	1.259	1.372	1.507
-.8	0	.062	.247	.555	.988	1.049	1.114	1.194	1.288	1.403	1.536
-1.0	0	.064	.256	.577	1.001	1.057	1.124	1.209	1.309	1.425	1.562
-1.2	0	.066	.263	.592	1.004	1.060	1.132	1.220	1.321	1.443	1.583
-1.6	0	.071	.284	.640	1.013	1.073	1.145	1.237	1.343	1.468	1.612
-2.0	0	.075	.300	.675	1.021	1.084	1.162	1.258	1.367	1.494	1.636

TABLE IX a

VALUES OF THE STREAM FUNCTION ABOVE THE PLANE OF THE ROTOR FOR V = 0

$\frac{r}{R}$ =	0	.2	.4	.6	.8	1.0	1.2	1.4	1.6	1.8	2.0
$\frac{z}{R}$	ψ/ψ_{total}										
0	0	.058	.225	.507	.904	1.200 1.413	.845	.768	.723	.694	.673
.2	0	.043	.168	.362	.586	.715	.711	.677	.648	.628	.618
.4	0	.031	.121	.252	.392	.500	.551	.565	.564	.559	.555
.6	0	.022	.087	.178	.276	.363	.422	.457	.478	.487	.493
.8	0	.018	.062	.128	.203	.272	.326	.368	.399	.419	.432
1.0	0	.012	.044	.094	.155	.212	.262	.302	.333	.357	.376
1.2	0	.009	.033	.073	.128	.170	.214	.253	.285	.308	.326
1.4	0	.006	.026	.056	.096	.138	.178	.212	.243	.269	.286
1.6	0	.006	.022	.046	.077	.111	.148	.180	.206	.233	.253
1.8	0	.005	.019	.036	.062	.090	.121	.149	.177	.200	.221
2.0	0	.001	.014	.030	.050	.073	.099	.123	.148	.170	.192

TABLE IX b

VALUES OF THE STREAM FUNCTION BELOW THE PLANE OF THE ROTOR FOR V = 0

$\frac{r}{R}$ =	0	.2	.4	.6	.8	1.0	1.2	1.4	1.6	1.8	2.0
$\frac{z}{R}$	ψ/ψ_{total}										
0	0	.057	.226	.510	.906	1.200 .987	.845	.768	.723	.694	.673
-.2	0	.069	.277	.623	.995	.955	.886	.825	.782	.748	.723
-.4	0	.075	.300	.676	.993	.959	.910	.864	.822	.794	.765
-.6	0	.076	.304	.685	.992	.965	.932	.894	.856	.828	.803
-.8	0	.075	.300	.676	.994	.971	.946	.917	.886	.859	.834
-1.0	0	.074	.296	.666	.994	.976	.953	.930	.906	.881	.861
-1.2	0	.073	.292	.657	.995	.978	.959	.939	.917	.899	.882
-1.4	0	.061	.244	.548	.975	.982	.964	.947	.930	.912	.896
-1.6	0	.054	.216	.487	.865	.989	.970	.955	.938	.923	.910
-1.8	0	.047	.187	.420	.747	.995	.980	.965	.950	.935	.922
-2.0	0	.040	.160	.360	.640	1.000	.988	.976	.962	.949	.935

TABLE X

THE NORMAL COMPONENT OF THE

INDUCED VELOCITY IN THE PLANE OF ROTATION

OF A UNIFORMLY LOADED, HOVERING ROTOR

$\frac{r}{R}$	$\frac{V_z}{v}$
1.1	-.44052
1.2	-.22110
1.4	-.09519
1.6	-.04865
1.8	-.03351
2.0	-.02434

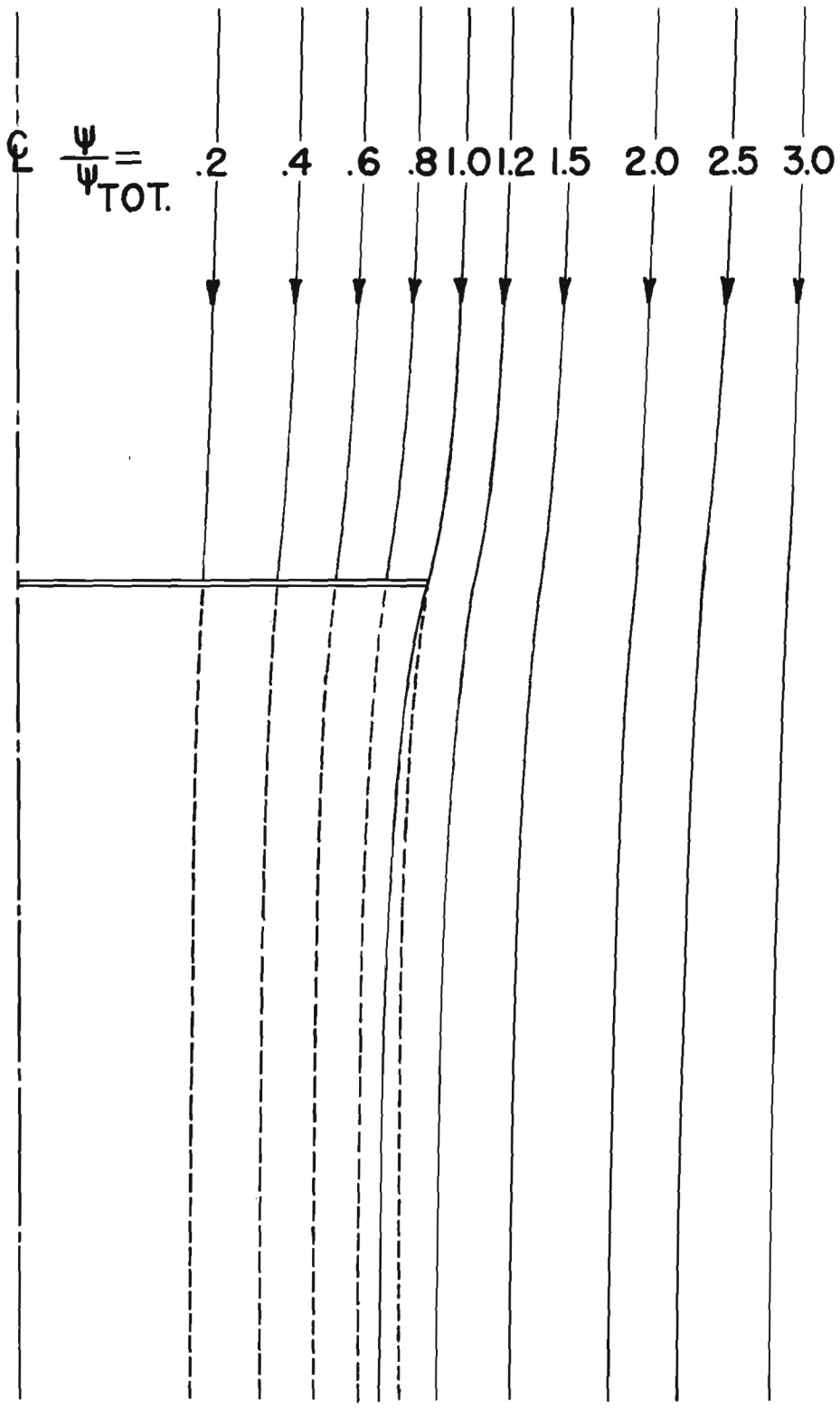

Figure 1. Streamlines for $V = 4\ v = 2\gamma$ for Wake Consisting of a Uniform Vortex-Cylinder.

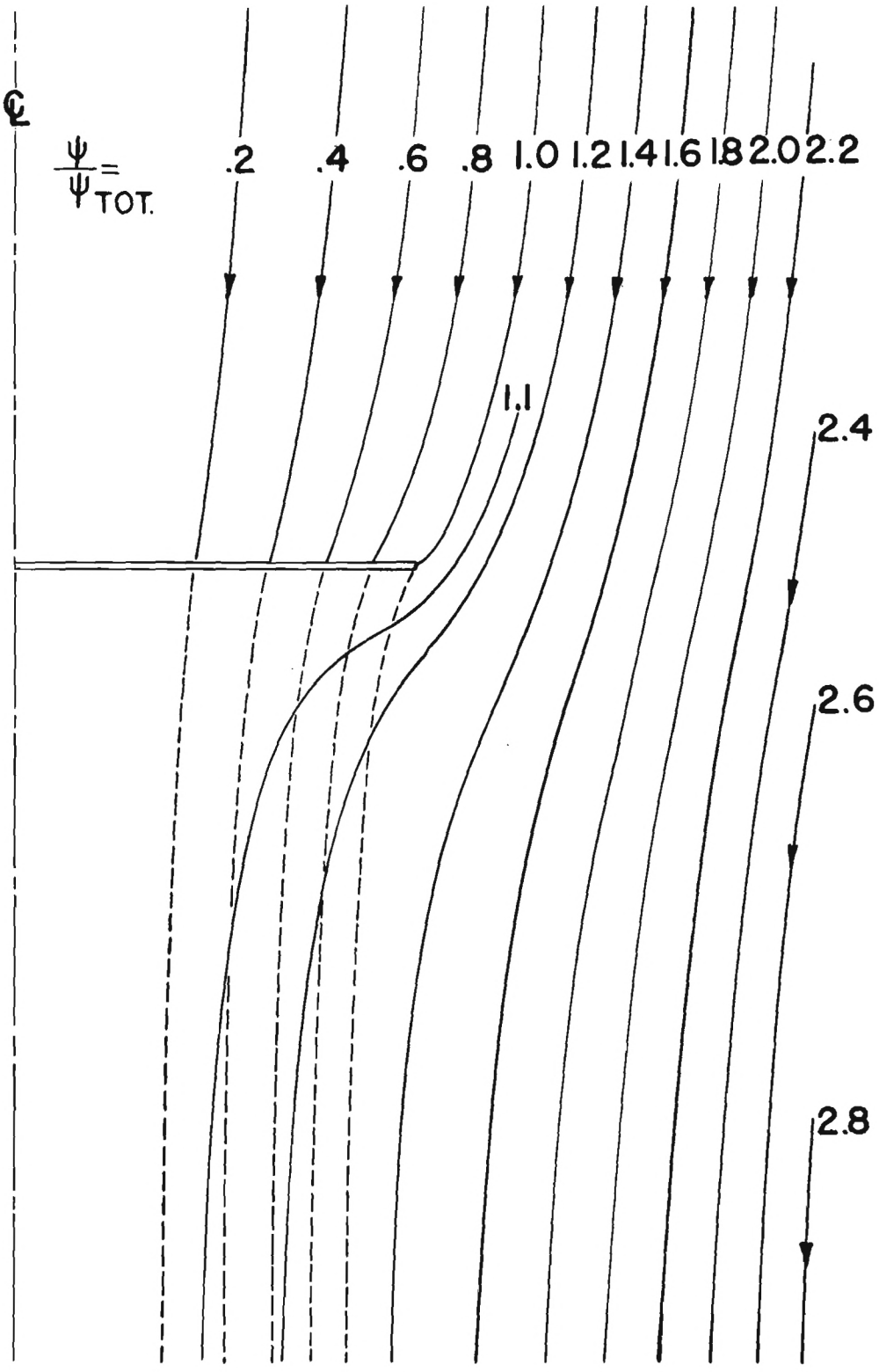

Figure 2. Streamlines for $V = v = \frac{1}{2}\gamma$ for Wake Consisting of a Uniform Vortex-Cylinder.

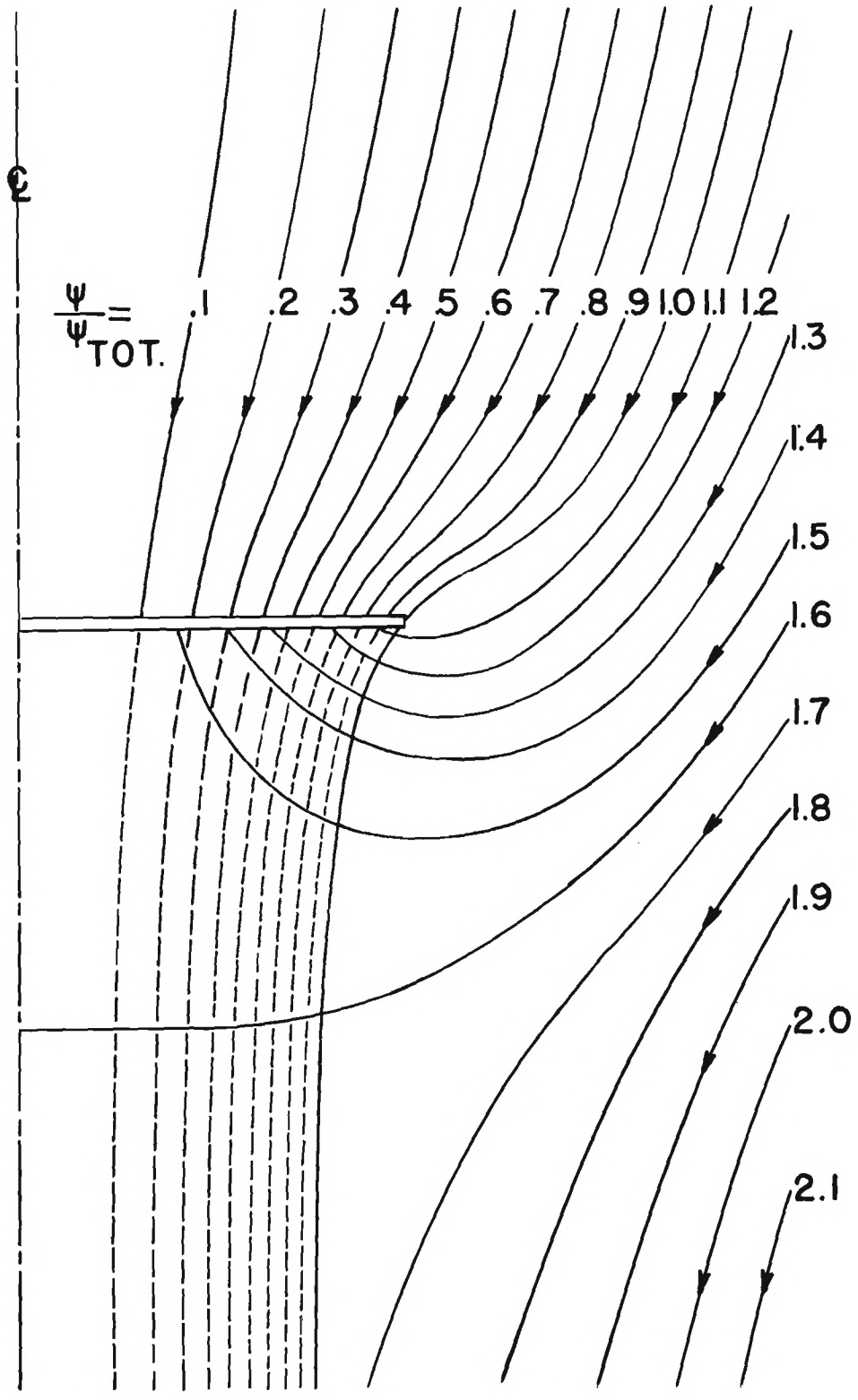

Figure 3. Streamlines for $V = \frac{1}{4}\, v = \frac{1}{8}\gamma$ for Wake Consisting of a Uniform Vortex-Cylinder.

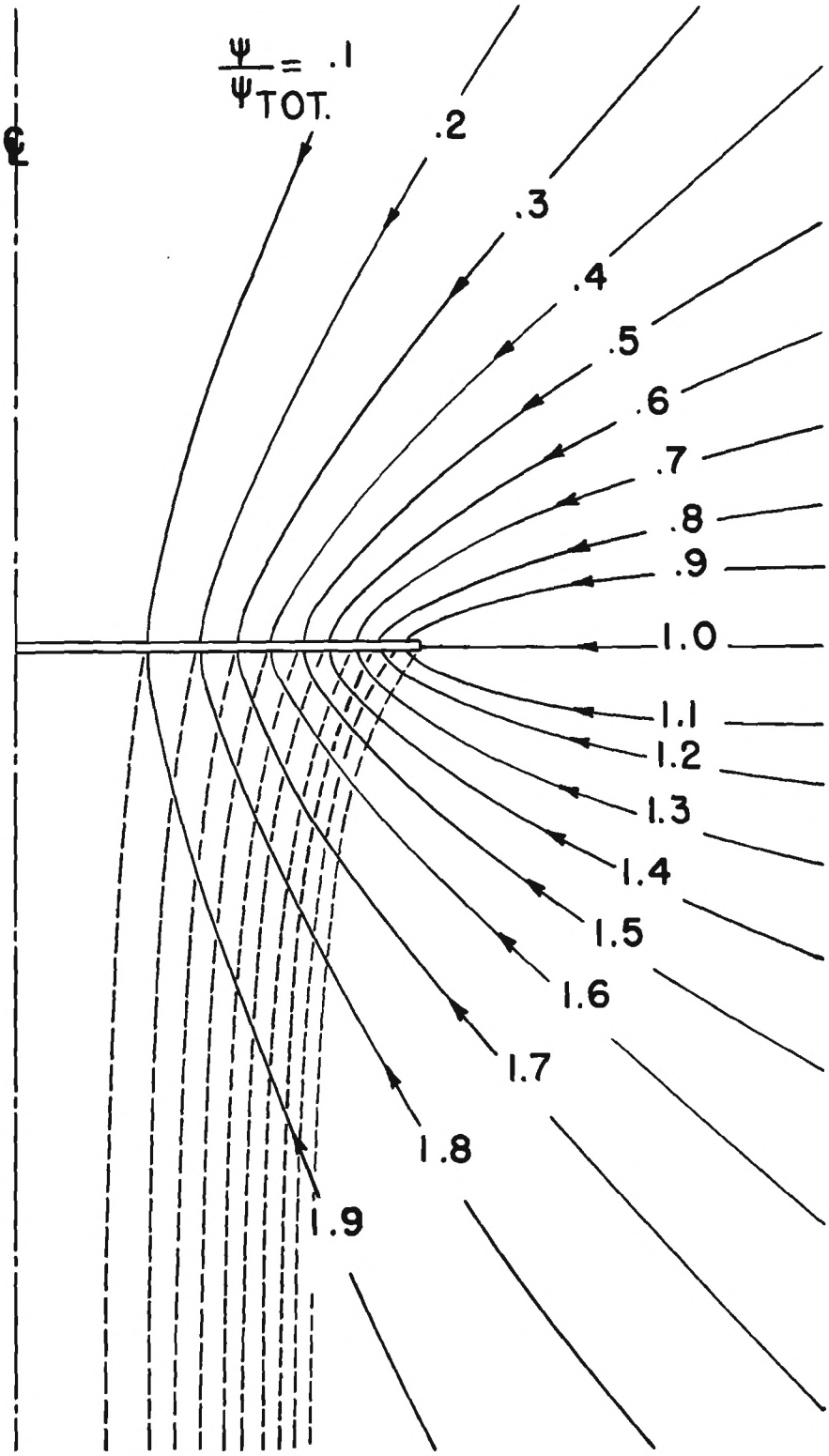

Figure 4. Streamlines for V = 0 (hovering) for Wake Consisting of a Uniform Vortex-Cylinder.

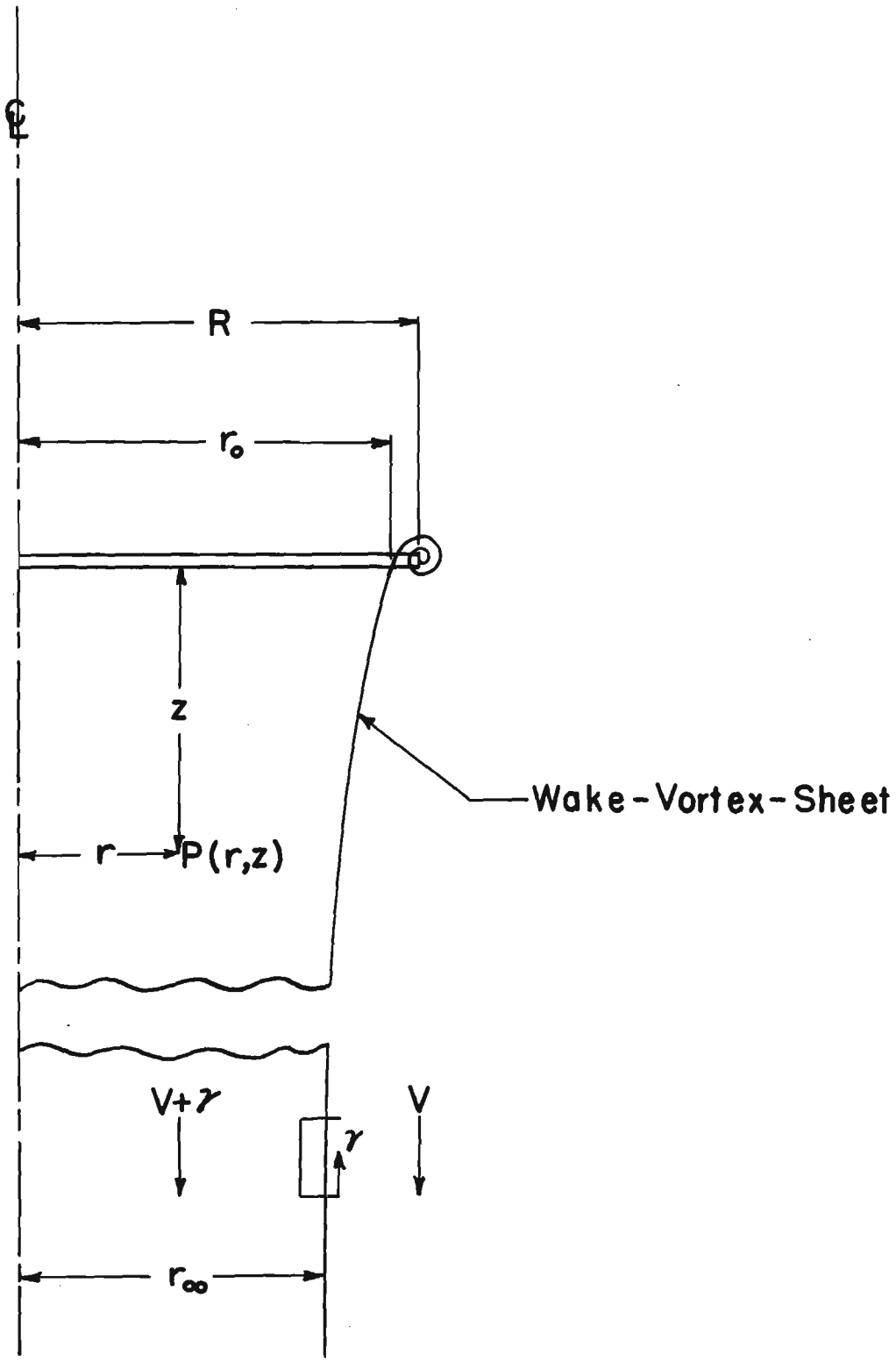

Figure 5. Schematic Section of Wake-Vortex-System.

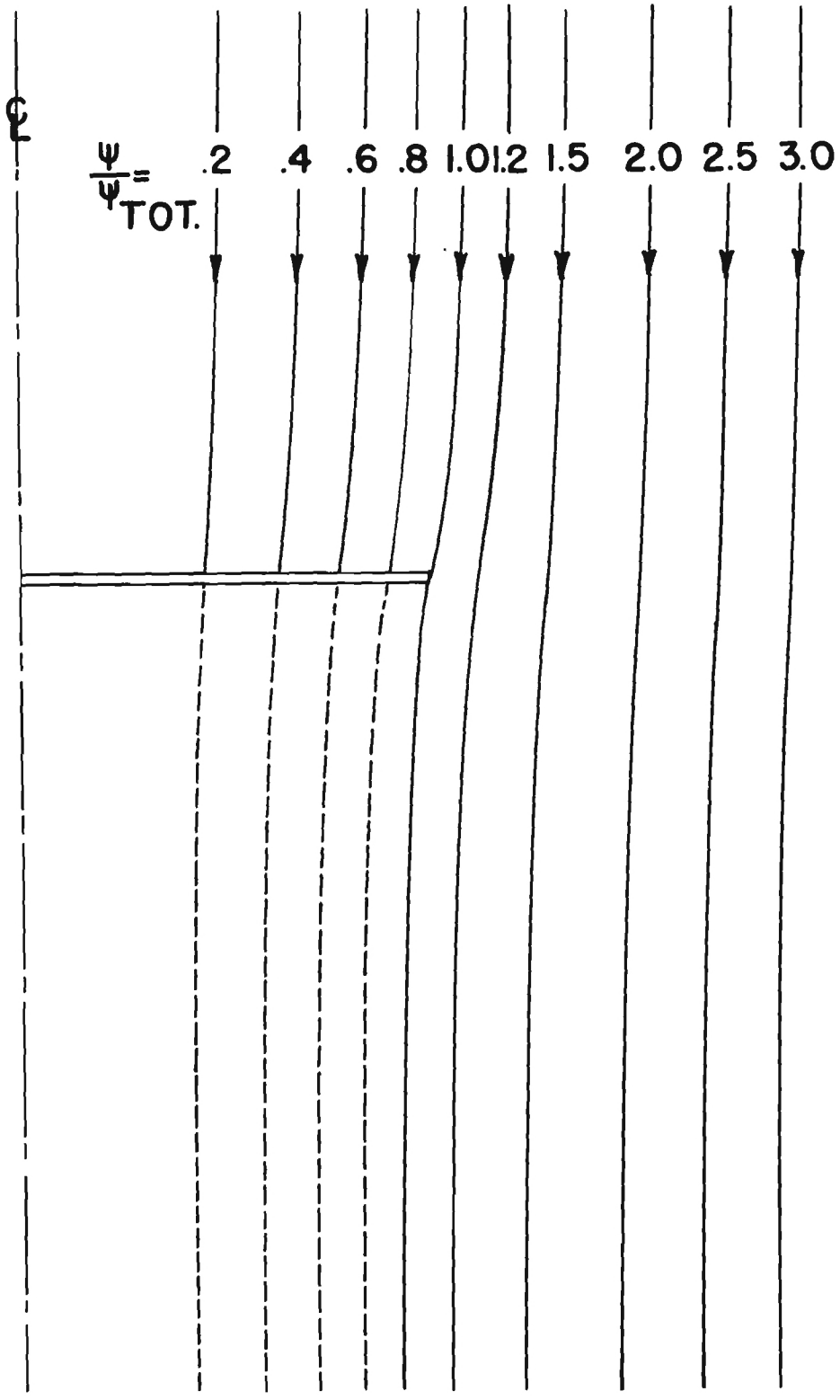

Figure 7. Streamlines for V = 4 v = 2γ.

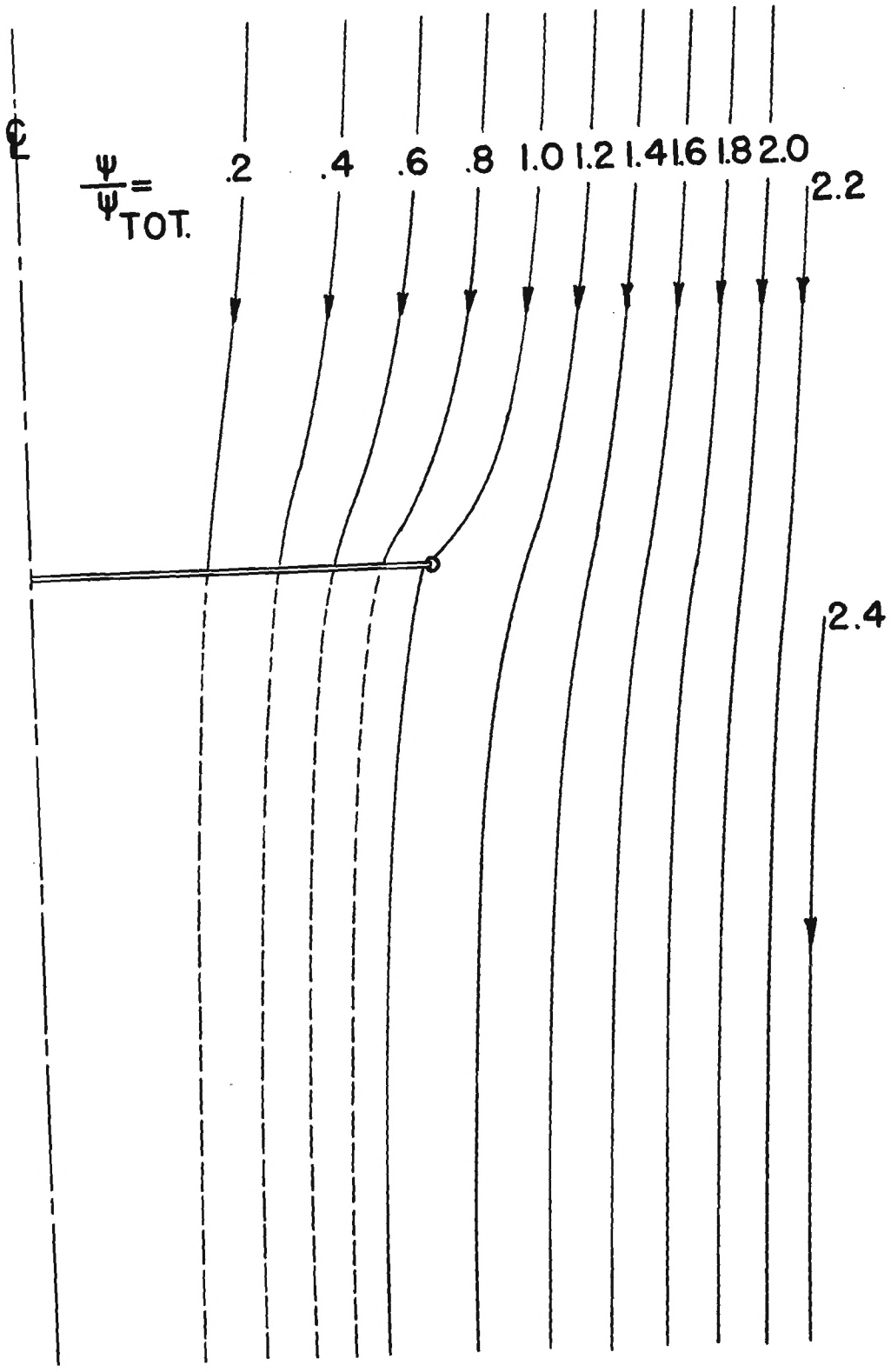

Figure 8. Streamlines for $V = v = \frac{1}{2}\gamma$.

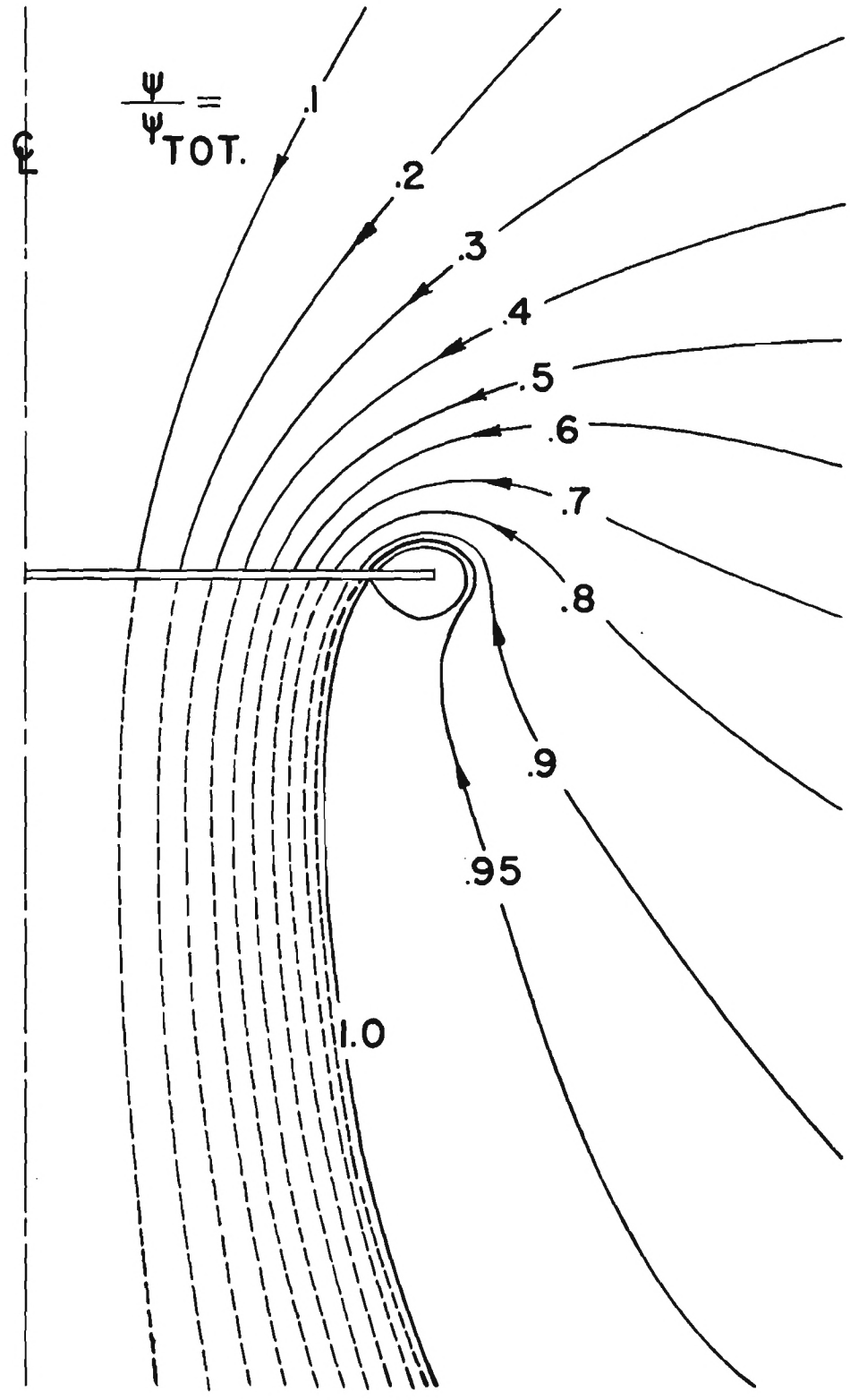

Figure 10. Streamlines for V = 0.

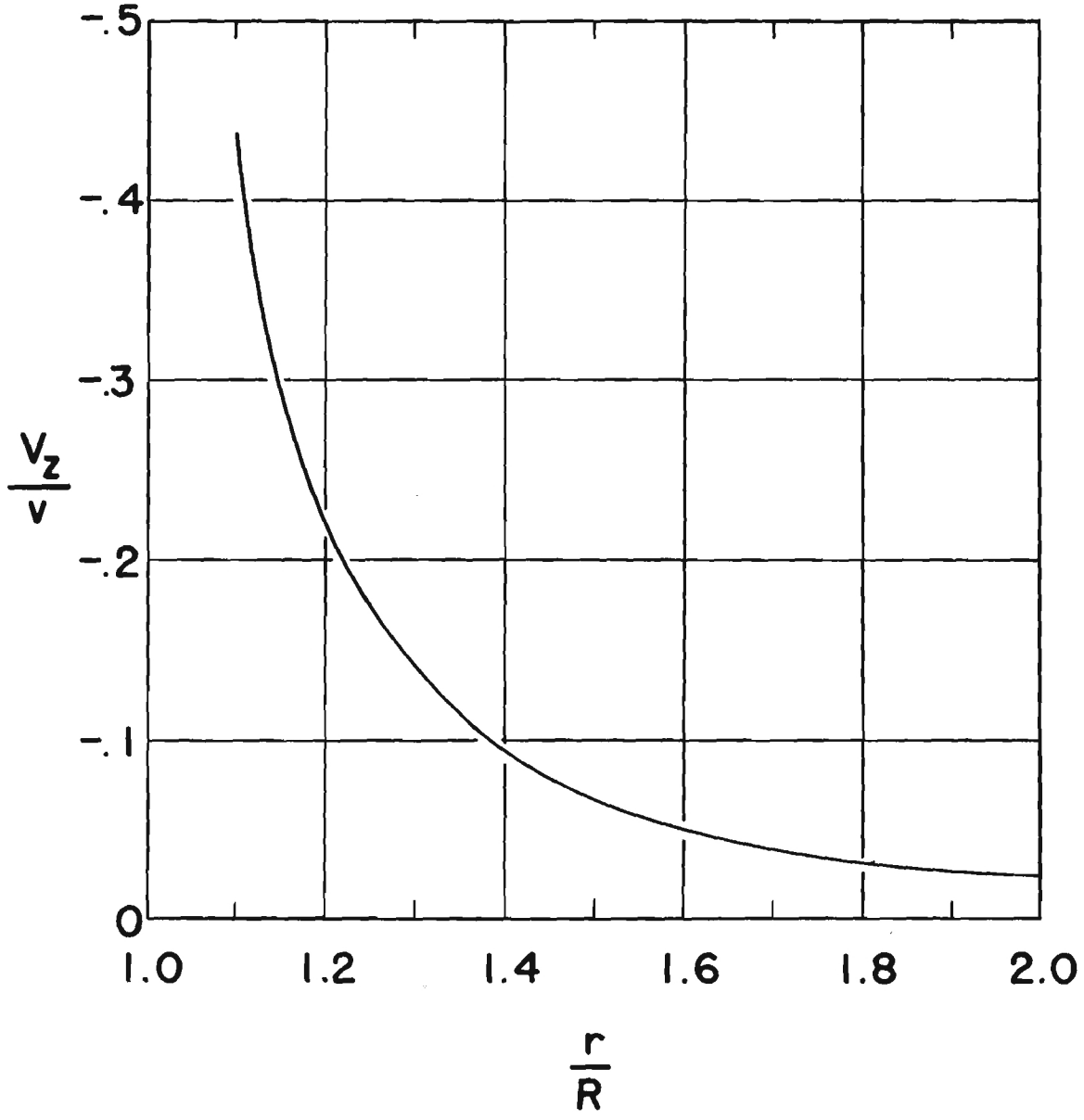

Figure 11. The Normal Component of the Induced Velocity in the Plane of a Uniformly Loaded, Hovering Rotor.

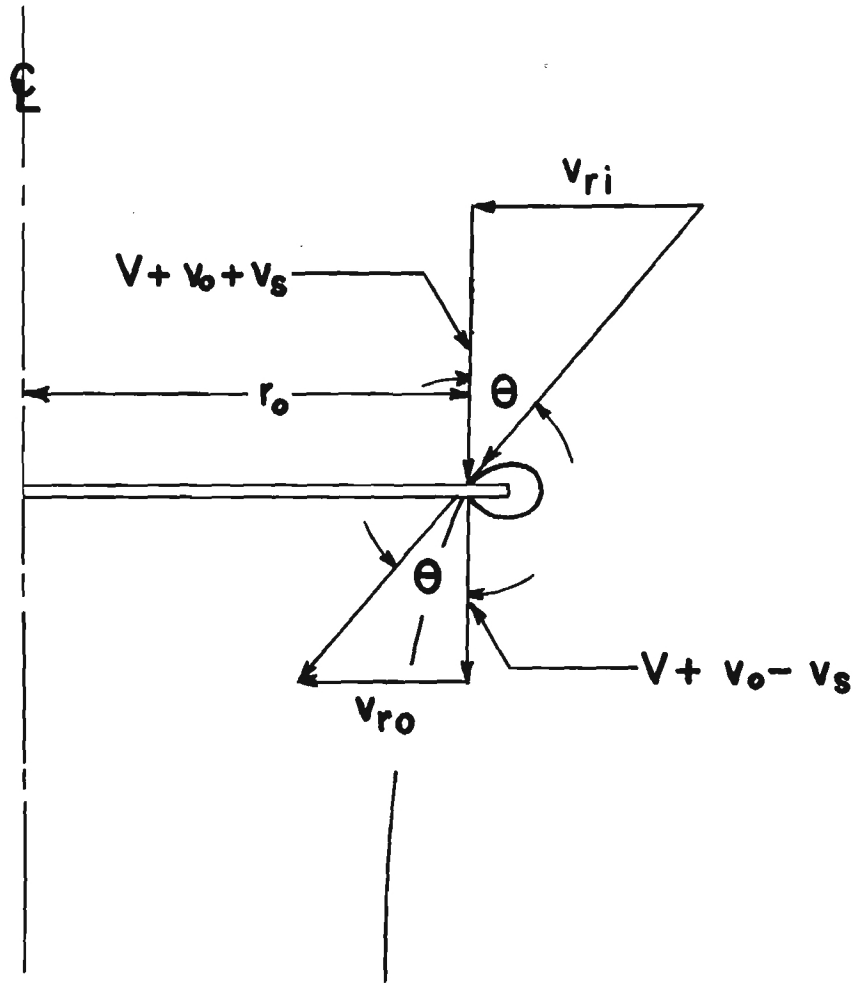

Figure 12. Velocity Diagram at Initial Wake Radius r_o.

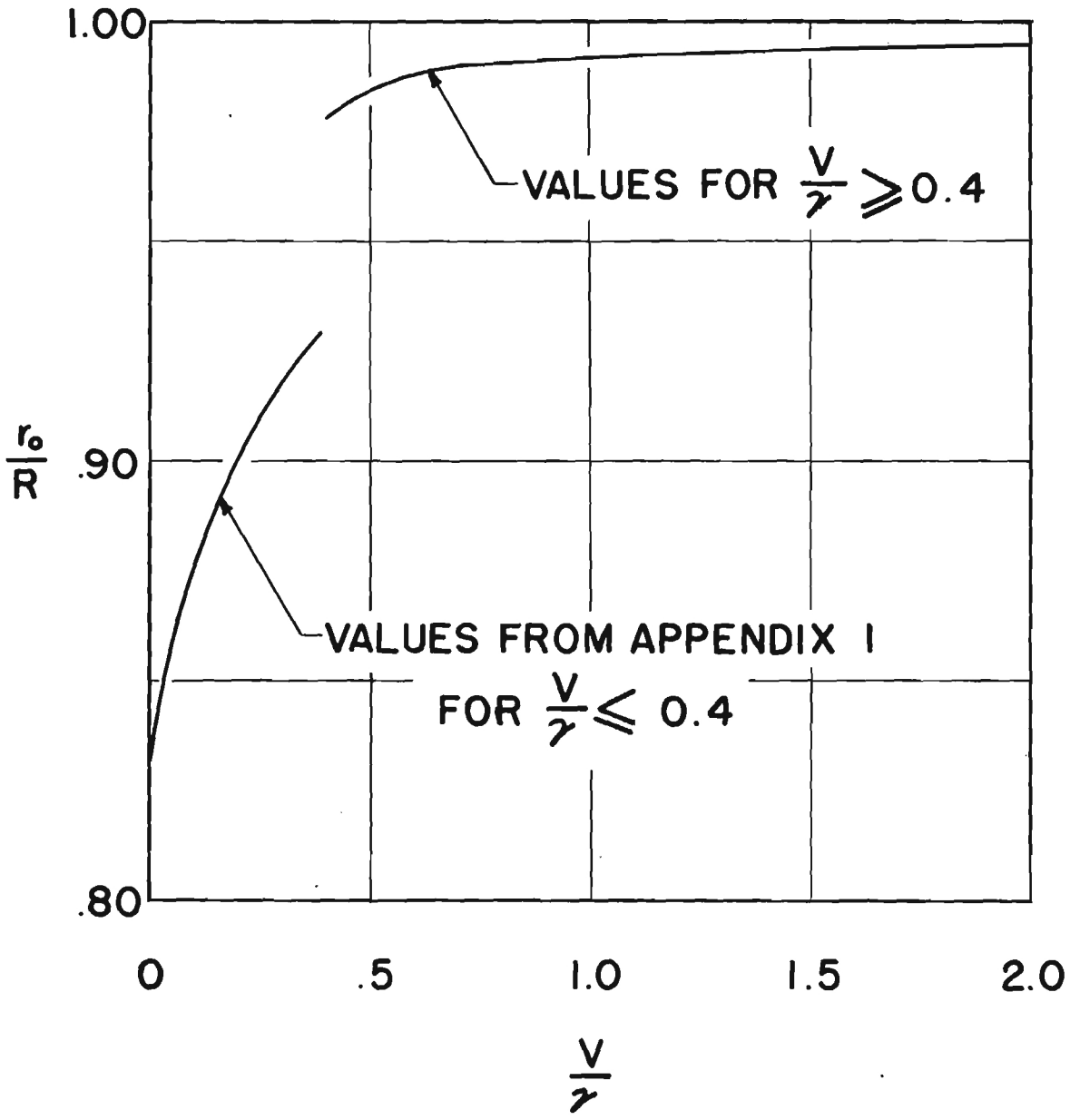

Figure 13. Values of Initial Wake Radius r_o.

Engineering Experiment Station
of the Georgia Institute of Technology
Atlanta, Georgia

A NOTE ON THE FLOW INDUCED BY A ROTOR IN POWER-ON VERTICAL DESCENT

By

Walter Castles, Jr.

Daniel Guggenheim School of Aeronautics

o - o - o - o - o - o - o - o - o - o - o

Contract No. Naw-6230

National Advisory Committee for Aeronautics

March 1957

Engineering Experiment Station
of the Georgia Institute of Technology
Atlanta, Georgia

A NOTE ON THE FLOW INDUCED BY A ROTOR IN POWER-ON VERTICAL DESCENT

By

Walter Castles, Jr.

Daniel Guggenheim School of Aeronautics

o - o - o - o - o - o - o - o - o - o - o

Contract No. Naw-6230

National Advisory Committee for Aeronautics

March 1957

A NOTE ON THE FLOW INDUCED BY A ROTOR IN POWER-ON VERTICAL DESCENT

By Walter Castles, Jr.

Prepared by [redacted]

Walter Castles, Jr., Associate Professor, Daniel Guggenheim School of Aeronautics

Approved by [redacted]

Thomas W. Jackson, Head
Mechanical Sciences Division

Released by [redacted]

Paul K. Calaway, Director
Engineering Experiment Station

TABLE OF CONTENTS

SUMMARY

Approximate equations are derived for the induced power required and blade loading of a lifting rotor operating in the power-on vertical descent range. The approximate relations, which are based upon certain assumptions as to the nature of the flow pattern, yield, for the induced power variation, results which are in general agreement with the avail - able experimental data.

INTRODUCTION

The induced power required in power-on vertical descent as predicted by elementary vortex theory or momentum theory based upon the assumption that a normal columnar wake extends a large distance below the rotor does not agree with the available experimental results as is seen from figure 1 reproduced from reference 1. Furthermore, the observed flow patterns about a rotor operating in power-on vertical descent are of a "vortex-ring" or recirculatory type for which it is necessary to consider the effects of viscosity and the resultant turbulent mixing in order to explain the existance of a steady thrust force.

Although the power-on vertical descent flight range has been of little practical interest in the past, on account of the operational limitations on single-engine helicopters, this flight range may be of considerable interest in the future if vertical landing approaches are required at certain locations for multi-engine helicopters or V.T.O.L. aircraft. A better understanding of the mechanics of the axially symmetric

flows that occur in vertical descent may also be of value in that it may furnish some insight for the more complicated flow patterns that occur in inclined descent.

The present report is an attempt to express the relations between the rotor thrust loadings and induced velocity distributions for the "vortex-ring" or recirculatory flow patterns that exist in power-on vertical descent in a simple approximate manner that is suitable for engineering computations.

NOTATION

a	slope of blade element lift curve
b	number of blades in rotor
c	blade chord at radius r
c_{d_o}	local blade profile drag coefficient at radius r
c_ℓ	blade element lift coefficient
k	slope of a linear variation of rotor disk loading along rotor radius
M'	mass flow through rotor
p	static pressure
p_o	atmospheric pressure
P_c	climb power, rate of change of potential energy
P_i	induced power required
Q	rotor torque

r radius of point on rotor

R rotor radius

T rotor thrust

v axial induced velocity at rotor for case of uniform disk loading

v_o axial induced velocity at hovering for hypothetical rotor with uniform disk loading, $v_o = \sqrt{T/2\ \rho\ \pi\ R^2}$

V freestream velocity or rate of descent

V_o $\sqrt{w/2\ \rho}$

V_i local axial induced velocity at radius r

V_w axial velocity at end of wake core

w disk loading at radius r

x nondimensional radius r/R

Z distance below rotor

θ blade angle at radius r

ρ mass density of air

Ω angular velocity of rotor blades

ANALYSIS

Section A. Case Of Uniform Disk Loading.

Consider the wake of an idealized lifting rotor hovering in a viscous fluid as sketched in figure 2. Let the radial distribution of loading be such as to impart a uniform increase in total pressure to the fluid passing through the rotor. In analogy with the case of the flow of a uniform, stationary, free jet as given in reference 2, there will be a central region of the wake located below the cross-section of minimum radius AA', denoted in figure 2 by the region between the axis and surface AB, within which the turbulent mixing has not penetrated and the flow will be essentially that of a non viscous fluid having a uniform axial velocity.

The mixing region between the sections AB and AC on figure 2 has slightly divergent streamlines and an axial velocity distribution such that the velocity decreases with radius from the wake center-line and with distance from the rotor.

In the case of the stationary free jet, it is remarked in reference 2 that experimental measurements show the static pressure to be "practically constant in the mixing zone" and only very slightly above atmospheric static pressure by the amount of the velocity head of the radial velocity at the outer turbulent mixing boundary AC. It might reasonably be supposed that a very similar situation exists with respect to the uniformity of the static pressure in the mixing region at the boundary of a rotor wake for the portion below the cross-section of minimum wake radius AA'.

It is to be noted that there is some surface, denoted by line AD on figure 2, along which the axial velocity will be constant and some small part, say equal to V, of the axial velocity at the rotor disk. The radial components of velocity along such a surface of constant axial velocity will be small compared to the axial velocity components and will be directed outwards.

Consider now the effect of imposing some small descent velocity, say equal to the previously chosen value V, on the hovering flow pattern of figure 2. Within the core of the wake previously enclosed by the surface AB the principal effect will be similar to that obtained by superposition of the velocity V , that is, there will be a decrease in the axial velocities and little change in the radial velocities somewhat as shown in figure 2. It would appear that the rate of decrease of velocity along a streamline through the turbulent mixing region between surfaces AB and AD will now be greater on account of the path length being shorter, and the previous surface AD, somewhat altered in position, will now constitute a surface of zero axial velocity as sketched in figure 3. It would consequently follow that, except for the effect of the very small radial velocity components, surface AD now constitutes a surface of constant pressure similar to the surface AC which existed in the hovering flow and along which, for the case of the analogous free jet, the static pressure is practically constant. Since surface AD in figure 3 contains the free stream "stagnation point" D at which point the static pressure is very nearly equal to the freestream total head, it might reasonably be supposed that the static pressure in the turbulent mixing region between surfaces AB and AD

on figure 3 is approximately this same value.

As a check on the above hypothesis, static pressure surveys were made through the turbulent mixing region "below" a 12 inch fan operating in the vertical descent condition in the center of the four foot square free jet at the exit of the Georgia Tech Low Turbulence Wind Tunnel. The surveys, at three different radii and free jet velocities along lines parallel to the free jet and fan axes, were taken with a small pitot tube first directed towards the free stream and then toward the fan. The results of the static pressure surveys are given in table 1 and shown in figure 4. The test free-jet velocities were limited to the speed range given in table 1 by the reversal of rotation of the fan at higher velocities and the extreme distortion of the free jet boundaries at lower jet velocities. The lower velocity test conditions gave static pressure peaks in the turbulent mixing region which were below the freestream total head as would be expected from a consideration of the lack of constraint on the free jet boundaries.

It can be seen from figure 4 that, within the accuracy of the present small scale measurements, the static pressure in the turbulent mixing region at the end of the primary wake extending below a rotor operating at small rates of power-on vertical descent is of the order of the freestream total head.

Referring to figure 3 it is seen that, although there will be a certain amount of mixing over the whole of the local flow pattern, the greater part of the loss in total head in a fluid circuit must occur in the region ABDA of figure 3 which is the only region where there is a

large velocity gradient. For steady state conditions to exist, the loss in total head around a fluid circuit must be equal to the change in total head across the rotor or very nearly equal to the rotor disk-loading for the idealized rotor under consideration. Similarly it can be seen from figure 3 that the total head loss along a streamline within the core of the wake and extending from the rotor to section AB should be very small on account of the nearly uniform velocity distributions and consequent absence of turbulent mixing across these wake cross sections.

Consider now the effect of the small rate of vertical descent V on the outer boundary of the turbulent mixing region, represented by section AC on figure 2 for the case of hovering. For the descent case the outer turbulent mixing zone boundary AC of figure 2 will be folded back on itself and shrink to a line coinciding with the edge of the rotor and be replaced by some section indicated by DE on figure 3. The momentum loss of the freestream flow and the vorticity shed by the rotor will be confined within this outer wake boundary DE which, at large distances above the rotor, might be expected to have a diameter very nearly proportional to the cube root of the distance from the rotor in analogy with the wake at large distances behind any three dimensional body exerting a drag force. There will be some dividing streamline, represented schematically by DF on figure 3, outside of which the retarded freestream flow within the outer wake boundary will continue to flow downstream and within which the fluid will recirculate through the rotor. For small rates of descent the upper "stagnation point" F will be a considerable distance above the rotor in a region of very low velocity flow and nearly ambient

static pressure p_o. The total head along the axial entering streamline is thus of the order of p_o. The total head loss in a circuit, which is the same for all the re-entrant streamlines since it must be equal to the assumed uniform disk loading for steady-state flow, is thus very nearly equal to the total head at the end of the wake core at section AB less the total head on an entering streamline, a value of the order of the ambient atmospheric pressure p_o.

Let the velocity at section AB where the static pressure is very nearly equal to the freestream total head be denoted by V_w. Then the disk loading $T/\pi R^2$ is about equal to the total head at section AB minus the entering total head p_o. Thus

$$\frac{T}{\pi R^2} \approx \frac{1}{2} \rho V_w^2 + \frac{1}{2} \rho V^2 \tag{1}$$

or

$$V_w \approx \sqrt{\frac{2T}{\rho \pi R^2} - V^2} \tag{2}$$

It is to be noted that for the greater part of the energy loss in a circuit to occur in the high shear region between the section AB, where the total head is about $p_o + \frac{1}{2} \rho (V_w^2 + V^2)$, and section AD, where the total head is about $p_o + \frac{1}{2} \rho V^2$ plus some small radial velocity head, it is necessary that

$$V_w \geqq V \tag{3}$$

or from equation 2

$$V \leqq \sqrt{\frac{T}{\rho \pi R^2}} \tag{4}$$

The requirement that the downward directed wake core velocity V_w at section AB on figure 3 be at least equal in order of magnitude to the freestream velocity V can perhaps be seen more clearly from the standpoint of vortex theory. The rate of transport of vorticity downward across some horizontal plane, say Y - Y on figure 3, between sections AB and AD must be at least equal to the subsequent rate of transport of the same vorticity upwards across Y - Y between sections AD and DE for the presently assumed steady state viscous flow. If the respective layers of vorticity be considered to compose diffuse "vortex sheets", the vertical rates of transport of vorticity are equal to one-half the square of the respective vertical components of "sheet strength" or difference in vertical component of velocity across the "sheets", since the axial velocity component on the dividing section AD is zero by definition. If, as a first approximation, the effects of radial induced velocity components be neglected, the vertical velocity difference across the outer wake "vortex sheet" between sections AD and DE is equal to the freestream velocity V, and thus the vertical velocity difference V_w across the inner wake "sheet" between sections AB and AD must be, to the same order of approximation, at least as great as V.

Another equation relating the thrust T and the wake core velocity V_w can be obtained from a consideration of the momentum exchange. Since linear momentum is preserved in the turbulent mixing process and the fluid recirculates, the rotor thrust can be no less than the rate of transport of axial momentum across section AB where the velocity is V_w and the total head is above the freestream value. Let v be the mean axial component of induced velocity at the rotor. Then the mean resultant axial

velocity at the rotor is $v - V$ and the mass flow M' through the rotor is

$$M' = \rho \pi R^2 (v - V) \tag{5}$$

Thus the rate of change of axial momentum is

$$T = \rho \pi R^2 (v - V) V_w \tag{6}$$

Substituting the value of V_w from equation 2 in equation 6 and solving for the thrust

$$T = \rho \pi R^2 (v - V) \left[(v - V) + \sqrt{(v - V)^2 - V^2} \right] \tag{7}$$

Solving equation 7 for the induced velocity v gives

$$v = V + \frac{v_o^2}{\sqrt{v_o^2 - \left(\frac{V}{2}\right)^2}} \tag{8}$$

where

$$v_o = \sqrt{\frac{T}{2 \rho \pi R^2}}$$

or in nondimensional form

$$\frac{v}{v_o} = \frac{V}{v_o} + \frac{1}{\sqrt{1 - \frac{1}{4}\left(\frac{V}{v_o}\right)^2}} \tag{9}$$

It follows from equation 4 that the flight range for which equations 7, 8, and 9 are useful is

$$0 \leqq \frac{V}{v_o} \leqq \sqrt{2} \tag{10}$$

Values of the nondimensional induced velocity v/v_o versus the nondimensional rate of descent V/v_o are given in table 2 and shown in figure 5 along with the experimental curve for the values obtained in reference 1 for a model rotor with 12 degrees blade twist and thus nearly uniform loading over the outer blade sections.

It is to be noted that for the rotor with uniform disk loading the relation

$$\frac{T\,v}{T\,v_o} = \frac{P_i}{T\,v_o} = \frac{v}{v_o} \qquad (11)$$

where P_i = induced power required

holds so that figure 5 also gives the induced power ratios as indicated.

Section B. - Case of Triangular Distribution of Disk Loading Along Rotor Radius.

The problem of finding the radial distribution of load, induced velocity, and thus the induced power required for a rotor with given blade geometry operating at a given rate of power-on descent by the method to be derived in the subsequent section involves the solution of a fourth degree equation for the tangent of the inflow angle at the blade elements. Consequently the analysis of the present section will be restricted to a solution for the induced power required for a rotor with a given triangular distribution of disk loading along the rotor radius. This load distribution corresponds closely to that of a lifting rotor having blades with zero or small twist and it thus appears that, whereas the case of uniform loading is purely hypothetical, the case of triangular loading may be of considerable interest for purposes of performance estimation.

Let

$$w = k \left(\frac{T}{\pi R^2} \right) x \tag{12}$$

be the local disk loading at nondimensional radius x.

Then

$$T = 2 \pi k \left(\frac{T}{\pi R^2} \right) R^2 \int_0^1 x^2 \, dx \tag{13}$$

Integrating, solving the result for the constant k and substituting the value of k back in equation 12 gives

$$w = \frac{3}{2} \left(\frac{T}{\pi R^2} \right) x \tag{14}$$

Define

$$V_o = \sqrt{\frac{w}{2 \rho}} \tag{15}$$

in analogy with the value $v_o = \sqrt{\frac{T}{2 \rho \pi R^2}}$ for the hypothetical case of uniform loading.

Then assuming that there is no turbulent mixing in the primary wake core or, what amounts to the same thing, applying the working hypotheses of the "independence of blade elements" over the outer rotor annuli for which equation 9 applies, gives

$$\frac{V_i}{V_o} = \frac{V}{V_o} + \frac{1}{\sqrt{1 - \frac{1}{4} \left(\frac{V}{V_o} \right)^2}} \tag{16}$$

where V_i is the local axial component of induced velocity at radius r for the radii for which

$$0 \leqq \frac{V}{V_o} \leqq \sqrt{2} \tag{17}$$

Substituting the values of w and V_o from equations 14 and 15 in equation 17 it is found that equation 16 is applicable for the nondimensional radii

$$\frac{1}{3}\left(\frac{V}{v_o}\right)^2 \leqq x \leqq 1 \tag{18}$$

The nondimensional induced power $(P_i)_1 / T\, v_o$ required for the outer rotor annulus for which equation 18 holds is thus

$$\frac{(P_i)_1}{T\, v_o} = \frac{2\pi R^2}{T\, v_o} \int_{\frac{1}{3}\left(\frac{V}{v_o}\right)^2}^{1} w\, V_i\, x\, dx \tag{19}$$

or

$$\frac{(P_i)_1}{T\, v_o} = 3 \int_{\frac{1}{3}\left(\frac{V}{v_o}\right)^2}^{1} \left[\frac{V}{v_o} + \frac{3x}{\sqrt{6x - \left(\frac{V}{v_o}\right)^2}}\right] x^2\, dx \tag{20}$$

Integrating equation 20 gives

$$\frac{(P_i)_1}{T\, v_o} = \left(\frac{V}{v_o}\right) - \frac{133}{1890}\left(\frac{V}{v_o}\right)^7 +$$

$$+ \frac{\sqrt{6 - \frac{V}{v_o}^2}\left[1080 - 216\left(\frac{V}{v_o}\right)^2 + 192\left(\frac{V}{v_o}\right)^4 + 4\left(\frac{V}{v_o}\right)^6\right]}{2520} \qquad (21)$$

It follows from setting $x = 1$ in equation 18 that the range of vertical descent for which equation 21 applies over some outer annulus of the rotor is

$$0 \leqq \frac{V}{v_o} \leqq \sqrt{3} \qquad (22)$$

For the flight range specified by equation 22 the total pressure just beneath the rotor and inboard of nondimensional radius $x = \frac{1}{3}\left(\frac{V}{v_o}\right)^2$ is less than the static pressure in the turbulent mixing region at the lower end of the wake core. If the effects of turbulent mixing be neglected within the wake core as was implied by the use of the "independence of blade elements" in deriving equation 21, this inner circle, for which $0 \leqq x \leqq \frac{1}{3}\left(\frac{V}{v_o}\right)^2$, constitutes a closed region as far as energy transfer from the rotor to the fluid is concerned, since the fluid passing through these inner annuli would not have sufficient energy to penetrate the adverse pressure gradient above the turbulent mixing region. The total rotor torque due to lift for the sections of blades within the circle must thus be assumed to be zero. Using the hypothesis that the power input to the inner circle of the rotor for which $0 \leqq x \leqq \frac{1}{3}\left(\frac{V}{v_o}\right)^2$ is negligible, it follows that the induced power $(P_i)_2$ for this region is equal to the product of the thrust over the region and the rate of descent. Thus

$$(P_i)_2 = 2\pi V \int_0^{\frac{1}{3}\left(\frac{V}{v_o}\right)^2 R} w\, r\, dr \qquad (23)$$

Substituting the value of the disk loading w from equation 14 and dividing both sides by $T\,v_o$ gives the nondimensional induced power increment

$$\frac{(P_i)_2}{T\,v_o} = 3\left(\frac{V}{v_o}\right)\int_0^{\frac{1}{3}\left(\frac{V}{v_o}\right)^2} x^2\,dx = \frac{1}{27}\left(\frac{V}{v_o}\right)^7 \qquad (24)$$

The nondimensional induced power for the rotor with triangular loading operating in the power-on vertical descent range is the sum of the parts given by equations 21 and 24. The computed values are given in table 3. Figure 6 shows the comparison of the computed values with the experimental values given in reference 1 for a 6 foot diameter constant chord model rotor with untwisted blades. The values obtained on a full scale flight test of a rotor with untwisted blades as given in reference 3 are also shown. The flight test results include the effects of fuselage drag which tend to make these experimental values too large at low descent velocities and probably too small at large descent velocities.

Section C. - Loading Over Outer Blade Elements of a Rotor With Arbitrary Blade Geometry.

From two dimensional airfoil theory it follows that, for small inflow angles, the thrust dT on a rotor annulus of radius r and width dr is

$$dT = \frac{1}{2}\,\rho\,a\,b\,c\,(\Omega r)^2\left[\theta - \left(\frac{V_i - V}{\Omega r}\right)\right]dr \qquad (25)$$

where c_{d_o} = profile drag coefficient for blade element at radius r and lift coefficient

$$c_\ell = a\left[\theta - \left(\frac{V_i - V}{\Omega r}\right)\right] \tag{29}$$

The simplest consistent assumption for the distribution of the inflow angle over the inner radii for which $V_i < 2V$ in equation 28 is that $V_i = V$ for this inboard region. However such a zero value for the inflow angle really constitutes a weighted average for the induced torque rather than an actual distribution. Consequently, if this assumption is made, it would be necessary to assume also a reasonable blade thrust distribution such as a parabolic variation from the calculated value at the limiting radius $x = \frac{1}{3}\left(\frac{V}{v_o}\right)^2$ to a zero value at the hub. It appears that the above approximation should be adequate for small rates of vertical descent where the limiting radius is small and the thrust in question is an immaterial part of the total.

CONCLUDING REMARKS

The present analysis appears to yield results for the variation of induced power with rate of vertical power-on descent for a lifting rotor which are in satisfactory agreement with the available experimental data. It may thus be useful in performance estimation and in furnishing some insight into the mechanics of the "vortex ring" or recirculatory flows that occur in these flight conditions.

As there are no experimental blade load or direct induced velocity measurements available for comparison, some judgement should be exercised in the application of the theoretical blade load equations given in Section C.

It might be pointed out that the present analysis gives no steady state solution for the (hypothetical) rotor with uniform disk loading operating in the power-on descent range $\frac{V}{v_o} > \sqrt{2}$. In the case of any actual lifting rotor the disk loading will go to zero at the hub and the radial distribution of disk loading will be dependent upon the rate of descent. Consequently it might be expected that the range of stable operation for any actual rotor will be larger than that for the hypothetical case of uniform loading.

The question arises as to why an analysis of the present type should predict the ideal autorotation point or rate of descent at which the induced power required is equal to the rate of decrease of potential energy and the resultant mean normal component of velocity at the rotor

is consequently zero. One explanation of this question might be as follows.

The idealized flow pattern or perfect fluid flow patterns for a lifting rotor operating at the ideal autorotation point would have to be of the Kirchhoff or "free streamline" type where the whole of the wake above the rotor and extending downstream to infinity constitutes a closed energy region. In the corresponding viscous fluid flow pattern a closed energy region bounded by the turbulent mixing zone would also exist within which the flow could be considered to be of perfect fluid type. However, in this case it would be a closed region bounded by the upper surface of the rotor and some surface of revolution extending a limited distance downstream.

The present analysis hypothecates the existence of such a closed energy region enveloping the inboard blade elements at some small rate of vertical descent and increasing in diameter with rate of descent until, at the ideal autorotation point, it includes the full rotor radius. The growth in diameter of the closed energy region with rate of descent would necessarily be determined by the external flow and consequently the ideal autorotation point would occur when the downflow through the outer rotor annulus vanishes. The prediction of the rate of descent at which the downflow through the outer blade elements disappears thus gives the rate of descent at the ideal autorotation point.

REFERENCES

1. Castles, Walter, Jr. and Gray, Robin B.: Empirical Relation Between Induced Velocity, Thrust, and Rate of Descent of a Helicopter Rotor As Determined By Wind-Tunnel Tests on Four Model Rotors. NACA TN 2474

2. Prandtl, L.: The Mechanics of Viscous Fluids. Spread of Turbulence. Vol. III of Aerodynamic Theory, div. G., sec. 25, W. F. Durand, ed., Juluis Springer (Berlin), 1935, pp. 170-175.

3. Stewart, W.: Flight Testing of Helicopters. Journal R.A.S., vol. 52, no. 449, May 1948, pp. 261-292; discussion, pp. 293-304.

Table 1. - Results Of Static Measurements

Run 1 - Fan 5 Diameters from Free Jet Exit. Free Jet Velocity = 17.5 ft/sec. Survey along a line at $\frac{1}{2}$ R from axis. The starred values are for pitot facing fan.

$\frac{Z}{D}$	$\frac{p - p_o}{\frac{1}{2} \rho V^2}$
0.96	0.83
1.17	1.00
1.33	0.92
1.50	.83
1.67	.75
2.50	.25
3.33	.08

$\frac{Z}{D}$	$\frac{p^* - p_o}{\frac{1}{2} \rho V^2}$
0.42	0.25
.58	.33
.75	.67
.83	.75
.92	.83
1.00	.92
1.08	1.00
1.17	1.00
1.33	.92

Run 2 - Fan 4 Diameters from Free Jet Exit. Free Jet Velocity = 16.5 ft/sec. Survey along a line at 0.6 R from axis.

$\frac{Z}{D}$	$\frac{p - p_o}{\frac{1}{2} \rho V^2}$
0.58	0.60
.83	.82
1.33	.97
1.83	.67
2.33	.40
2.83	.25
3.33	.12

$\frac{Z}{D}$	$\frac{p^* - p_1}{\frac{1}{2} \rho V^2}$
0.25	0.60
.46	.64
1.00	.97
1.50	.75
2.00	.45

Run 3 - Fan 5 Diameters from Free Jet Exit. Free Jet Velocity = 14.2 ft/sec. Survey along a line at 1/3 R from axis

$\frac{Z}{D}$	$\frac{p - p_o}{\frac{1}{2} \rho V^2}$
1.13	0.75
1.25	.75
1.33	.87
1.42	1.00
1.50	1.00
1.67	1.00
2.00	.75
2.50	.50
3.33	.12

$\frac{Z}{D}$	$\frac{p^* - p_o}{\frac{1}{2} \rho V^2}$
0.58	0.00
.83	0.00
1.08	.25
1.17	.37
1.25	.75
1.33	.87
1.42	.87
1.50	.75

Table 2. - Values of the Nondimensional Induced Velocity Versus Nondimensional Rate of Descent For Idealized Rotor with Uniform Loading

V/v_o	v/v_o
0.0	1.000
.2	1.205
.4	1.420
.6	1.658
.8	1.892
1.0	2.155
1.2	2.450
1.4	2.801
$\sqrt{2}$	$2(\sqrt{2}$

Table 3. - Theoretical Values Of The Nondimensional Induced Power Ratio $P_i/T\,v_o$ Versus Nondimensional Rate of Descent V/v_o for Rotor with Triangular Distribution of Disk Loading Along Radius

V/v_o	$P_i/T\,v_o$
0	1.049
.2	1.238
.4	1.407
.6	1.568
.8	1.737
1.0	1.907
1.2	2.079
1.4	2.185
1.6	2.069
1.65	1.974
1.70	1.841
$\sqrt{3}$	$\sqrt{3}$

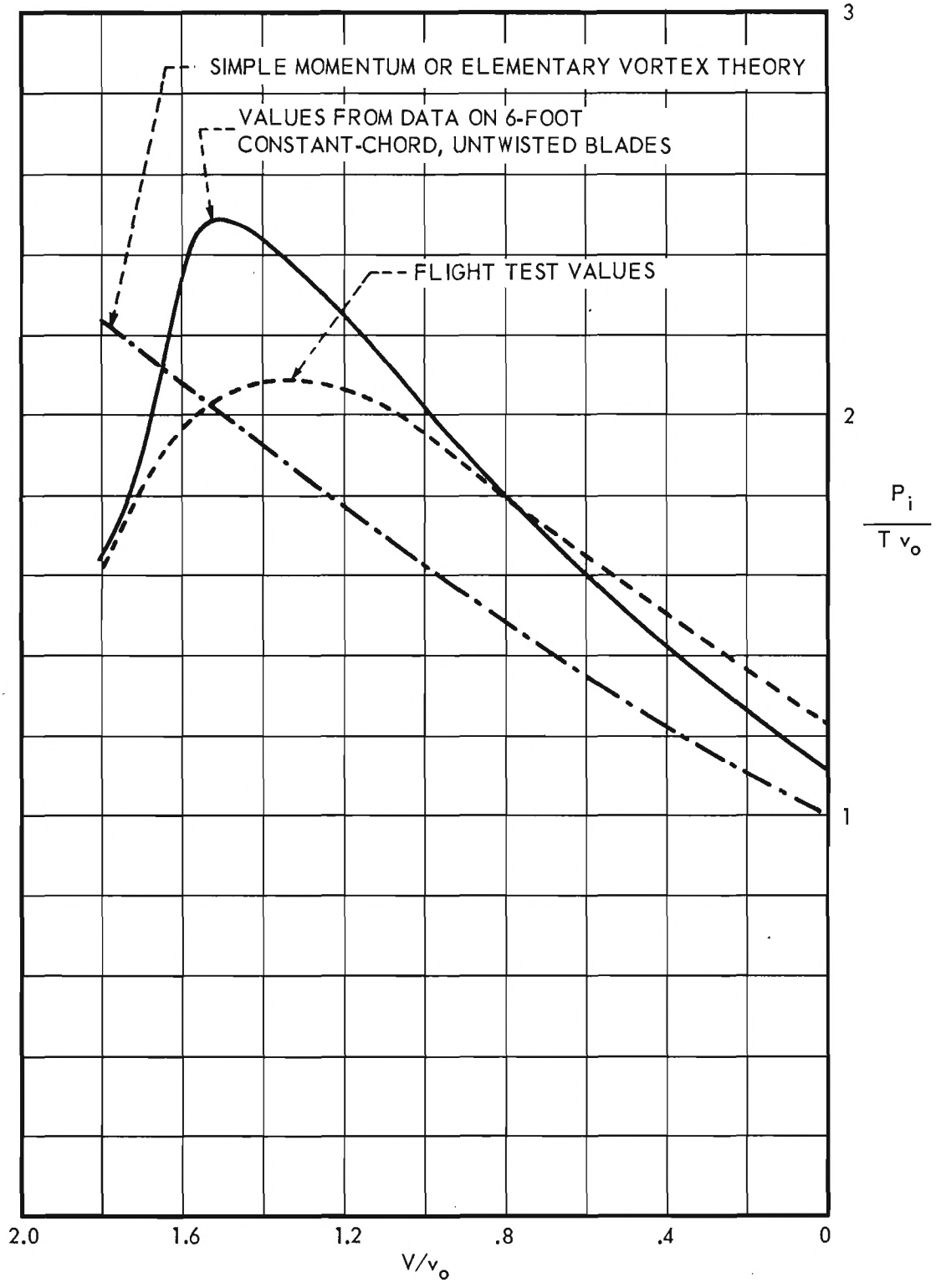

Figure 1. Comparison of Values of the Nondimensional Induced Power for Power-on Vertical Descent Given by Simple Momentum Theory or Elementary Vortex Theory with Experimental Values.

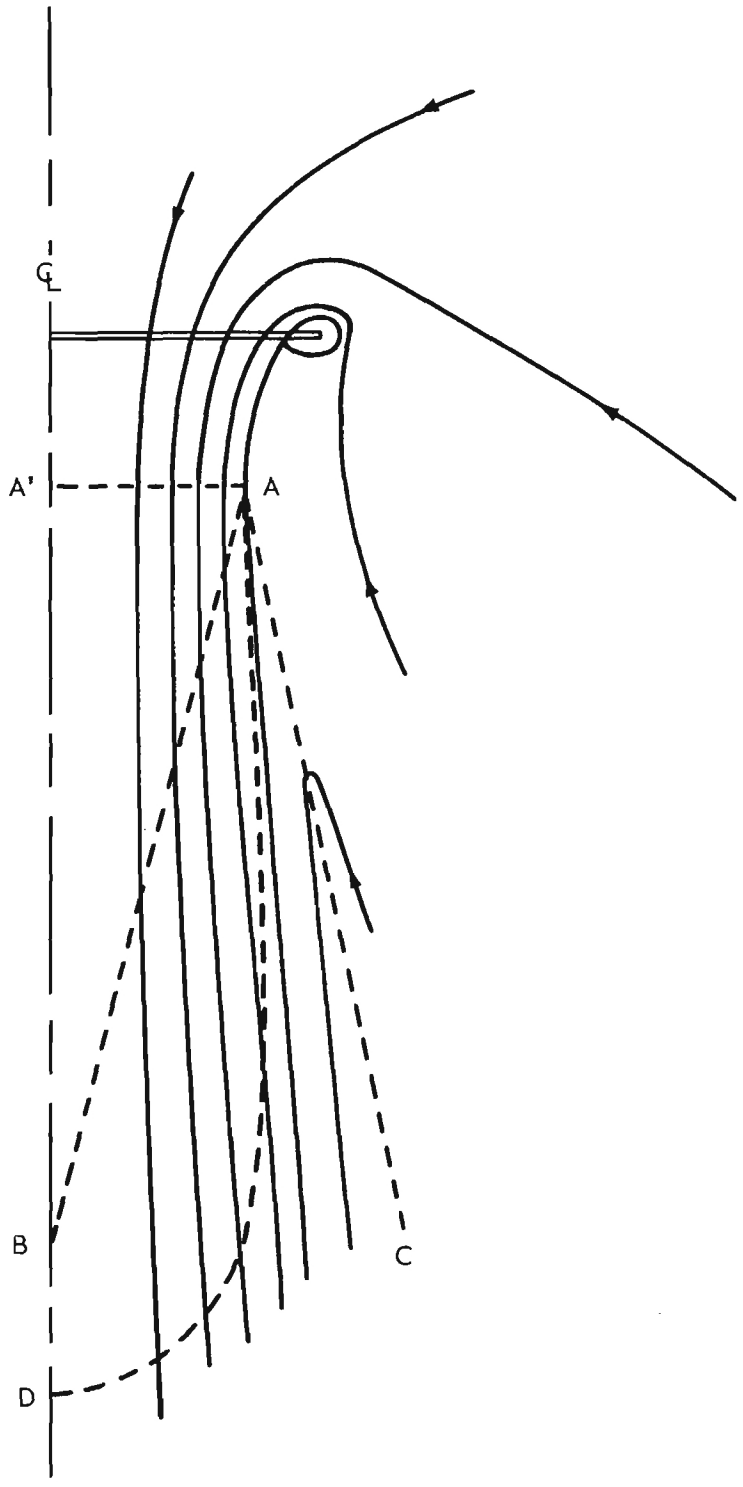

Figure 2. Sketch of Idealized Hovering Flow Pattern.

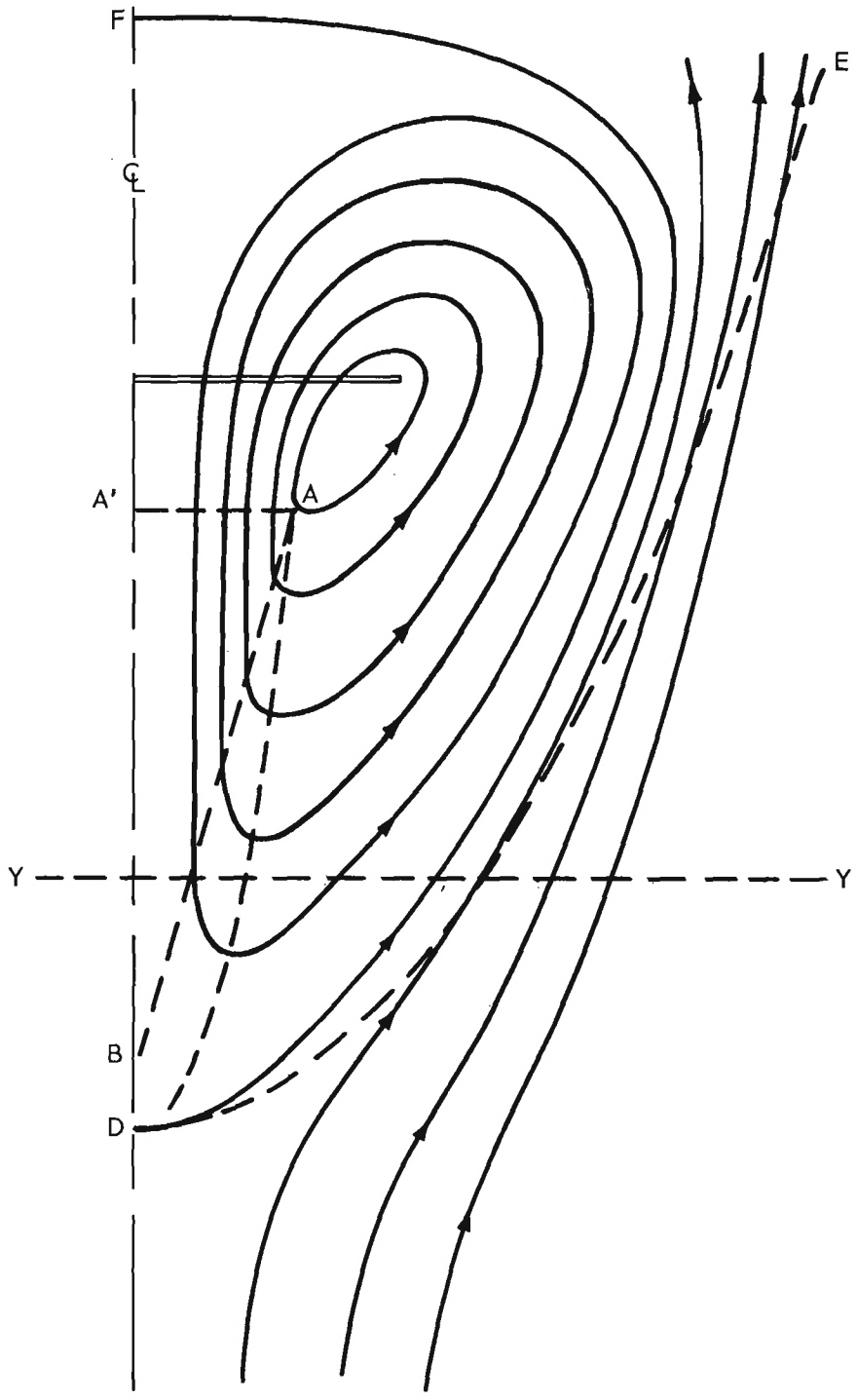

Figure 3. Sketch of Idealized Flow Pattern At Small Rate of Vertical Descent for Rotor with Uniform Loading.

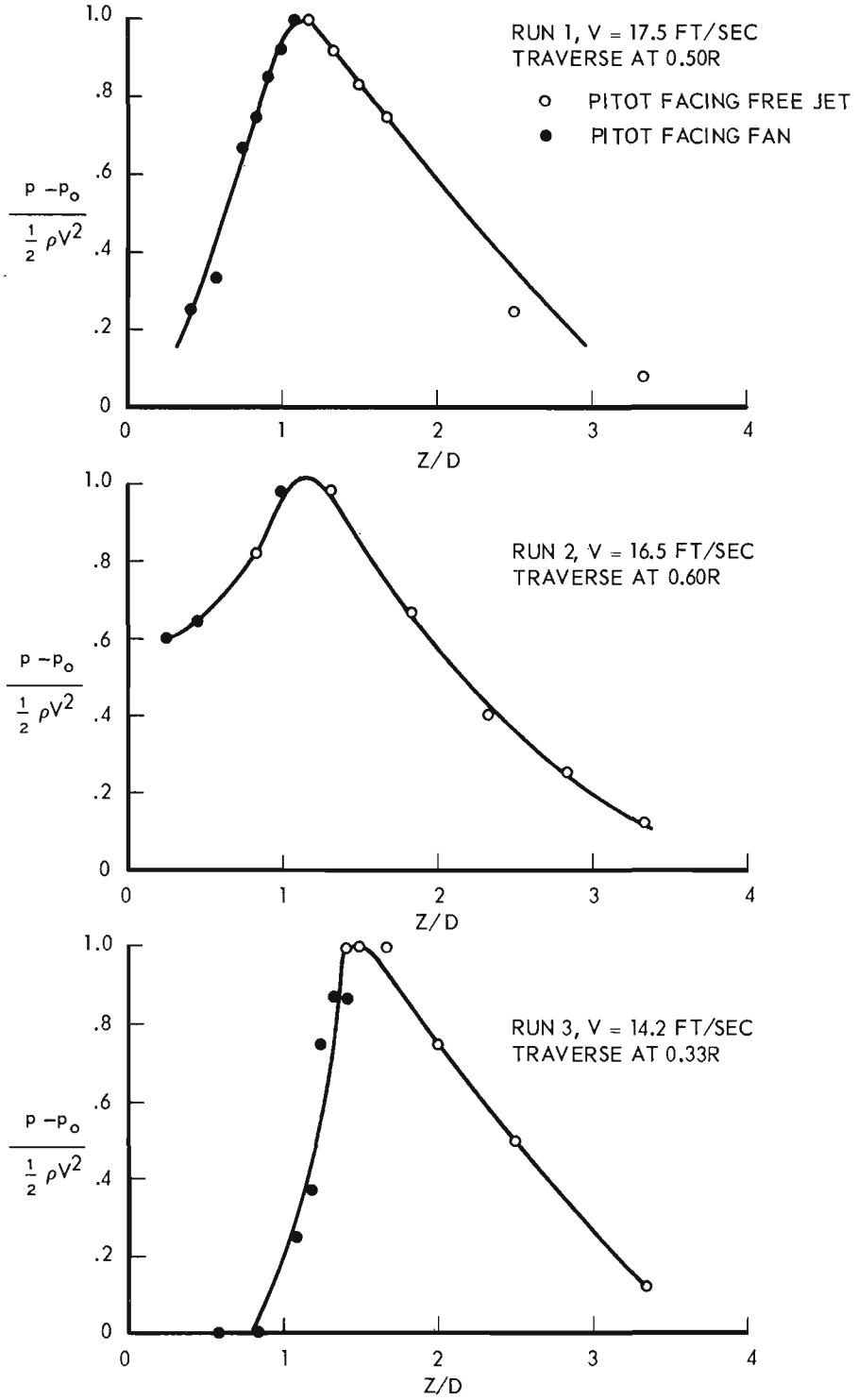

Figure 4. Variation of Static Pressure Through Turbulent Mixing Region.

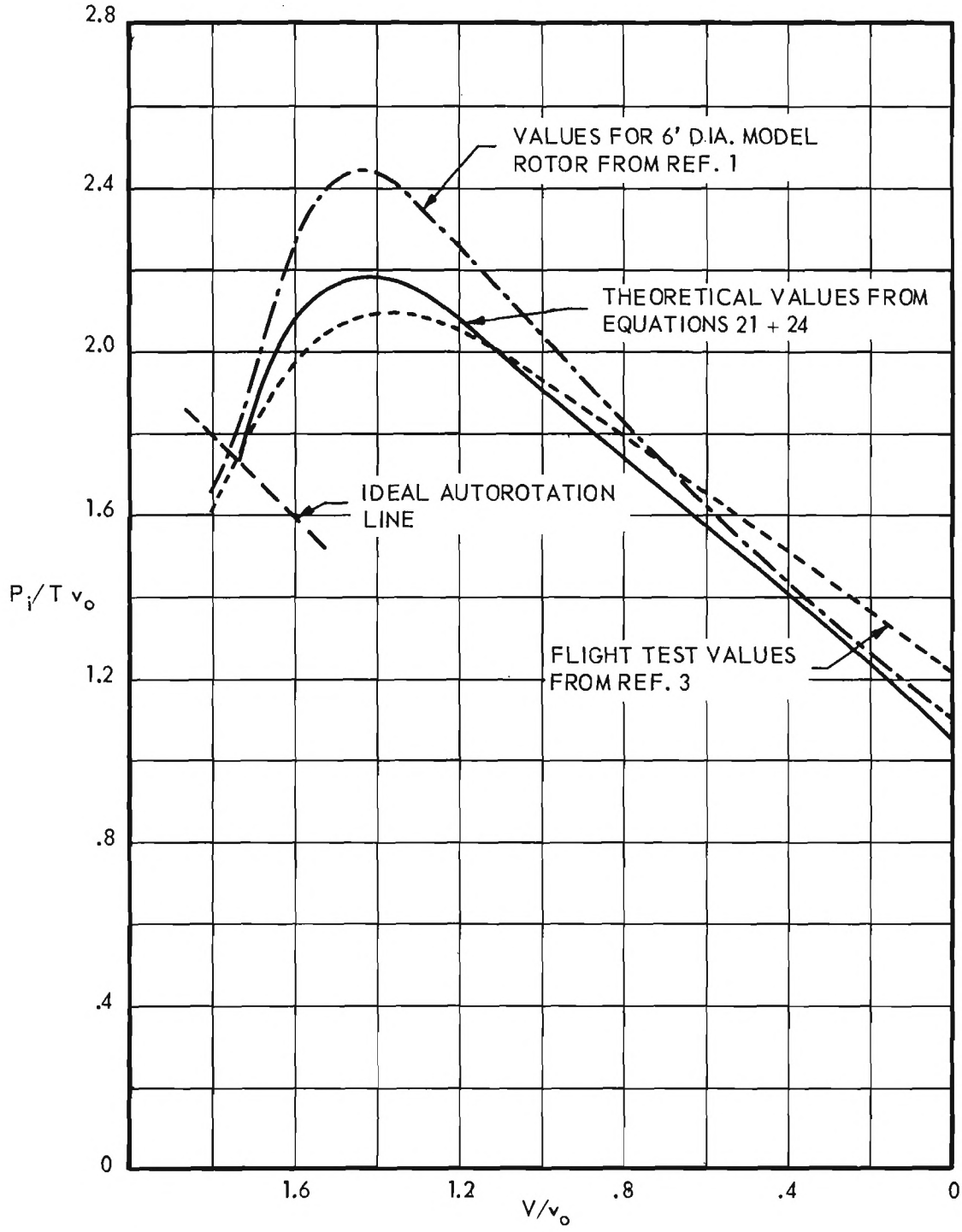

Figure 6. Theoretical Induced Power Ratio Versus Nondimensional Rate of Vertical Descent for Rotor with Triangular Radial Disk Load Distribution Compared with Experimental Values for Rotors with Untwisted Blades.